UNIVERSITÀ DEGLI STUDI DI MILANO

Doctorate School of Biochemical Sciences
Dipartimento di Biotecnologie Mediche e Medicina Traslazionale

Cycle XXXI

The role of HDAC3 in the pathophysiology of adipose tissue

BIO/10

Raffaella Longo

Matr. R11372

Tutor: Prof. Maurizio Crestani

Coordinator: Prof. Sandro Sonnino

Academic year 2017-2018

“πάντες ἄνθρωποι τοῦ εἰδέναι ὀρέγονται φύσει”

“All men by nature desire knowledge”
Aristotle, Metaphysics, 980 **a**

Table of contents

Abstract

INTRODUCTION

Obesity is a metabolic disorder considered as a risk factor for cardiovascular disease, one of the major cause of death worldwide. The upsurge in obesity fueled investigations in the effort to understand the pathophysiology of adipose tissues. Recently recognized as an organ, adipose tissue is divided in white (WAT) and brown fat (BAT). While WAT is mainly considered as energy storage site, BAT is involved in thermogenesis, by oxidizing fatty acids and dissipating energy as heat. The presence of thermogenic active adipocytes in WAT, resulting from a phenomenon called browning, has been recognized. The induction of browning confers protection against obesity and related disorders, paving the way for possible new therapeutic approaches. Moreover, the interaction between environmental cues and the organism has gained importance in the study of metabolic diseases. Epigenomic mechanisms of transcriptional regulation are viewed as an interface mediating the capacity of cells to adapt its own function to environment. Histone acetylation/deacetylation is one of the most intensely studied epigenomic modifications. Histone deacetylases (HDACs), by removing acetyl groups from histones, lead to transcriptional repression. HDACs have been involved in the regulation of metabolism in several organs.

PRELIMINARY RESULTS & AIM

We have previously demonstrated that class I HDAC inhibition reduced body weight and ameliorated glucose tolerance in murine models of obesity. HDAC3 has been identified as main actor involved in these mechanisms. Therefore, we next investigated the role of HDAC3 in the physiology of adipose tissues.

MATERIALS AND METHODS

We used models of *Hdac3* genetic inactivation, *in vivo* (adipose tissue specific *Hdac3* knock out mouse) and *in vitro* (*Hdac3* silencing in adipocyte cell line).

RESULTS

Adipose *Hdac3* ablation induced a transcriptional switch leading to metabolic rewiring toward a futile cycle of fatty acid β-oxidation and *de novo* lipogenesis that sustained browning of WAT. Exposure to high fat diet (HFD) offset the effects of *Hdac3* ablation, by interfering with lipid metabolism. We also observed remodelling of immune population resident in WAT in knock out vs. wild type mice.

CONCLUSIONS

Based on our results, we propose HDAC3 as a regulator of the thermogenic response to cold in WAT, acting as a molecular brake of the metabolic rewiring that sustains WAT browning.

Introduction

Globesity: prevalence, classification and aetiology

Obesity and overweight are defined as conditions where excessive accumulation of fat negatively affects health (Kopelman 2000). Fat accumulation, in turns, is caused by intake of excessive calories not counterbalanced by energy expenditure. The classic parameter that defines overweight and obesity is Body Mass Index (BMI), obtained with the following formula: weight (kg)/ height $(m)^2$. BMI is used for weight classification, as following:

- BMI between 18.5 and 24.9: healthy weight;
- BMI ≥ 25: overweight;
- BMI ≥ 30: obesity.

However, BMI does not take into account different adiposity locations and ethnic differences. Therefore, other parameters are now currently used as, for example, waist circumference, waist to hip ratio, skinfold thickness and bioelectric impedance (Williams et al. 2015).

Obesity and overweight are very common worldwide. Obesity is present in both industrialized and developing countries. WHO estimated that in 2016 39% of adults over 18 years (1.9 billion people) were overweight and 13% of these subjects were facing obesity (source: http://www.who.int/features/factfiles/obesity/en/). For these reasons, obesity is considered epidemic, defined by WHO with the term "globesity". BMI distribution in a population is strictly correlated to socio-economic conditions and industrialization. Improved economic condition is accompanied by a tendency to increased number of people affected by overweight or obesity. In the first phases of economic transition, obesity seems to be associated to the wealthier parts of the society. However, in later phases of economic transition increased prevalence of high BMI has also been observed in the poorest parts of the society (Kopelman 2000). The adoption of dietary habits and sedentary lifestyle similar to western and industrialized countries in developing countries, the so-called "westernization" of the diets, could explain this phenomenon.

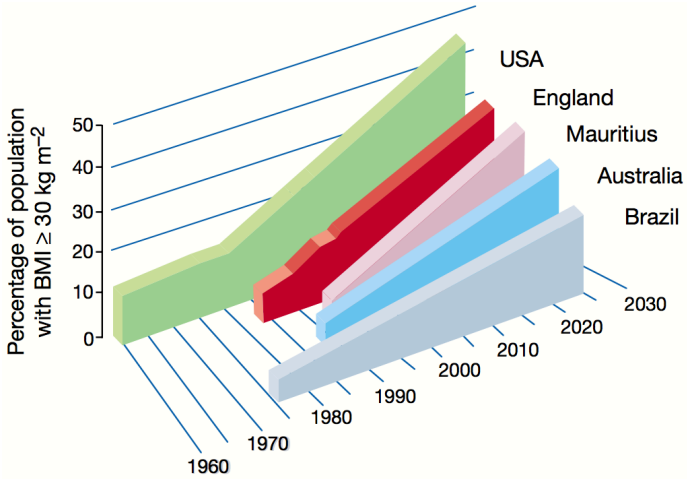

Figure 1: from Kopelman et al. (Kopelman 2000).
Obesity prevalence rates from 1960 to 2025.

Obesity is considered as a major risk factor for cardiovascular disease, mainly stroke and heart disease. Moreover, it is associated to type II diabetes, insulin resistance, hypertension and hyperlipidaemia (Williams et al. 2015). Other conditions often associated to obesity are osteoarthritis, respiratory problems and increased prevalence of some cancers. In addition, overweighed and obese people are often discriminated; therefore this condition is often associated to psychological problems, such as depression, particularly in women (Haslam & James 2005).

Increase of abdominal fat deposition, also known as visceral obesity, has a major role in determining the onset of insulin resistance, hypertension and hyperlipidaemia (Kopelman 2000). This is probably due to increased influx in portal circulation of fatty acids, cytokines and hormones, especially to the liver (Haslam & James 2005).

Regarding factors that contribute to obesity, more than 50% of BMI variation on individuals could be explained by genetic contribution. However, polygenic susceptibility-environment interactions play a major role (Haslam & James 2005). In fact, monogenetic defects leading to obesity are very rare. This highlights the importance of environment as major contributor in the development of overweight and obesity. In particular, increased energy intake, promoted by intense industrial competition, seems to be the major determinant for the onset of obesity, accompanied by reduced physical activity (Haslam & James 2005).

Obesity epidemic is nowadays one of the major medical challenge. The recent upsurge in obesity and related disorders prompted scientific community to find

and validate new therapeutic approaches to face this problem. However, contribution of stakeholders, community and health professionals should not be underestimated in developing new strategies to prevent and manage these diseases (Haslam & James 2005).

The adipose organ

The recent interest on pathophysiology of adipose tissues has been pushed by obesity epidemic. Adipose tissue has been recognized as an organ very recently. It has diverse functions: it helps to protect organs from mechanical hits, but also it has a role in regulation of hormonal reproductive axis. Most importantly, it is a central actor for regulation of systemic metabolism and energy homeostasis (Rosen & Spiegelman 2013). Classically, adipose tissue has been divided in two subtypes: brown and white adipose tissue. However, a third subtype has demonstrated to exist both in humans and rodents: beige fat.

White adipose tissue

White adipose tissue (WAT) is located in subcutaneous and visceral regions. In mice, visceral fat is found in gonadal (epididymal in males), perirenal, mesenteric and epicardic areas. These depots correspond to omental area in humans. The distinction between these two subtypes is not only related to location but adipocytes may display distinct metabolic and functional features according to their subtype. This is probably due to cell-autonomous mechanisms, specific innervation and vascularization (Rosen & Spiegelman 2013). White adipocytes are typically characterized by the presence of unilocular lipid droplet that occupies almost entirely cellular volume. For this reason, white adipocytes have been seen merely as energy storage sites.

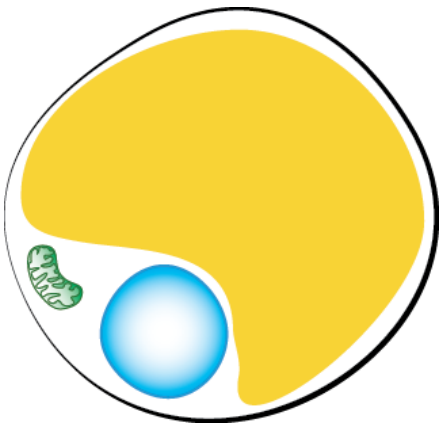

Figure 2: white adipocyte with unilocular lipid droplet. Nucleus is represented in blue, mitochondrion in green.

Only recently this cell has been recognized as a central player in the regulation of energy homeostasis. Furthermore, WAT secretes a plethora of molecules, defined as adipokines, which regulate systemic metabolism through interaction with other metabolic organs. Adiponectin and leptin are the most famous adipokines regulating appetite behaviour and systemic metabolism. Leptin is secreted after a meal and, by regulating hypothalamic neuronal circuits, negatively affects appetite (Choe et al. 2016). Adiponectin, on the other hand, possesses anti-diabetic protective properties, ameliorates insulin resistance and stimulates lipid oxidation (Choe et al. 2016). Other secreted adipokines are resistin, TNFα (Tumor Necrosis Factor α) and also lipid molecules, such as palmitoleic acid (Rosen & Spiegelman 2013). White adipocytes evolved to store lipids during a good nutrition state and to release them during fasting to provide energetic molecules to energy-demanding tissues (Rosen & Spiegelman 2013). Energy storage is realized by the condensation of three free fatty acids (FFAs) to glycerol in triacylglycerols (TGs), which are stored in the lipid droplets. On the other hand, lipolysis is performed by three enzymes that subsequently catalyse the hydrolysis of FFAs from TGs: ATGL (Adipose Triglyceride Lipase) is the enzyme that catalyses the first hydrolysis, HSL (*Lipe,* hormone-sensitive lipase) is the diacylglycerol lipase and, finally, MGL (Monoglyceride Lipase) releases the last FFA from glycerol. FFAs are then released in the circulation and used by skeletal muscle or other tissues. *De novo* lipogenesis (DNL) also takes place in adipose tissue. Herman et al. (Herman et al. 2012) showed that DNL is regulated by glucose cellular flux in adipocytes via ChREBPβ. Increased glucose flux, mediated by *Glut4* overexpression, enhanced expression of *ChREBP*, which, in turns, activates the expression of *Fasn* (Fatty Acid Synthase) and *Acaca* (Acetyl-CoA Carboxylase a), key enzymes for DNL. In particular, ChREBPβ isoform emerged as a novel regulator of DNL in adipose tissue in response to glucose. Of note, the authors also showed that high fat diet (HFD) reduced *ChREBPβ* expression in adipose tissue, thus reducing adipose DNL. In obese individuals both *CHREBPα* and *CHREBPβ* expression correlated with insulin sensitivity.

During the adoption of diets enriched in fat, white adipose tissue responds to caloric overload by increasing cellular volume (hypertrophy) and, though to a

lesser extent, by increasing cell number (hyperplasia). Hypertrophy disrupts adipocyte function and metabolism via inflammatory and non-inflammatory mechanisms, thus worsening systemic metabolism and insulin sensitivity (Choe et al. 2016). On the contrary, induction of hyperplasia seems to exert beneficial property with respect to glucose systemic homeostasis and insulin sensitivity during obesity, probably because newly differentiated adipocytes may buffer and correctly store excess lipids from diet (Choe et al. 2016). In fact, it has been demonstrated that high fat diet (HFD) profoundly affects WAT metabolism (Cummins et al. 2014). In particular, HFD induces metabolic rewiring toward lipid storage preventing excessive lipid oxidation. Nutrient overload promotes accumulation of acyl-carnitines to buffer carbons from metabolic intermediates before incorporation in fatty acids and, thus, TGs. Moreover, the same authors demonstrated that HFD also reprograms glucose, amino acids and nucleotide metabolism. Finally, HFD reduces mitochondrial proteins and induces autophagy, possibly to limit lipid oxidation.

Brown adipose tissue

Brown fat (BAT) is present in intrascapular and perirenal regions in mice. In humans, it is typically present in newborns. However, 18F-fluorodeoxyglucose positron-emission tomographic and computed tomographic (PET–CT) scans identified regions of active brown adipocytes in older humans, in particular in region from anterior neck to thorax (Cypess et al. 2009). Brown adipocytes are characterized by multilocular lipid droplets and higher mitochondria content.

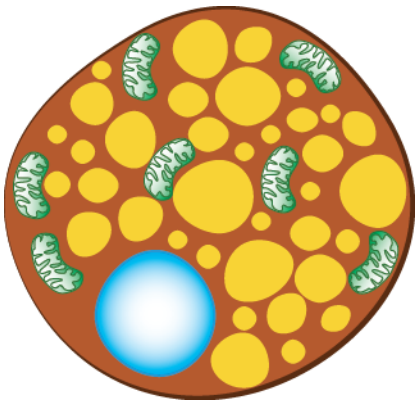

Figure 3: brown adipocyte with multilocular lipid droplets. Nucleus is represented in blue, mitochondria in green.

Brown fat participates in regulation of body temperature, by dissipating energy as heat. In particular, upon cold exposure, norephinefrine is released and activates thermogenesis in BAT primarily through β_3-adrenergic receptors, which are abundantly expressed in this tissue. Brown adipocytes are characterized by the presence of the uncoupling protein 1 (UCP1), which dissipates the mitochondrial proton gradient, thus uncoupling ATP synthesis from respiratory chain (Rosen & Spiegelman 2013). Long chain free fatty acids (LCFAs) in BAT are required for UCP1 activity (Fedorenko et al. 2012). In fact, UCP1 acts as an $LCFA^-/H^+$ symporter with LCFA bound to the protein. Fatty acids are taken up from circulation via LPL (Lipoprotein Lipase) and translocated to cytoplasm by CD36 (Cluster of Differentiation 36) (Calderon-Dominguez et al. 2015) or obtained by hydrolysis of TGs via lipolysis. Fatty acid β-oxidation is highly active in BAT, in fact deletion of genes important for this pathway (*Cpt1b, carnitin-palmitoyl transferase 1b and Acsl1, acyl-CoA synthethase 1*) demonstrated that β-oxidation is required for thermogenesis (Calderon-Dominguez et al. 2015).

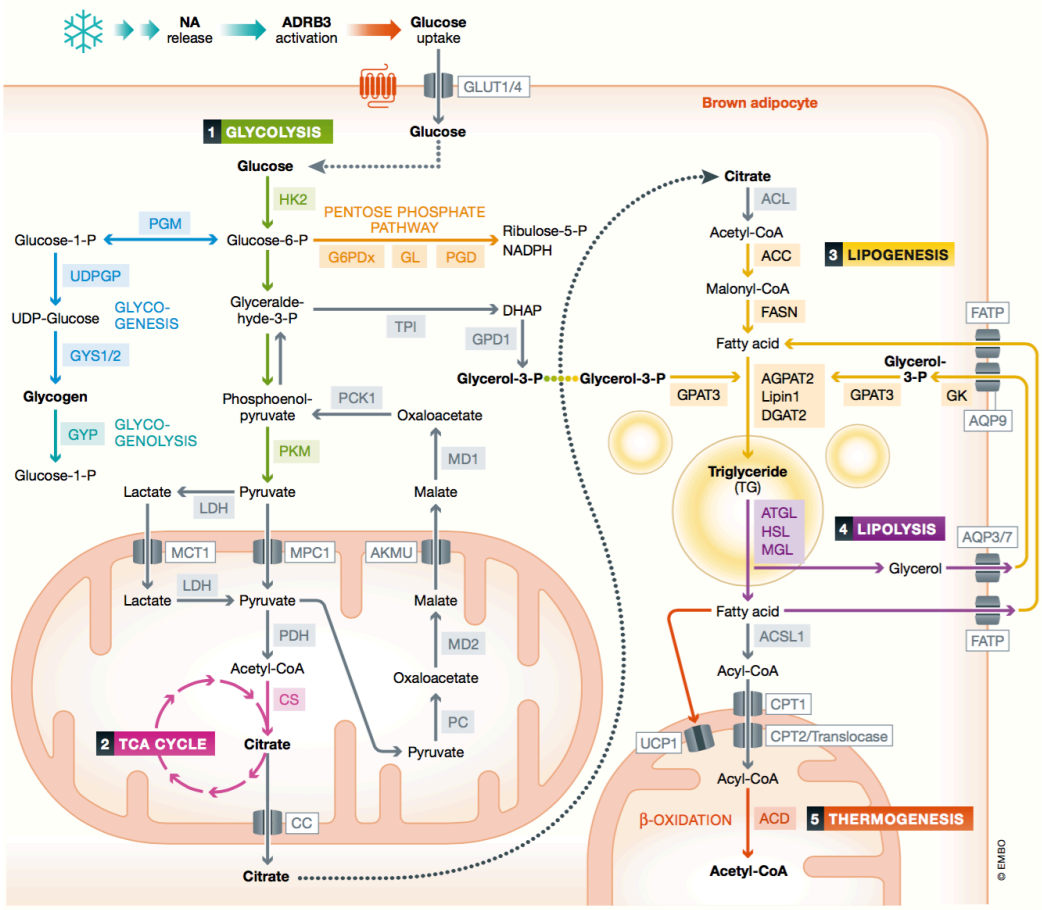

Figure 4: from Hankir et al. (Hankir et al. 2018).
Norephinefrine release by sympathetic nerves upon cold exposure activates β_3-adrenergic receptors. This induces glucose internalization by GLUT1/4. Glycolysis generates dihydroxyacetone phosphate (DHAP), which is converted in glycerol-3-phosphate, pyruvate and lactate. Simultaneously, pentose phosphate pathway generates ribulose-5-P and NADPH. Pyruvate and/or lactate are next transported in the mitochondria. Mitochondrial pyruvate is converted to acetyl-CoA by pyruvate dehydrogenase (PDH). Acetyl-CoA then enters in the TCA cycle as citrate, which is then exported to the cytosol. Citrate is converted back to acetyl-CoA by ATP-citrate lyase (ACLY), feeding DNL. Newly synthesized FAs are condensed in TGs. Upon cold exposure, TGs are rapidly hydrolyzed via ATGL, HSL and MGL. FFAs either activate UCP1 or enter in the mitochondria via ACSL1, CPT1, translocase and CPT2. Once inside the mitochondria, acyl-CoA is β-oxidized, generating proton gradient across the inner mitochondrial membrane as a result of oxidation of NADH and $FADH_2$ generated during fatty acid oxidation. Glycerol is phosphorylated by glycerol kinase (GK) into glycerol-3-phosphate. Similarly, anaplerotic conversion of pyruvate to oxaloacetate is catalyzed by pyruvate carboxylase (PC). Oxaloacetate, in turns, is converted to malate, which is exported to the cytosol and converted back to oxaloacetate. Finally, phosphoenolpyruvate carboxykinase 1 (PCK1) generates PEP from oxaloacetate, feeding glycerolneogenesis or used to obtain ATP via pyruvate kinase required for conjugation of FFAs with Coenzyme A. Fatty acids and glycerol released from lipolysis may enter an extracellular loop via fatty acid transport protein1 (FATP) and aquaporin 3/7/9 (AQP 3/7/9) as part of the fatty acid recycling pathway.

Fatty acid β-oxidation, in fact, produces high amount of reducing equivalents NADH and $FADH_2$ that feed electron transport chain and, thus, uncoupled respiration. However, glucose uptake is essential for thermogenesis, though to a lesser extent than lipids (Hankir et al. 2018). Glucose, in fact, has several roles in BAT: glucose-6-phosphate can supply pentose phosphate pathway producing NADPH, amino acids and nucleotides. Moreover, glucose provides glycerol for TG synthesis and glucose-derived pyruvate can be converted to lactate (Hankir et al. 2018). Finally, glucose is converted to pyruvate and, thus, to acetyl-CoA to feed TCA cycle. Importantly, glucose derived acetyl-CoA can be also converted to citrate by PDH (Pyruvate Dehydrogenase), which in turn exits the mitochondria and is converted back to cytosolic acetyl-CoA pool via ATP-citrate lyase (ACLY) to feed *de novo* fatty acid synthesis. At this regard, β_3-adrenergic stimulation or cold exposure stimulate the concomitant expression of genes belonging to lipid oxidation and *de novo* lipogenesis in BAT (Yu et al. 2018; Mottillo et al. 2014), inguinal and gonadic WAT (Mottillo et al. 2014). The concurrent and paradoxical activation of these opposite pathways provides fuel for higher oxidative metabolism and supply substrates to high rate of lipid oxidation

(Mottillo et al. 2014). A recent paper from Weir et colleagues (Weir et al. 2018) used microdialysis to quantify BAT metabolism in human subjects. They showed that glucose uptake was increased in BAT during cold exposure. According to this study, glucose seemed to not be fully oxidized during cold-induced thermogenesis, as lactate production and release was high in BAT and accounts for more than half of glucose uptake in cold activated BAT. However, authors showed that lipolysis and subsequent fatty acid oxidation supplied the majority of energy demand related to BAT thermogenesis. Glutamate uptake was also increased in activated BAT, indicating that BAT also uses additional energy sources other than glucose and fatty acids. Of note, BAT metabolism was active also in warm conditions.

Recently, it has been showed that BAT releases molecules with endocrine roles, collectively known as "batokines", as for example FGF21 (Fibroblast Growth Factor 21), NRG4 (Neuregulin4) and BMP8b (Bone Morphogenetic Protein 8b) (Kajimura et al. 2017).

Beige adipocytes and browning

A third type of adipocytes has been recognized very recently: beige adipocytes. These cells have been identified as UCP1+ cells within WAT depots. The appearance of beige adipocytes, a phenomenon defined as "browning", has been originally found after cold exposure or β-adrenergic stimulation in mice (Rosen & Spiegelman 2013).

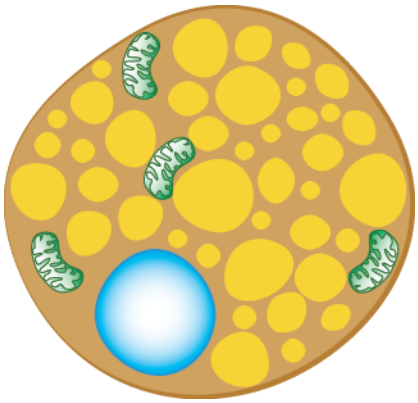

Figure 5: beige adipocyte. Nucleus is represented in blue, mitochondria in green.

Subcutaneous WAT (SubWAT) is more prone to undergo browning than visceral epididymal WAT (Kajimura et al. 2015). Importantly, beige adipocytes have been identified also in humans (Jespersen et al. 2013; Sparks et al. 2012; Shinoda et al.

2015). In addition to β-adrenergic stimulation and cold exposure, several inducers of browning and BAT activity have been identified, among which T3 (triiodothyronine), natriuretic peptides (ANP and BNP), bile acids, irisin, FGF21. As opposed to BAT, where UCP1 expression and uncoupled respiration are high without stimulus, beige cells acquire thermogenic capacity upon proper stimulation (Sparks et al. 2012).

Developmental origin of beige adipocytes is highly debated. It is clear that beige adipocytes do not share developmental program with classical brown adipocytes. Recent researches suggested that cold or β-adrenergic stimulation induce *de novo* beige adipocyte differentiation and activation of *Ucp1* expression in mature adipocytes, which likely derive from beige lineage (Kajimura et al. 2015).

The study from Shabalina et al. (Shabalina et al. 2013) showed that mitochondria from beige fat were functionally capable to perform UCP1-dependent thermogenesis. Of note, oxidative phosphorylation capacity was lower in BAT or beige mitochondria compared to heart mitochondria. In this study, however, BAT thermogenic capacity was still higher than that of beige fat. Proteomics analysis of beige fat mitochondria versus BAT mitochondria identified the arginine-dependent creatine metabolism as a peculiar characteristic of cold-activated beige adipocytes (Kazak et al. 2015). Importantly, the authors demonstrated the occurrence of a creatine-driven futile cycle, which increased ADP-dependent respiration and thermogenesis. In fact, futile cycle of phosphocreatine hydrolysis and creatine phosphorylation by CK (Creatine Kinase) increased ADP concentration in mitochondria, thus ADP-dependent electron transport chain. Accordingly, reduced creatine metabolism *in vivo* diminished oxidative metabolism in thermogenic tissues BAT and beige fat.

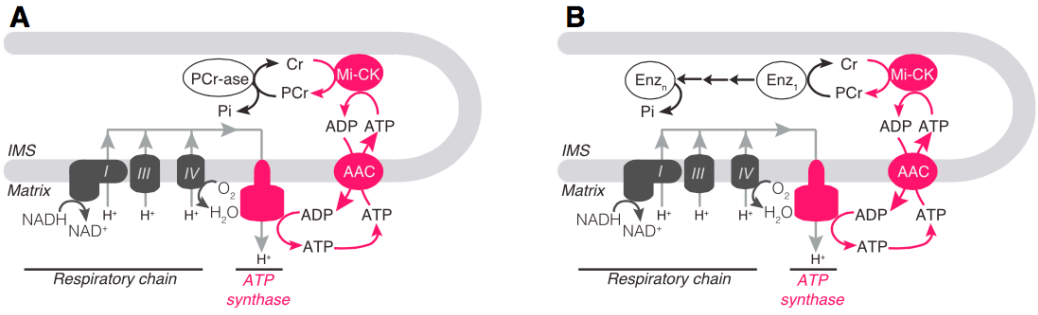

Figure 6: from Kazak et al. (Kazak et al. 2015).
Models of creatine futile cycle: a) model based on phosphocreatine direct hydrolysis; b) model based on multiple phosphotransfer events.

Moreover, inhibition of creatine metabolism reduced thermogenic capacity of *Ucp1*$^{-/-}$ mice, thus indicating that creatine metabolism role in thermogenesis is UCP1-independent. These results are indicative of metabolic pathways influencing thermogenesis in beige adipocytes and BAT that do not need UCP1 uncoupling activity. Furthermore, another study demonstrated that induction of browning by *Prdm16 (Pr domain containing 16)* overexpression (*Prdm16* Tg mice) was sufficient to increase thermogenic response in inguinal WAT, even in absence of *Ucp1* (*Prdm16* Tg x *Ucp1*$^{-/-}$ mice), further suggesting the existence of thermogenic mechanisms alternative to UCP1 activation (Ikeda et al. 2018). In particular, these authors found a role of SERCA2b (*Atp2a2,* ATPase Ca^{2+} transporting slow twitch 2*)*-RyR2 (Ryanodine Receptor 2) pathway in mediating UCP1-independent thermogenesis in beige adipocytes. *Prdm16* Tg x *Ucp1*$^{-/-}$ mice and *Prdm16* Tg mice displayed resistance to HFD-induced obesity and glucose intolerance, indicating that induction of beige adipocytes protected against obesity and related metabolic dysfunction without requirement of UCP1 activation. Interestingly, *Prdm16* Tg x *Ucp1*$^{-/-}$ mice displayed increased respiratory exchange ratio (RER) than *Ucp1*$^{-/-}$ mice, indicating that *Prdm16* Tg x *Ucp1*$^{-/-}$ mice preferentially utilized carbohydrates as energy source or, in other terms, beige adipocytes switched from fatty acid to glucose metabolism in absence of UCP1. To explain their results, the authors proposed the following model: norephinefrine, by interacting with α_1 and β_3-adrenergic receptors, increases Ca^{2+} flux in the cytoplasm, which is subsequently recycled in endoplasmic reticulum by SERCA2b, consuming ATP. Ca^{2+} is likely transported to the mitochondria where it activates PDH phosphatase 1c (PDP1c) and oxidation of glucose-derived pyruvate in TCA cycle and following ATP synthesis. Thermogenesis is achieved when uncoupling of ATP hydrolysis by SERCA2b and Ca^{2+} transport is occurring. This pathway seems to be operative in beige adipocytes, which display higher ATP synthase than BAT.

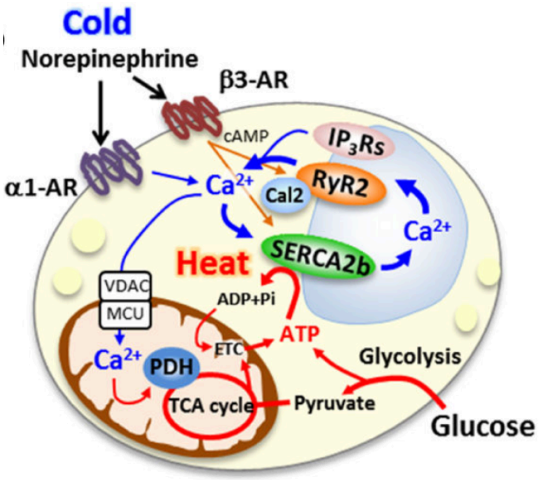

Figure 7: adapted from Ikeda et al. (Ikeda et al. 2018).
Model of UCP1-independent thermogenesis via uncoupling of Ca^{2+} transport and ATP hydrolysis by SERCA2b.

Several studies have clearly demonstrated that induction of beige adipocytes and/or activation of BAT by treatment with pharmacological agents or genetic modifications protect against diet-induced obesity and prevent dysfunction of systemic metabolism (Kajimura et al. 2015). Min et al. (Min et al. 2016) obtained human adipogenic progenitors that resembled many features of beige phenotype. When implanted in HFD-fed NOD-*scid IL2rg*^{null} mice, human derived adipocytes maintained enhanced systemic glucose tolerance. Of note, these cells displayed increased expression of *IL33 (Interleukin 33)* and *PCSK1 (Proprotein-Convertase Subtisilin/Kexin type 1)* and its substrate *PENK (Proenkephalin)*, thus suggesting that neuroendocrine secreted factors could contribute to amelioration of glucose metabolism related to human beige adipocytes implantation.

Immune cells are adipocytes partners that contribute in the regulation of adipose tissue pathophysiology

Adipose tissues are not only composed by adipocytes but other cell types reside within it: endothelial cells, fibroblasts, preadipocytes, stem cells and immune cells. Actually, mature adipocytes only constitute 20-40% of the entire tissue (Rosen & Spiegelman 2013). The role of immune cells in adipose tissue pathophysiology raised interest of scientific community because their pro-inflammatory functions exerted as consequence of HFD provide a link between obesity and dysregulation of systemic metabolism. However, immune cells in adipose tissue do not play only a pro-inflammatory role in obesity but also secrete anti-inflammatory cytokines that participate in regulation of tissue function.

Innate immune cells in WAT pathophysiology

Hypertrophic adipocytes have been linked to altered adipose tissue functionality. In fact, hypertrophy has been associated to increased expression and release of inflammatory cytokines, increased hypoxia and lipolysis with related increase in release of FFAs that are ectopically accumulated in other organs and tissues, such as liver and skeletal muscle, thus worsening systemic metabolism (Choe et al. 2016).

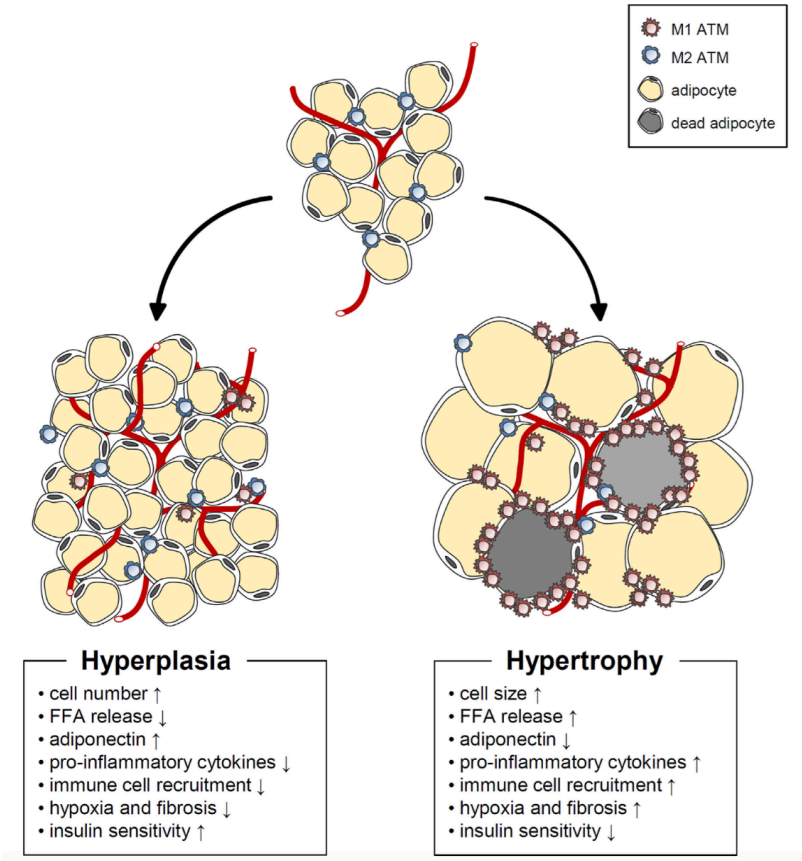

Figure 8: from Choe et al. (Choe et al. 2016).
Characteristics of hyperplastic versus hypertrophic adipocytes in obesity.

It has been demonstrated that, in obesity, hypertrophy drives necrotic-like adipocytes death. This, in turns, promotes accumulation of macrophages in WAT that surround dead cells in "crown-like structures" (CLSs) (Cinti et al. 2005). Crown-like structures are prevalent in visceral fat (ViscWAT), suggesting that visceral adipocytes are more prone to hypertrophy driven-death. Adipocytes size seems to be a critical factor to trigger death in ViscWAT, whereas it seems to be more tolerated by subcutaneous adipocytes. This peculiar characteristic associates

increased ViscWAT with increased incidence of metabolic disorders (Murano et al. 2008). Macrophages appearance has been linked with insulin resistance (Xu et al. 2003). This is related to increased release of pro-inflammatory cytokines. Actually, adipose tissue resident macrophages (ATMs) are divided in two subtypes: M1 or "classically activated" and M2 "alternatively-activated" macrophages. M1 macrophages typically express surface markers CD11c (*Itgax, integrin alpha X)* together with classical macrophages markers F4/80 (*Adgre1, adhesion G-protein coupled receptor E1*) and Cd11b (*Itgam, integrin alpha M)* (Huh et al. 2014). Polarization towards M1 macrophages is induced by factors as lipopolysaccharide (LPS) and interferon γ (IFNγ) and, in turns, M1 macrophages release pro-inflammatory molecules, such as tumor necrosis factor α (TNFα), interleukins 6 (IL6), 12 (IL12) and 1β (IL1β) and NO (nitric oxide) (Mathis 2013; Huh et al. 2014). In fact, *Il6* and *Nos2* (Nitric Oxide Synthase 2, inducible) are considered gene markers of M1 subtype, together with *Ccl2* (Chemokine C-C Motif Ligand 2). On the other hand, M2 macrophages are present in lean subjects and are characterized by the expression of surface markers CD206 (*Mrc1, mannose receptor, C type 1*), CD301 (*CLEC10A, C-type lectin domain containing 10A*) and Arg1 (Arginase 1). Conversely, M2 subtype releases anti-inflammatory cytokines, for example IL10 and IL1Ra (Interleukin 1 Receptor Antagonist) (Huh et al. 2014). However, a recent study identified different subtypes of macrophages that do not endow classical M1 or M2 phenotype. Hill et al. (Hill et al. 2018) showed the presence of $CD9^+$ ATMs, especially in CLSs. The $CD9^+$ macrophages presented lysosomal-like particles loaded with high amount of intracellular lipids. Transfer of $CD9^+$ macrophages to lean recipient donor caused a shift of gene expression toward a profile more similar to that of obese adipose tissue, indicating $CD9^+$ macrophages as primary actors in inflammation related to obesity. On the other hand, the authors also demonstrated the presence of another macrophage population, $Ly6C^+$, with no lipid particles and interspersed in the adipose tissue. These macrophages expressed genes related to angiogenesis and tissue organization; in fact their transfer to a lean recipient mouse was accompanied by increased expression of genes belonging to adipose tissue physiology. Importantly, the authors also showed $CD9^+$ ATM with lipid-laden structures associated to CLSs in human visceral fat of obese subjects. Furthermore, they showed a correlation between BMI and $CD9^+$ ATMs, further indicating that the presence $CD9^+$ ATMs is linked to obesity also in humans.

The presence of other immune cell types has been linked to obesity related metabolic dysfunctions. Talukdar et al. (Talukdar et al. 2013) showed the presence of neutrophils ($Ly6G^+$) in WAT (ATNs, adipose tissue neutrophils) after 3 days of HFD exposure which remained constant up to day 90 of exposure. Expression of neutrophil elastase *Ne* was higher in HFD fed mice and *Ne* genetic or pharmacologic inhibition reduced ATNs and improved hepatic and adipose tissue insulin sensitivity. Moreover, *Ne* knock out mice displayed increased expression profile of M2 macrophages in adipose tissue and, conversely, reduced expression of M1 subset genes, indicating that *Ne* may have a role in recruiting M1 macrophages. Moreover, also mast cells have been implicated in obesity-inflammation (Mathis 2013).
Eosinophils in the adipose tissue secrete cytokines such as IL4 and IL13 that polarize macrophages toward M2 subset (Huh et al. 2014). Davina et al. (Davina et al. 2011) demonstrated that 90% of IL4 competent cells in visceral WAT of chow diet fed mice were eosinophils. Moreover, HFD fed mice displayed reduced levels of eosinophils. The same authors elegantly demonstrated that eosinophils and Il4 and Il13 sustained the presence of alternatively activated macrophages in visceral WAT. Eosinophil-deficient mice displayed increased body fat and impaired glucose tolerance, suggesting that eosinophils play an anti-inflammatory role in obesity.
Finally, also recently discovered innate lymphoid cells (ILCs) and related release of IL5 and IL13 have been implicated in maintaining adipose homeostasis under normal conditions (Mathis 2013).

Adaptive immunity plays a role in adipose tissue pathophysiology

In addition to innate immune cells, also adaptive immunity has been implicated in adipose tissue pathophysiology. At this regard, Nishimura et al. (Nishimura et al. 2009) showed increased number of $CD8^+$ T lymphocytes within CLSs in adipose tissue of obese mice. In parallel, $CD4^+$ T lymphocytes were not associated to CLSs and their number was decreased in visceral WAT of obese mice. Moreover, $CD8^+$ T lymphocytes infiltration was detected within 2 weeks of HFD exposure, even before macrophages infiltration. Accordingly, treatment with α-CD8 antibody reduced M1 macrophages, number of CLSs and expression of *Tnfα* and *Il6* in HFD fed mice. CD8 block with specific antibody also ameliorated glucose tolerance. By performing *in vitro* co-culture experiments, the same authors

demonstrated that obese visceral WAT induced T cell proliferation. Additionally, interaction between visceral epididymal adipose tissue and $CD8^+$ T lymphocytes was essential to induce monocyte differentiation to macrophages, macrophages migration and activation, measured as *Tnfα* expression.

B cells have been also found in visceral WAT of HFD fed mice within 4 weeks of diet exposure (Winer et al. 2011), together with IgG and IgM associated to CLSs. HFD fed B^{null} mice, a model with genetic B cells deprivation, showed improved glucose tolerance and insulin sensitivity with reduced number of M1 macrophages and $CD8^+$ T cells. In fact, the same authors demonstrated that T lymphocytes were required for B cells-driven metabolic impairments during HFD and that, in turn, B cells modulated $CD8^+$ T lymphocytes, via MHC II (major histocompatibility complex II), and $CD4^+$ T lymphocytes, via MHC I. Moreover, IgG produced by B cells in ViscWAT also participated in worsening glucose homeostasis and insulin sensitivity. Importantly, insulin-resistant obese human subjects displayed a peculiar serum IgG panel different from that of insulin-sensitive obese human subjects, highlighting the importance of B cell function and activity in human pathology.

Winer et al. (Winer et al. 2009) also characterized $CD4^+$ T lymphocytes and related sublineages in obese mice and human subjects. HFD fed mice and obese subjects displayed increased T helper1 (Th1) subset and reduced level of $CD4^+$ $Foxp3^+$ T cells (Treg, T regulatory), with increased Th1:Treg ratio. This peculiar T cells subset was, at least in part, determined by antigen-driven mechanisms. $CD4^+$ T lymphocytes transfer in HFD fed RAG^{null} mice, which lacked lymphocytes, caused reduced weight gain, reduced levels of obesity-related adipokines leptin, resistin and Mcp1 (*Ccl2, chemokine (C-C motif) ligand 2*) and ameliorated glucose tolerance. Interestingly, immunotherapy increasing $CD4^+$ $Foxp3^+$ T cells improved glucose tolerance during HFD exposure and increased also Il10-secreting M2 macrophages in ViscWAT. The authors proposed that Th2 and Treg gradually fail to modulate Th1 expansion in obesity, leading to the onset of pro-inflammatory environment in WAT that worsens systemic glucose tolerance.

With respect to $CD4^+$ $Foxp3^+$ cells, Feuerer et al. (Feuerer et al. 2009) demonstrated that these cells represent half of $CD4^+$ T cells in ViscWAT of lean mice with lower number in subcutaneous WAT. The abdominal WAT $CD4^+$ $Foxp3^+$ cells displayed 136-fold increase in *Il10* expression compared to lymphnodes Treg. By analyzing T cell receptor (TCR) repertoire the authors

found that fat Treg endowed TCR repertoire different from that of fat T conventional cells (Tconv), indicating that Treg population in ViscWAT is not derived from local conversion of Tconv cells. The author also raised the possibility that the TCR-driven high frequency of Treg in adipose tissue may be related to the local recognition of specific antigen. Importantly, Treg resulted to have a role in regulating glucose homeostasis in obesity. *In vitro* assays demonstrated that Treg-specific cytokine IL10 reduced the TNFα-mediated insulin resistance in 3T3-L1 adipocytes by cell-autonomous mechanisms, thereby showing the importance of Treg in regulating adipose tissue homeostasis and systemic metabolism.

Finally, natural T killer cells (NTK) have been somewhat implicated in inflammation related obesity but their exact role remains to be further elucidated (Mathis 2013).

Thus, it appears that innate and adaptive immunity cooperate both in normal adipose tissue physiology and in metabolic disorders. In fact, anti-inflammatory cells (mainly M2 macrophages and Treg cells) act as brake of inflammatory response in early stages of obesity. However, excess energy and adipocyte dysfunction lead to unbalanced equilibrium between anti- and pro- inflammatory immune cells that, in turn, induce dysregulation in the immune response and metabolic systemic dysfunction. However, immune cells unbalancing in adipose tissue during obesity is a dynamic and reversible phenomenon (Choe et al. 2016).

Immune cells have been implicated in inflammation and obesity not only in ViscWAT but also in BAT, though they are present in a lesser extent (Brown et al. 2018). Inflammatory mechanisms in obesity seem to impair thermogenic response in BAT and beige adipocytes recruitment.

Immune cells are not only implicated in inflammation and obesity. For example, during fasting and weight loss macrophages are recruited to fat to buffer excessive free fatty acids (Rosen & Spiegelman 2013). Moreover, it has been suggested that ATMs modulate extracellular matrix thus playing a role in adipose tissue remodeling and angiogenesis, also during adipogenesis (Choe et al. 2016). Importantly, both innate and adaptive immune cells play a role in thermogenesis and browning (Brown et al. 2018). In particular, M2 macrophages, eosinophils, ILC2 cells, Treg and iNTK cells have been implicated in regulation of BAT activation and/or WAT browning. Several mechanisms of macrophages involvement in BAT- and beige-related thermogenesis have been proposed: their role in producing norephinefrine is still debated. However, these cells have been

involved in clearance and degradation of this neurotransmitter, thus reducing response to cold and thermogenesis. Finally, a role in innervation has also been showed (Brown et al. 2018).

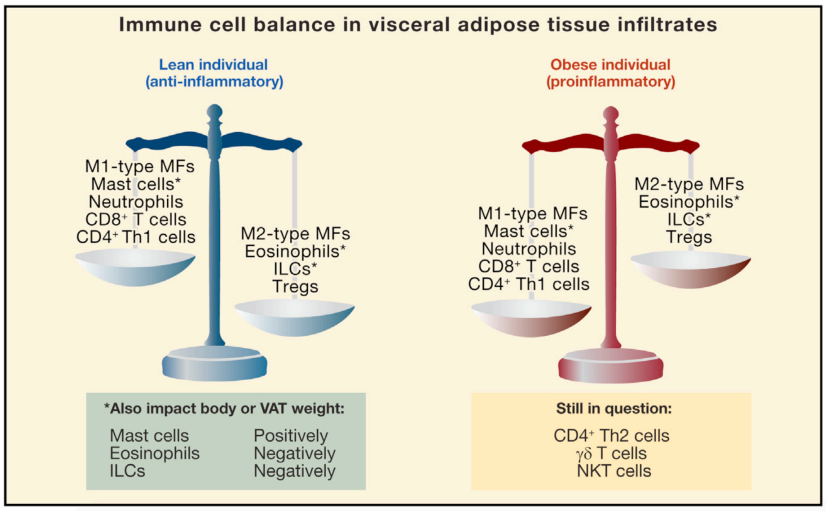

Figure 9: from Mathis (Mathis 2013).
Immune cells in the pathophysiology of adipose tissue.

Epigenetics

The term "epigenetics" refers to heritable changes in gene expression that do not imply changes in DNA sequences. Epigenetic mechanisms comprise chromatin modification, DNA cytosine modifications (methylation and hydroxymethylation) and non-coding RNAs-driven silencing. Epigenetic regulation of gene expression is viewed as a way to sense the external environment and modulate genome function. Therefore, modulation of chromatin organization is one of the mechanisms by which cells can modulate their functions in response to changing environmental conditions. In fact, chromatin can be viewed as an "interface" between environment and nuclear function throughout lifespan (Benayoun et al. 2015). Regulation of chromatin organization is exerted by chemical modifications on DNA cytosine or histone aminoacidic residues. The role of these modifications is to regulate DNA accessibility to transcriptional factors and coregulators and/or proximity of regulatory elements to gene sequences. To simplify the complexity of chromatin 3D organization, the state of opened chromatin is defined as "euchromatin", whereas the state of lower DNA accessibility is defined as "heterochromatin". However, chromatin condensation in a particular locus is a much more dynamic phenomenon and the final result in terms of gene expression

is actually due to the contribution of different epigenomic marks in the same locus. In fact, chromatin modifications constitute the epigenomic code, as already hypothesized since 2000 (Strahl & Allis 2000). Amino acid residues in histone tails can be modified via phosphorylation, methylation, acetylation, ADP-rybosilation, SUMO-ylation, biotinylation and ubiquitinylation. Epigenomic enzymes that are responsible of adding a particular chemical modification to histone or DNA are classically defined as "writers". Enzymes defined as "erasers" catalyze the opposite reaction. Finally "readers" are the enzymes that actuate the final epigenetic response. To mention some elements of the histone code, active promoters are usually marked by histone 3 lysine 4 trimethylated (H3K4me3); active enhancers by histone 3 lysine 4 mono and dimethylated (H3K4me1/me2) and histone 3 lysine 27 acetylated (H3K27ac); genes actively transcribed by histone 3 lysine 36 or 79 trimethylated (H3K36me3, H3K79me3). Whereas, silenced chromatin is associated to histone marks such as histone 3 lysine 9 trimethylated (H3K9me3), histone 3 lysine 27 di- and trimethylated (H3K27me2/me3), histone 4 lysine 27 di- and trimethylated (H4K27me2/me3) and histone 4 lysine 20 trimethylated (H4K20me3) (Longo et al. 2017).

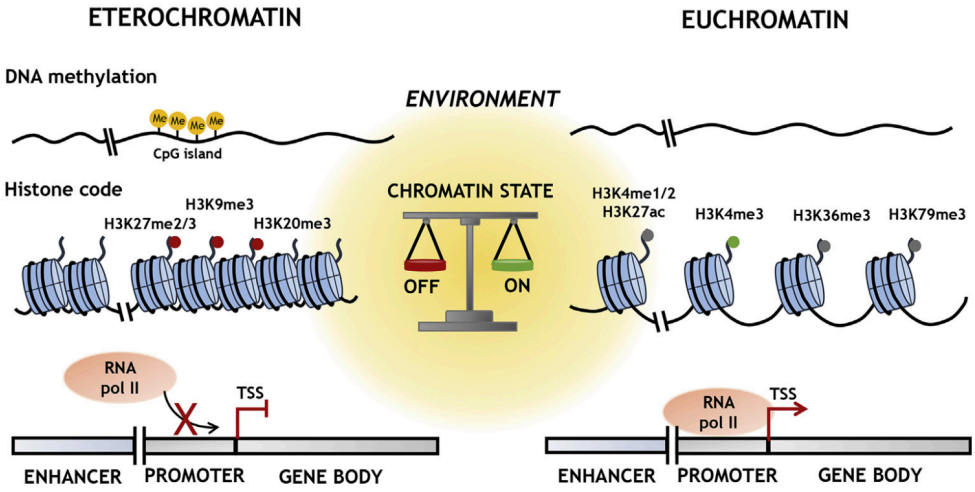

Figure 10: adapted from Longo et al.(Longo et al. 2017).
Chromatin spatial organization regulates gene expression. Gene expression patterns result from combination of different epigenomic marks.

Recently, the idea that metabolic status of the cells is integrated in epigenetic regulation of genome has emerged (Lu & Thompson 2012). At this regard, epigenomic enzymes use as cofactors or substrates molecules that are part of intermediate metabolism. This observation suggests a tight link between

metabolism and epigenomic regulation. Thus, metabolite levels in a particular metabolic state can influence epigenomic enzymes activity, thereby regulating gene expression (Ferrari et al. 2018).

Acetylation of histone tails is catalyzed by a class of enzymes called histone acetyltransferases (HATs) and acetyl-CoA is used as substrate for histone acetylation. At this regard, Wellen et al. (Wellen et al. 2009) demonstrated that ATP-citrate lyase (ACLY) is fundamental to provide acetyl moieties to HATs in the nucleus. In fact, these authors showed that ACLY is present not only in the cytoplasm but also in the nucleus. Cytoplasmic citrate enters in the nucleus and is used by ACLY, obtaining nuclear acetyl-CoA, which, in turn, is used by HATs. Moreover, they also showed that glucose is the principal source to sustain histone acetylation. However, fatty acids and, in certain conditions, acetate, can be also used as source of acetyl-CoA for histone acetylation (McDonnell et al. 2016; Gao et al. 2016). On the other hand, histone deacetylases (HDACs) are erasers of histone acetylation. Shimazu et al. (Shimazu et al. 2012) demonstrated that ketone body β-hydroxybutyrate inhibits endogenously class I HDACs. Class III HDACs, also known as sirtuins, activity is regulated by NAD^+/NADH ratio, thus these epigenomic enzymes are defined as "sensors of energy status" of the cell.

Methylation of DNA or of lysine or arginine residues on histone tails is the result of equilibrium between methylation and demethylation activity. Methylator enzymes are DNA methyltransferases (DNMT) and histone methyltransferases (HMT) which use S-adenosylmethionine (SAMe) for transferring methyl groups to the proper substrate, forming S-adenosylhomocisteine (SAH) as by-product. Both SAMe and SAH are intermediate metabolites of the so-called "one-carbon metabolism". Methionine, folate, choline and vitamins B12 and B6 also influence this pathway and, in turn, epigenetic methylation. Histone demethylation may occur thanks to the activity of LSDs (Lysine-Specific Demethylases), which use FAD as cofactor, or JHDMs (Jumonji-C domain containing Histone Demethylases), which use for their enzymatic reaction O_2, Fe(II) and α-ketoglutarate, which is converted to succinate. Whereas, DNA methylation is probably exerted by two step reactions: the first conversion of 5-methylcytosine (5-mC) in 5-hydroxymethylcytosine (5-hmC) is catalysed by TETs (Ten-Eleven Translocation), which share catalytic mechanisms with JHDMs. In addition, fumarate and succinate exert by-product negative inhibition to TETs and JHDMs, competing with α-ketoglutarate.

Overall, both methylation/demethylation and acetylation/deacetylation activities are modulated by molecules that play central roles in cellular metabolism.

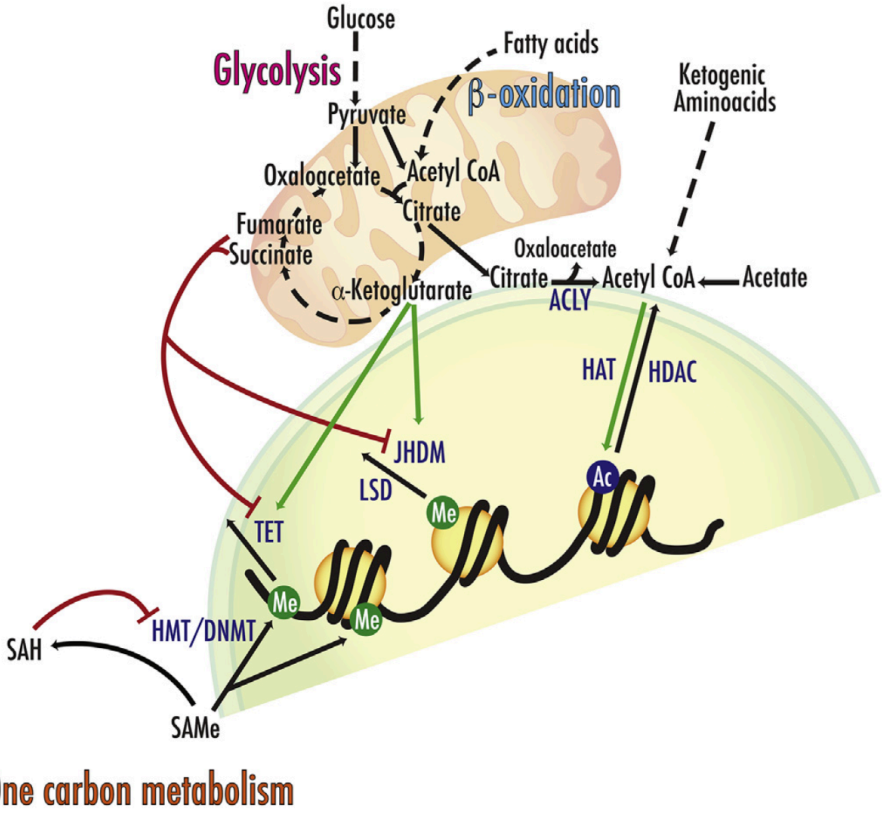

Figure 11: from Ferrari et al. (Ferrari et al. 2018).
Metabolic intermediates are substrates of chromatin modifying enzymes.

Obesity and epigenetics

Obesity and related metabolic complications are multi-faceted disorders and environment plays an important role in their onset. From this perspective, a link between obesity and epigenomic-based pathological mechanisms has been hypothesized. Several investigations are focusing on how nutritional effects during gestation are maintained in the following generation, as epigenetic memory of a former metabolic state. This phenomenon is also known as "transgenerational epigenetic inheritance" (Longo et al. 2017). At this regard, one of the most famous evidences is the "Dutch Hunger Winter famine" case study, that refers to the famine occurring in Netherlands from November, 1944 to May, 1945 (Lumey et al. 2007). By studying offspring of mothers exposed to famine, the association between exposure to famine during gestational period and higher body mass

indexes of female offspring at the age of 59 years has been established (Stein et al. 2007). In a follow-up study, females exposed to famine during early gestational period, i.e. periconceptional period, showed hypomethylation at *IGF2 (Insulin Growth Factor 2)* differentially-methylated regions, a gene important for growth, after nearly 60 years from the event. This study was the first to highlight that environmental conditions during human gestation are associated to epigenetic changes that are maintained later in life. Recently, epigenome-wide association studies (EWAS) lead to the identification of several epigenomic traits linked to obesity and metabolic disorders. For example, EWAS conducted in African American adult population identified numerous methylation variants associated with BMI and waist circumference (WC) (Demerath et al. 2015). The authors observed that over 100 biological pathways were enriched for methylation pattern associated to BMI and WC. In particular, they found pathways related to lipid and energy metabolism, immune function, adipocyte, neuronal and chondrocyte differentiation and development. To mention some of the genes, CPT1A (Carnitine Palmitoyl Transferase 1A, implicated in fatty acid β-oxidation), ABCG1 (ATP-Binding Cassette subfamily G member 1, implicated in macrophage cholesterol and phospholipid transport and lipid homeostasis) and HIF3A (Hypoxia Inducible Factor 3 subunit alpha) methylation loci were previously suggested to be associated to obesity. In fact, another study identified DNA methylation on *HIF3A* locus associated with BMI in adult population with European origin (Dick et al. 2014). This association was recorded both in whole blood DNA and in adipose tissue sample. Moreover, the authors suggested that increased BMI possibly caused increased *HIF3A* methylation.

Overall, the main challenges of this field of investigation are to validate epigenetic marks in blood circulating cells as early markers of the onset of metabolic diseases and to find environmental cues that alter gene expression and, ultimately, metabolism in order to envision new possible therapeutic strategies (Ferrari et al. 2018).

Histone deacetylases

One of the most intensely studied histone modifications is acetylation/deacetylation. Acetylation of ε-amino group of histone lysines, by neutralizing the positive charge, relaxes chromatin structure and increases the accessibility of transcription factors and coregulators to DNA consensus

sequences. Acetylated histone marks are binding sites for bromodomain proteins (readers), which often activate transcription (Haberland et al. 2009). The opposite reaction is catalysed by epigenomic modifiers histone deacetylases (HDACs). The removal of acetyl groups compacts chromatin, thereby repressing transcription. HDAC family comprises 18 proteins with highly conserved deacetylase domain, divided in four subclasses (Haberland et al. 2009).

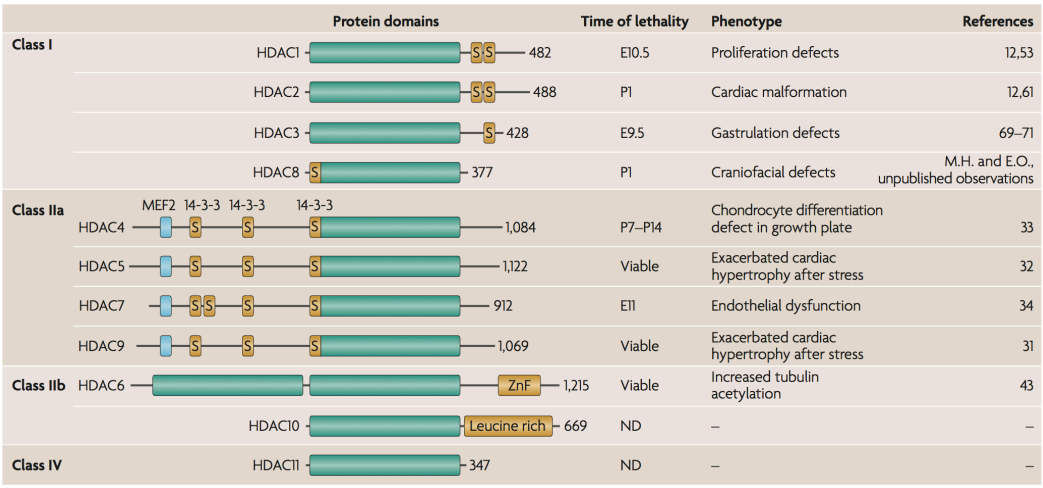

Figure 12: from Haberland et al. (Haberland et al. 2009).
Class I, class IIa and IIb and class IV histone deacetylases features.

Members of class I HDACs are HDAC1, HDAC2, HDAC3 and HDAC8. They are ubiquitarian and have nuclear localization.

Class II HDACs are further divided in IIa and IIb subclasses. Class IIa comprises HDAC4, 5, 7 and 9. Class IIa HDACs are cytoplasmic and, once phosphorylated, they shuttle in the nucleus where they act as adaptors for recruiting other coregulators for formation of protein complexes. Class IIb comprises HDAC6 and 10. HDAC6 exerts its activity on cytoplasmic proteins, such as tubulin and other cytoskeleton proteins, whereas HDAC10 function is not known.

Class III HDACs are also known as sirtuins and their activity is dependent on NAD^+/NADH ratio. Therefore, cell energetic state modulates sirtuins activity.

Finally, HDAC11 is the only protein constituting class IV HDACs and its activity is poorly understood.

Overall, HDACs function is highly specific for each isoform, as murine models with specific ablation of *Hdac* isoforms have shown (Haberland et al. 2009). Several studies showed the role of HDACs in the regulation of metabolism

(Ferrari et al. 2012). Our laboratory has previously demonstrated that HDAC7, 3 and 1, together with corepressors NCOR1/2 (*Ncor1*, nuclear receptor corepressor 1, and *Ncor2/Smrt*, silencing mediator of retinoic and thyroid receptors), regulated the expression of *Cyp7a1*, encoding for the protein that catalyzes the key-limiting step of bile acid synthesis from cholesterol in the liver (Mitro et al. 2007). In particular, HDAC7 played a pivotal role in these mechanisms. Mihaylova et al. (Mihaylova et al. 2011) showed that class II HDACs shuttle in the nucleus in response to glucagon in the liver. In the nucleus they mediate the induction of gluconeogenetic genes through, at least in part, deacetylation and activation of FOXO (Forkhead box) transcription factors. Furthermore, shRNA-mediated silencing of these HDACs reduced blood glucose levels in several models of obesity. Several studies demonstrated the involvement of HDACs in the regulation of metabolic gene program in skeletal muscle (Ferrari et al. 2012).

HDAC3 is a regulator of metabolism in several organs

HDAC3 is a member of class I HDACs. HDAC3 forms protein complexes with NCOR1 or NCOR2/SMRT (Sun et al. 2013). Watson et al. (Watson et al. 2012) showed the structure of HDAC3/SMRT-DAD (DAD: deacetylase activation domain) complex. HDAC3 protein structure is formed by eight-stranded parallel β-sheets surrounded by α-helices. A tyrosine adjacent to the active site tunnel is present only in this HDAC isoform, possibly providing substrate specificity. The SMRT-DAD interacts with HDAC3 N-terminal region. Moreover, the authors observed the presence of D-myo-inositol-1, 4,5,6-tetrakisphosphate (Ins(1,4,5,6)P_4 or IP_4) tightly bound in a highly basic pocket at the interface of HDAC3 and DAD. IP_4 appeared to be required for the formation of the complex, acting as "intermolecular glue" between two proteins. In fact, Both IP_4 and SMRT-DAD were required for HDAC3 enzymatic activity. Of note, IP_4 binding is general requirement for class I HDACs, with the exception of HDAC8. In addition, another group showed that Tyr298 was important for HDAC3 activity in the presence of SMART-DAD (Sun et al. 2013). However, by genetic *Hdac3* manipulation the authors showed that the deacetylase activity was dispensable for HDAC3-mediated gene repression. Rather, formation of NCOR/SMRT-HDAC3 complex was absolutely indispensable for HDAC3 genomic recruitment and transcriptional repression in the liver.

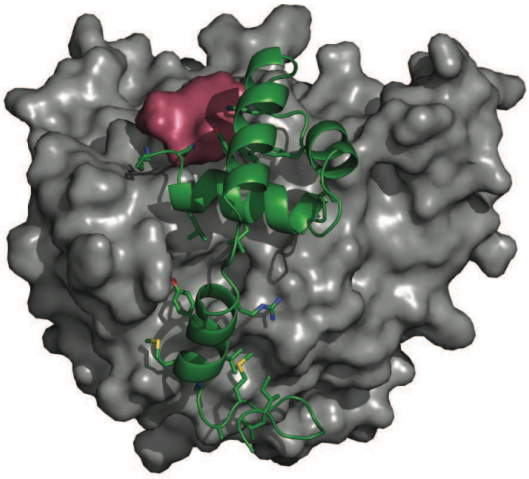

Figure 13: adapted from Watson et al. (Watson et al. 2012).
Interaction between SMRT-DAD (green), HDAC3 (grey) and IP_4 (dark red).

Several studies showed a clear role of HDAC3 in regulating lipid metabolism in different organs and tissues.

Hepatic *Hdac3* deletion caused de-repression of genes important for lipid and steroid metabolism, thus inducing increased lipid accumulation in the liver (Knutson et al. 2008). These effects were due to *Pparg* upregulation and consequent activation of PPARγ gene networks. A study from another group using a different liver-specific knock out mouse proposed a model whereby HDAC3 in the liver regulates metabolism in circadian fashion (Feng et al. 2012). In particular, these authors observed that HDAC3 was recruited to over 14.000 sites in the liver during the diurnal period (non-active phase in mice). However, HDAC3 recruitment dropped during the dark phase (active period in mice). Moreover, they observed decreased H3K9ac in the same sites and decreased RNA polymerase II recruitment at TSS of genes downstream HDAC3 binding within 10 kb, indicating that they were actively repressed. HDAC3 recruitment during light period overlapped with that of NCOR and REV-ERBα, a nuclear receptor key regulator of the circadian clock, indicating that REV-ERBα recruits HDAC3-NCOR complex in an oscillatory circadian mode. Liver-specific *Hdac3* knock out increased hepatic fat content, accompanied by increased *de novo* fatty acid synthesis. In a following study, the same group of research (Sun et al. 2012) proposed a model whereby during non-active and fasting period HDAC3 is recruited to the genome and represses the expression of genes involved in lipid synthesis and sequestration, thereby routing metabolic intermediates to gluconeogenesis. During the active and feeding period HDAC3 is not recruited to

the genome, leading to de-repression of lipogenic genes, thus inducing storage of energy in the form of lipids. Intriguingly, hepatic *Hdac3* knock out model displayed severe hepatosteatosis but insulin sensitivity was not impaired. In fact, expression of genes associated to lipid droplets, *Cidec* (Cell-death Inducing DFFA-like Effector c), *Plin2* (Perilipin 2), *Fitm1* (Fat-storage Inducing Transmembrane protein 1) and *G0S2* (G0/G1 switch 2), was upregulated upon *Hdac3* knock out, suggesting that lipid sequestration in droplets prevented both lipotoxicity and lipid-driven insulin resistance in the liver. In addition, hepatic *Ncor* knock out showed similar lipid and metabolic phenotype, indicating the importance of coregulators recruitment for HDAC3 activity in the liver (Sun et al. 2013).

HDAC3 is a key regulator of energy metabolism also in the heart (Montgomery et al. 2008). Cardiomyocyte-specific *Hdac3* deletion induced cardiac hypertrophy and fibrosis, resulting in cardiac dysfunction and in lethality by 16 weeks of age. Cardiac hypertrophy was caused by increased activation of PPARα target genes (*Pdk4*, *Acadl*, *Acadvl*, *Acox*, *Ucp2* and *Ucp3*), thus increasing fatty acid oxidation potential and mitochondrial uncoupling. In fact, the authors showed that in wild type mice PPARα and HDAC3 were co-recruited and repressed gene expression, while, upon *Hdac3* gene deletion, PPAR-responsive elements increased H3 acetylation and the expression of target genes was induced. In addition, another study adopted a murine model with *Hdac3* ablation in cardiac and skeletal muscle only after birth by means of Mck-Cre mice (muscle creatine kinase promoter) (Sun et al. 2011). This murine model did not show abnormalities when fed normal diet, but displayed severe cardiac contractile dysfunction and hypertrophic cardiomyopathy on HFD, leading to heart failure and lethality. Indeed, heart *Hdac3* knock out impaired fatty oxidation potential that resulted detrimental upon dietary lipid overload.

The same group has recently generated a mouse model with *Hdac3* ablation in skeletal muscle (HDAC3-SkMKO), by means of MLC-Cre mouse (myosin light chain 1f promoter) (Hong et al. 2016). HDAC3-SkMKO mice showed systemic insulin resistance and glucose intolerance. Moreover, glucose uptake was reduced upon exercise with concomitant increase in anaplerotic flux from amino acid metabolism. However, HDAC3-SkMKO mice showed enhanced endurance, possibly due to increased mitochondrial oxidative capacity. Indeed, HDAC3-SkMKO mice displayed increased fatty acid oxidation and reduced RER, indicating fuel preference switch towards fatty acids. This increased preference of

fatty acids as energy source was due to increased amino acid catabolism, particularly that related to branched chain amino acids (BCAAs), and increased anaplerosis via purine nucleotide cycle. By using different "omics" approaches, the authors demonstrated that REV-ERBα recruited HDAC3 during late afternoon to enhancers, thus inducing HDAC3-mediated repression of metabolic genes. In fact, metabolic genes repressed by HDAC3-REV-ERBα complex showed circadian rhythmicity in expression patterns. Overall, the authors proposed a model whereby in nocturnal animals the circadian clock dissociates HDAC3 from metabolic genes just before the start of light and fasting period, thus activating BCAA catabolism and anaplerosis, lipid oxidation and mitochondrial oxidative capacity and concurrently reducing glycolysis. This mechanism spares glucose for brain and red blood cells. Conversely, before night and feeding period, REV-ERB recruits HDAC3 to the genome, thus inducing glucose utilization in skeletal muscle.

Finally, the same authors showed results from generation of *Hdac3* knock out specifically in BAT (Emmett et al. 2017). Loss of *Hdac3* resulted in impaired thermogenic response upon cold exposure and mitochondrial dysfunction, leading to lethality upon cold. In fact, HDAC3 KO BAT displayed repression of genes important for oxidative phosphorylation, TCA cycle, energy and metabolic pathways, among which *Ucp1*. The authors observed upon *Hdac3* ablation reduced H3K27ac near repressed genes and increased H3K27ac peaks near upregulated genes. *De novo* motif analyses identified that HDAC3 coactivated ERRα, thus inducing the thermogenic program in BAT. Moreover, HDAC3 activated PGC1α (*Ppargc1a,* PPARγ Coactivator 1 a) both transcriptionally and via lysine deacetylation. Considering that PGC1α is indispensable for ERRα-driven gene expression, these data indicated that HDAC3 strengthened ERRα-driven gene expression also activating its partner PGC1α. By observing gene expression at thermoneutrality and at room temperature (RT), the authors concluded that BAT HDAC3 is required to maintain minimal basal expression of *Ucp1* and metabolic genes so that BAT thermogenesis is readily activated to maintain body temperature upon cold exposure.

Aim of the study

Recently obesity has been described as epidemic: it has been, in fact, estimated that over 50% of European people are overweight or obese. Obesity is often accompanied by a plethora of comorbidities such as insulin resistance and type II diabetes, metabolic syndrome, neurological dysfunctions and increased prevalence of cancer. This pathological condition is also considered one of the major risk factors for cardiovascular diseases. For these reasons, obesity has become an urgent and worrisome health problem. To face this important challenge, many researchers worldwide have focused their scientific interest in the study of the pathophysiology of adipose tissues. Adipose tissue is a complex organ and metabolic homeostasis is maintained by a physiologic interplay between different cellular actors: adipocytes, regulatory immune cells and others. This fine-tuned communication is altered as a consequence of diets enriched in fat, causing a low-grade inflammatory condition, defined "metaflammation", which results detrimental for whole body metabolism and health status. The discovery that it is possible to induce thermogenic capacity of adipose tissue opened a new era for scientific investigations in the metabolic field. Firstly, it is common knowledge that brown adipose tissue contributes to non-shivering thermogenesis, burning fatty acids and dissipating energy as heat. However, it has been described that specific environmental cues, i.e. cold, can induce thermogenesis even in white adipose tissue, a phenomenon called browning (Kajimura et al. 2015). Upon exposure to these stimuli, specific adipocytes, interspersed within WAT, acquire metabolic characteristics of brown fat cells (e.g., thermogenesis). The induction of browning in animal models of obesity reduced body weight and ameliorated whole body metabolic dysfunctions (Rosen & Spiegelman 2013). This discovery shed a new light to find new promising therapeutic strategies to fight obesity. How environment interferes with functions of metabolic organs has gained more and more attention. Epigenetic mechanisms lead to adapt genomic functions to changed environmental conditions. Epigenetic machinery takes advantages of enzymes and regulatory proteins that dynamically modulate chromatin architecture so that gene expression and cellular function can be rapidly and finely regulated in response of external stimuli. Moreover, epigenetic enzymes use as cofactors or substrates metabolic intermediates, thus metabolism and epigenetics may be reciprocally and simultaneously regulated (Ferrari et al. 2018). At this regard, a huge amount of scientific publications is focused on the role of different epigenomic modifiers in regulating whole body or tissue specific metabolism. One of the epigenomic modifiers' family intensely investigated includes histone

deacetylases (HDACs). HDACs catalyse the removal of acetyl groups from lysine residues of histone tails, thus leading to increased chromatin condensation and repression of gene transcription. Their activity is counterbalanced by histone acetyltransferases (HATs), which catalyse the opposite reaction and therefore induce chromatin relaxation and gene activation. HDACs are also recruited with coregulators of transcription as part of protein complexes that may also modulate proximity of regulatory genomic regions to genes. HDACs are divided in four classes according to their homology to yeast HDACs. Several groups demonstrated that HDACs regulate energy homeostasis and metabolism in several organs (Montgomery et al. 2008; Knutson et al. 2008; Sun et al. 2012; Sun et al. 2011; Clearance et al. 2016; Emmett et al. 2017; Ferrari et al. 2012). At this regard, our laboratory demonstrated that inhibition of class I HDACs strongly ameliorated metabolic phenotype in models of obesity (Galmozzi et al. 2013; A. Ferrari et al. 2017). Treatment with MS-275, class I HDAC specific inhibitor, caused reduction of body weight (Figure 14a) in diet-induced obese mice (DIO mice) and *db/db* mice (data not shown). Moreover, it has also been observed an amelioration of glucose clearance as measured by glucose tolerance test (Figure 14b). DIO mice treated with MS-275 were able to maintain higher levels of body temperature than vehicle-treated mice upon cold exposure (Figure 14c), suggesting higher thermogenesis.

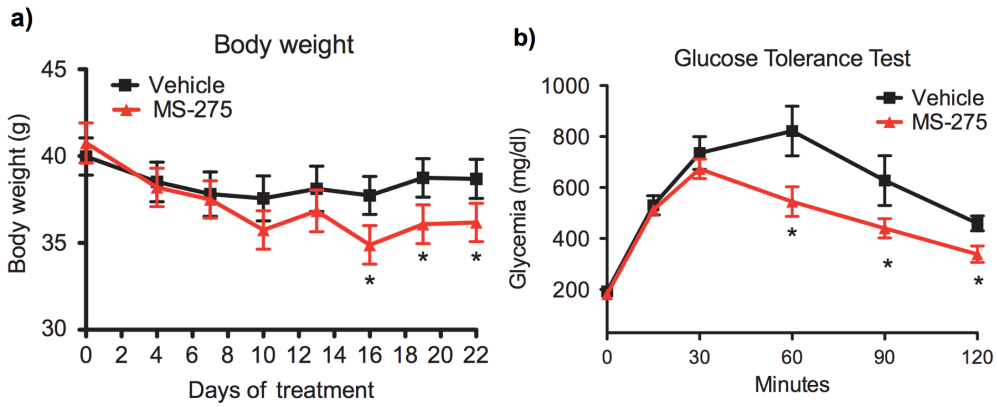

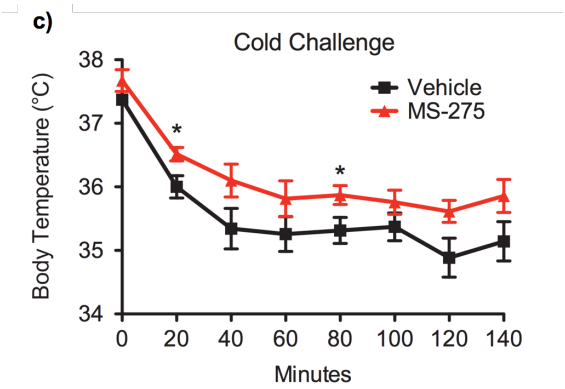

*Figure 14: a) Body weight measurements of DIO mice treated with vehicle or MS-275. b) Intraperitoneal glucose tolerance test (ip-GTT) of DIO mice treated with vehicle or MS-275. c) Cold challenge of DIO mice treated with vehicle or MS-275. *p<0.05.*

This was accompanied by a reduction of subcutaneous WAT mass (Figure 15a), adipocyte size (Figure 15b) and increased expression of genes for lipid catabolism (*Atgl, Cpt1b, Acadl*) (Figure 15c) and brown phenotype (*Ucp1, Adrb3, Cidea, Dio2, Ppara*) (Figure 15d), suggesting that MS-275 induced browning of white adipose tissue.

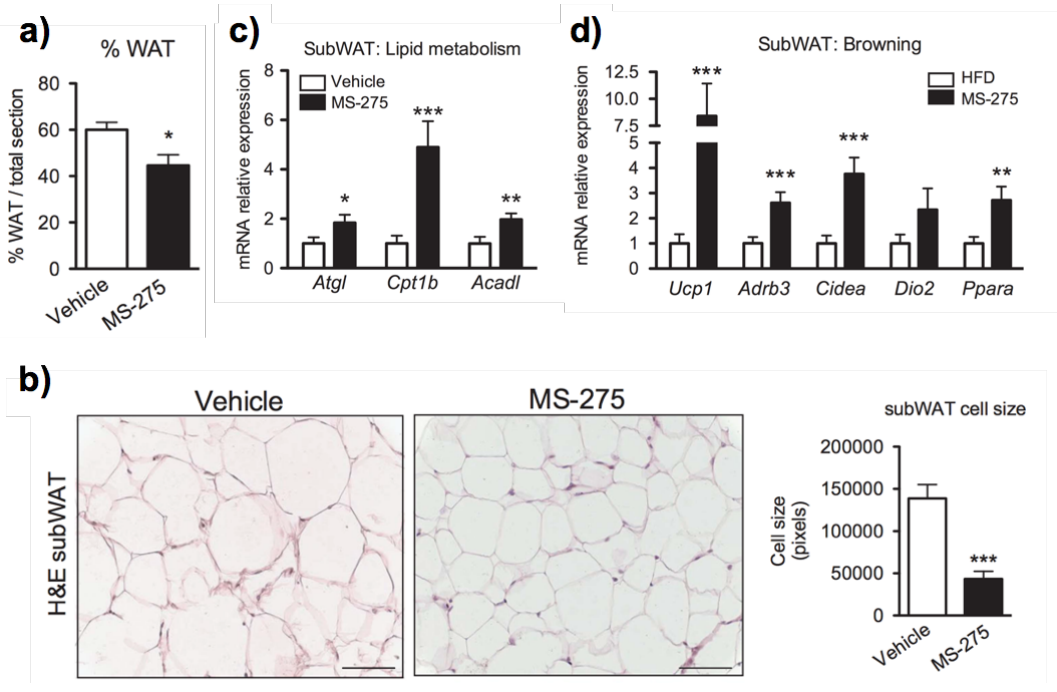

Figure 15: a) SubWAT weight of DIO mice treated with vehicle or MS-275. b) H&E staining of DIO mice SubWAT treated with vehicle or MS-275 and related calculation of SubWAT cell size. c) SubWAT expression of genes related to lipid metabolism of DIO

*mice treated with vehicle or MS-275. d) SubWAT expression of browning markers of DIO mice treated with vehicle or MS-275. *p<0.05; **p<0.01; ***p<0.001.*

Furthermore, another set of experiments demonstrated that only *Hdac3* silencing *in vitro* resembled the effects observed *in vivo* with MS-275 treatment, therefore suggesting HDAC3 as the major class I HDAC isoform involved in these mechanisms (Figure 16).

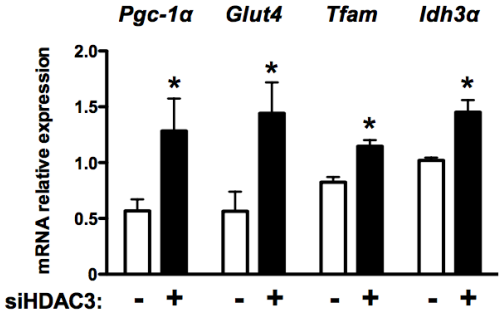

*Figure 16: silencing of C2C12 myoblasts showed Hdac3 silencing mimicked MS275 in vivo treatment. *p<0.05.*

Based on these results, the principal aim of my PhD project was to investigate the role of HDAC3 in adipose tissue pathophysiology. Our laboratory generated a mouse model with specific ablation of *Hdac3* in the adipose tissue (H3atKO mice). Briefly, by using this *in vivo* murine model, we discovered that *Hdac3* ablation induced rewiring of metabolism toward a futile cycle of fatty acids usage and re-synthesis, that sustained thermogenesis and browning. The rearrengement of WAT metabolic phenotype was associated with strong reprogram of gene expression with induced oxidative and mitochondrial gene program and activation of PPARγ- and PPARα-dependent regulatory networks. Moreover, we also conducted *in vitro* experiments by silencing *Hdac3* in C3/H10T1/2 cell line, which can be differentiated to adipocytes. *In vitro* results confirmed *in vivo* findings, establishing a solid tool to deeply investigate molecular mechanisms underlying *Hdac3* ablation. Thanks to this *in vitro* model, we demonstrated that carbons from fatty acids are used as source for *de novo* lipogenesis. Moreover, the flux of acetyl groups from mitochondria to cytosol and nucleus, controlled by ACLY, resulted to be fundamental in these mechanisms. We then exposed H3atKO mice to high fat feeding. Surprisingly, we did not observe any difference between H3atKO and Floxed (i.e., WT) mice in terms of body weight gain, metabolic and molecular features. To explain this unexpected result, we focused on regulation of lipid metabolism exerted by high fat diet. As a matter of fact,

high fat feeding not only differently regulated PPARs expression and activity but also lipogenesis via reduced *ChREBPβ* expression. The disruption of the equilibrium between metabolism and gene regulation of H3atKO blunted the effect of *Hdac3* ablation. We also explored immunophenotyping of visceral WAT in H3atKO mice. FACS analysis demonstrated increased number of monocytes, neutrophils and macrophages in H3atKO mice. Furthermore, we also observed increased percentage of M1 macrophagic subset. Interestingly, when we exposed H3atKO mice to a shorter period of high fat feeding, M1 macrophage levels were no further exacerbated by diet exposure. This preliminary observation led us to hypothesize that *Hdac3* ablation not only strongly impacted metabolism but also immune functionality of WAT. Finally, we explored the possibility that HDAC3 is involved in the physiological induction of browning upon cold exposure. *In vivo* findings demonstrated analogies in terms of gene expression between *Hdac3* ablation and exposure to cold in inguinal WAT. These evidences support the idea that HDAC3 can be a novel regulator of adipocyte response to cold. This hypothesis has been, at least in part, confirmed by other investigators (Liao et al. 2018; Yuliana et al. 2018). In conclusion, the results presented in the following thesis unravelled novel mechanisms of regulation of adipocyte functionality and plasticity. In perspective, possible molecules able to unlock these mechanisms will constitute a promising therapeutic approach against obesity and related disorders.

Materials and Methods

In vivo experiments

Generation of *Hdac3* adipose specific knock out mouse model (H3atKO)

All experiments including animal models were conducted following European regulations EU Directive 86/609/-CEE and 2010/63/EU and Italian regulations DL 116/1992 and 26/2014. Animal protocols used in this study were approved by Italian Health Ministry (protocols 06/2012 and 898/2015-PR).
Hdac3 Floxed mice ($Hdac3^{fl/fl}$) in C57Bl/6J background, kindly provided by Dr. Scott W. Hiebert Laboratory, Vanderbilt University, were crossed with B6; FVB-Tg (Adipoq-Cre)1Evdr/J mice (The Jackson Laboratory) to obtain *Hdac3* adipose tissues specific deletion. To identify H3atKO and Floxed mice, tail or ear biopsies were collected and DNA was extracted with NucleoSpin Tissue kit (Macherey Nagel). PCR with specific primers was performed on DNA extracted.
Floxed and H3atKO mice at 8 weeks of age were fed standard diet (4rf21 GLP certificate, Mucedola), low fat diet (LFD, D12450H, Research Diet) and high fat diet (HFD, D12451, Research Diet) for 24 weeks. Body weight was monitored before, during and at the end of the diet experiment. At the end of the diet exposure, mice were euthanized and blood samples and tissues were collected from individual animals. Specifically, inguinal subcutaneous (IngWAT), brown adipose tissue (BAT) and epididymal visceral (EpiWat) white adipose tissue were collected and snap frozen for following experiments. Plasma triglycerides, NEFA and cholesterol levels were measured using commercial kits (respectively Plasma Triglycerides Kit -Sentinel, NEFA kit -Wako Chemicals and Plasma Cholesterol Kit -Sentinel).

Cold challenge test

Basal rectal temperature was measured at room temperature (RT) at the beginning of the experiment. Then, mice were housed at 4° C and rectal temperature was measured every 20 min. LFD fed mice were exposed to 4° C up to 24 h, whereas HFD fed mice underwent cold challenge only for 100 min to avoid possible hypothermia. To collect IngWAT at 4° C, LFD mice were housed at 4°C for 24 hours. After this period mice were euthanized and IngWAT was collected at 4° C from individual animals.

Intraperitoneal glucose tolerance test (ip-GTT)

HFD fed mice were fasted for 16 hours. Basal glycaemia was measured at the beginning of the experiment using OneTouch Glucometer. Then 1 g/kg glucose was intraperitoneally injected and glycaemia was measured 30, 60, 90, 120, 150 and 180 min after injection.

Immunophenotyping

Immunophenotyping experiments were performed in collaboration with Prof. Catapano and Prof. Norata Laboratory of Lipoproteins, Immunity and Atherosclerosis, Università degli Studi di Milano. Floxed and H3atKO mice at 8 weeks of age were fed LFD and HFD for 4 weeks. Body weight was monitored before, during and at the end of the diet experiment. At the end of the diet exposure, mice were euthanized and blood and tissues were collected. Fresh collected blood was stained after lysis of red blood cells with ACK solution ($KHCO_3$ 10mM, NH_4Cl 150 mM, EDTA 0.1 mM) for 10 minutes at RT. Fresh visceral adipose tissues (ViscWAT) were placed on ice in a 6 well plate and cut in small pieces in 2 mL of PBS 5% BSA solution, then collagenase (200 mg/ml final concentration, NB4 standard grade, Serva) and $CaCl_2$ (5 mM final concentration) were added and samples were incubated at 37°C for 40 minutes under agitation. Samples were then top up with MACS (PBS, 2% FCS, 2 mM EDTA) and filtered on a sterile bandage and subsequently on a 100 µm and 70 µm cells strainers. After lysis of red blood cells with ACK for 5 minutes on ice, samples were washed, spun and resuspended in antibody mix. All flow cytometry antibodies were used at 1:100 dilutions unless otherwise specified, optimal antibody concentrations for staining were calculated based on manufacturer instructions. For immunophenotyping, cell suspension containing $1x10^6$ cells or 50 µL of blood were acquired with or Novocyte 3000 (ACEA Biosciences). The following anti-mouse antibodies were used: CD4 BV786, CD8 ev655, CD44 PE, CD25 PECy7, Ly6C ef450, Ly6G FITC, CD11b Af700, CX3CR1 PerCP Cy5.5, CD115 APC, CD62L ev605, CD45 FITC, CD44 ef450, FoxP3 APC, F4/80 PE, CD11c APC, CD206 PECy7, MHCII BV650.

Histology

Tissues were submerged immediately after collection in Carnoy fixation solution (60% EtOH 100%, 30% chloroform, 10% glacial acetic acid) and fixed for 24 hours at 4°C. Tissue were then stored in 100% EtOH at 4°C. Before starting

histological analysis, tissues were paraffin embedded and 8 μm sections were obtained using microtome.

Haematoxylin and eosin staining

8 μm sections were deparaffinized and stained with haematoxylin and eosin (H&E). 20x magnification images were taken and IngWAT adipocytes cell size was quantified using Adobe Photoshop CS6 (Adobe System Inc., San Jose, CA, USA).

Immunohistochemistry

8 μm IngWAT sections were deparaffinized and then incubated with 0,05 M NH_4Cl for 30 min to retrieve antigens. 20 min incubation with 1% H_2O_2 was performed to block endogenous peroxidase activity, then 1% BSA in 0,1% Triton X100 blocking buffer was applied for 1 hour. Anti-UCP1 (Abcam) antibody was applied at 1:300 dilution overnight at 4° C. Sections were then incubated with biotinylated secondary antibody at 1:3000 dilution. Presence of UCP1 was then revealed by DAB reaction.

Immunofluorescence

8 μm IngWAT sections were deparaffinized and then incubated with 1 N HCl for 10 min at 4°C, 2 N HCl for 10 min RT and 20 min at 37 °C to retrieve antigens. 5% BSA in 0,1% Triton X100 blocking buffer was applied for 1 hour. Anti-ACLY (Abcam) antibody was applied at 1:200 dilution overnight at 4°C. Sections were then incubated with AlexaFluor 488 secondary antibody at 1:1000 dilution to reveal presence of ACLY (green signal). Nuclei were then stained using Hoechst solution 1:1000 for 30 minutes (blue signal). 40X magnification images were taken and nuclei positive for green signal were counted and divided by the total number of nuclei for each section as indication of ACLY nuclear localization (n:3 H3atKO mice vs Floxed mice).

Cell cultures

C3H/10T1/2 cells were purchased from ATCC (CCL-226). For culturing and differentiate cells to adipocytes following media were used:

- Culturing medium: Dulbecco's Modified Eagle's Medium (DMEM, Sigma Aldrich) with 10% inactivated Foetal Bovine Serum (FBS, Euroclone), 1%

glutamine (Life Technologies), 1% penicillin/streptomycin (Pen/Strep, Life Technologies)

- Differentiation medium: culturing medium supplemented with 5 µg/ml insulin (Sigma Aldrich), 0,5 mM 3-isobutyl-1-methyl-xanthine (IBMX, Sigma Aldrich), 5 µM rosiglitazone (Cayman Chemicals) and 2 µg/ml dexamethasone (Sigma Aldrich)
- Maintenance medium: culturing medium supplemented with 5 µg/ml insulin (Sigma Aldrich)

To induce differentiation to mature adipocytes, cells were seeded at 70000 cells/ml concentration and maintained confluent for 24 hours (day 0). Culturing medium was then replaced with differentiation medium for 72 hours (day 3). At day 3 differentiation medium was replaced with maintenance medium, which was renewed every other day until day 9.

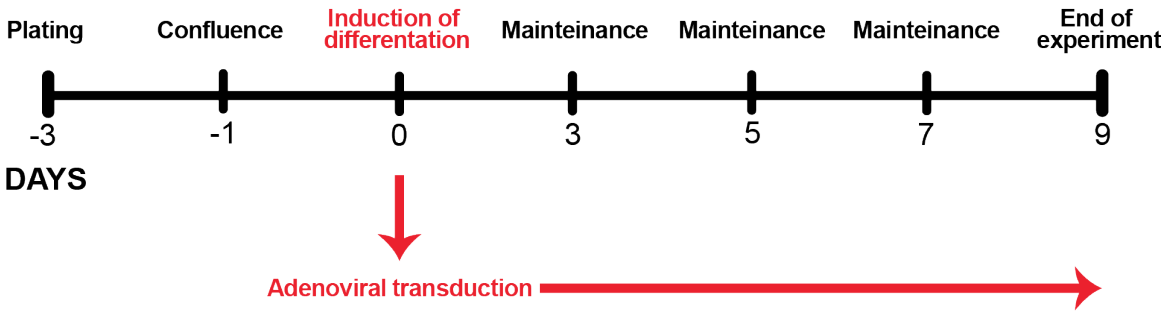

Figure 17: treatment scheme of C3H/10T1/2 cell line.

To inhibit PPARα, DMSO (vehicle) or 10 µM GW6471 were added at day 0 and maintained until day 9.

In vitro knock down by RNAi

To knock down *Hdac3*, at day 0 100 MOI Scramble or ShHdac3 adenoviral vectors (Vector BioLabs) were added to differentiation medium. To evaluate lipolysis, glycerol content in cell medium was measured at day 9 with Triglyceride Dosage Kit (Sentinel) and normalized to protein content.
To knock down *Acly* and *Acss2,* at day 0 50 MOI ShAcly or ShAcss2 adenoviral vectors (Vector BioLabs) were added to differentiation medium.
To simultaneously knock down *Hdac3* and *Acly* or *Hdac3* and *Acss2,* at day 0 50 MOI ShAcly or ShAcss2 + 100 MOI ShHdac3 adenoviruses were added to

differentiation medium, using 150 MOI Scramble treated cells as negative control.

^{13}C tracing experiments

At day 9 C3H/10T1/2 Scramble or ShHdac3 treated cells were incubated with 100 μM [U-^{13}C] palmitate (Sigma Aldrich) and 1 mM carnitine (Sigma Aldrich) for 30 minutes at 37 °C. Cells were then washed with cold PBS and lysed with MeOH 100 % (LC-MS grade). Extracts were analyzed by electrospray ionization flow injection analysis tandem mass spectrometry (FIA-MS/MS). Each isotopomer was resolved by m/z ratios and quantitated by Mass Distribution Vector (MDV). % MDV was then normalized to protein content.

Oil Red O staining

Oil Red O (ORO) staining was performed to quantify lipid content in C3H/10T1/2 at day 9. C3H/10T1/2 cells were seeded in 12-well plates and differentiated as described for 9 days. At the end of differentiation (day 9) cell were fixed with 100% formaldehyde for at least 1 hour and then washed with H_2O. Fixed cells were incubated with 1 ml 60% isopropanol for 2-5 minutes. ORO solution was applied for 10 minutes. Stained cells were then washed 3 times with 1 ml H_2O and images were taken. For quantification ORO was eluted incubating with 1,5 ml 100% isopropanol for 10 minutes. Staining absorbance was then measured at 500 nm wavelength, 0,5 second of reading. Quantification of ORO was normalized to protein content.

Chromatin-Immunoprecipitation qPCR (ChIP-qPCR)

IngWAT or Scramble and ShHdac3 treated C3H/10T1/2 cells at day 9 were cross-linked for 10 min with 1% formaldehyde, which was stopped by addition of 125 mM glycine solution. Cells and tissue were lysed and chromatin was sheared by sonication (SLPe sonicator, Branson). H3K27ac antibody (1 μg, ab4729, Abcam) was pre-incubated with 20 μl G protein DynaBeads (Life Technologies) for 1 h RT, to allow the binding of the antibody to Dynabeads. Sheared chromatin was incubated with Dynabeads solution overnight at 4 °C. After reversing crosslinking by incubating overnight at 65 °C, DNA was cleaned on QIAquick gel extraction kit columns (QIAGEN). Inputs and

immunoprecipitated samples were analyzed by qRT-PCR using gene-specific primers. Data are expressed as 10% of input.

RNA extraction and gene expression

For gene expression analysis, C3H/10T1/2 cells at day 9 or adipose tissues were lysed with TRIzol (Invitrogen) or Qiazol Reagent (Qiagen). Cell cultures were alternatively lysed with RA1 reagent (Macherey Nagel) supplemented with β-mercaptoEtOH. RNA from cell cultures extracts was purified with commercial kits (NucleoSpin RNA II, Macherey Nagel). RNA from adipose tissues was purified with commercial kits (RNeasy Lipid Tissue Mini kit, Qiagen). Total RNA was quantified by Nanodrop (Thermo Scientific). Specific mRNA was amplified with specific primers and quantitated by Real Time PCR, using SYBR Green (iScript One-Step qRT-PCR kit for SYBR Green, Bio-Rad Laboratories) or specific TaqMan probes (iScript One-Step qRT-PCR kit for Probes, Bio-Rad Laboratories) on CFX384 instrument (Bio-Rad Laboratories). Each specific mRNA was normalized to 36b4 RNA. Specific primers and probes were designed using IDT software and synthesized by Eurofins MWG Operon. Primers and probes for *Pparg* and *Adrb3* were purchased from Applied Biosystems, Thermo Fisher Scientific. Gene expression data of C3H/10T/1/2 cells treated with Scramble or ShHdac3 were obtained from four independent experiments (n= 4).

RNA-sequencing

RNA-sequencing (RNA-Seq) analysis of subcutaneous IngWAT was performed in collaboration with Dr. Béatrice Desvergne Laboratory, Centre Intégratif de Génomique, Université de Lausanne. Analysis was obtained from three pooled samples, each of whom contained 500 ng of total RNA from 2-3 individual animals. RNA-Seq libraries were prepared with PolyA selection using 500 ng of total RNA and the Illumina TruSeq Stranded RNA reagents (Illumina; San Diego, CA, USA) on a Sciclone liquid handling robot (PerkinElmer; Waltham, MA, USA) using a PerkinElmer developed automated script. Cluster generation was performed with the resulting libraries using the Illumina TruSeq SR Cluster Kit v3 reagents and sequenced on the Illumina HiSeq 2500 using TruSeq SBS Kit v3 reagents. Sequencing data were processed using the Illumina Pipeline Casava 1.82. Purity-filtered reads were adapted and quality trimmed with Cutadapt (v. 1.3, and filtered for low complexity with seq_crumbs (v. 0.1.8). Reads were

aligned against Mus musculus (version GRCm38) genome using STAR (v. 2.4.2a). The number of read counts per gene locus was summarized with htseq-count (v. 0.6.1) using Mus musculus (Ensembl v. GRCm38.82) gene annotation. Statistical analysis was performed for genes in R (R version 3.2.3). Genes with low counts were filtered out according to the rule of 1 count per million (cpm) in at least 1 sample. Library sizes were scaled using TMM normalization (EdgeR package version 3.12.1), and log-transformed with limma voom function (Limma package version 3.26.9). Differential expression was computed with limma. We used DAVID to highlight the biological functions enriched in differentially expressed genes. The annotated terms were grouped according to the degree of their co-association genes with the functional annotation clustering feature. The Group Enrichment Score, namely the geometric mean (in -log scale) of member's p-values in a corresponding annotation cluster, is used to rank their biological significance.

Protein analysis

Reagents and buffers

- SDS Sample Buffer 2x: 100 mM TrisHCl pH 6.8, 20% glycerol, 4 % SDS, 100 mM dithiothreitol, 0,002% BBF, protease inhibitor 1X (Sigma Aldrich)
- Blocking buffer: 5% non-fat milk in TBS 1X + 0,1 % Tween-20
- Washing buffer: TBS 1X + 0,1 % Tween-20
- Antibody dilution buffer: TBS 1X + 0,1 % Tween-20
- Secondary antibodies: horse radish peroxidase-conjugated goat anti-mouse (Sigma-Aldrich) or horse radish peroxidase-conjugated goat anti-rabbit (Cell Signaling)

C3H/10T1/2 at day 9 and adipose tissues (IngWAT, EpiWAT and BAT) were disrupted with SDS SampleBuffer 2x on Tissue Lyser (Qiagen) and suitable beads. After centrifugation, appropriate amount of samples was incubated at 95°C for 5 min and immediately put on ice. Samples were separated on SDS-PAGE and then electro-transferred to nitrocellulose membranes. Proper transfer of proteins on nitrocellulose membranes was checked by Ponceau staining. Blocking buffer was then added to membranes for 1 hours RT with gentle agitation. Primary antibodies were then added at proper dilutions overnight at 4°C with

gentle agitation. Membranes where then washed with washing buffer and incubated with secondary antibodies at proper dilutions for 1 hour RT with gentle agitation. Detection of proteins was performed with ECL Chemiluminescence (Pierce). Quantification of proteic bands on films was performed using ImageJ software and normalized to loading control proteins.

Analysis of metabolome by mass spectrometry

Subcutaneous inguinal and visceral epididymal fat were disrupted with Tissue Lyser (Qiagen), after addition of MeOH and suitable beads. For each sample an aliquot of methanolic extracts was used to quantify acylcarnitines and metabolites. This aliquot was subjected to analysis in the positive ion mode by electrospray ionization flow injection analysis, using O-Propionyl-L-carnitine-HCl-D3,C3 as internal standard. Another aliquot of methanolic extracts was used to quantify total fatty acids: after addition of heneicosanoic acid (C21:0) and ^{13}C-linoleic acid (Sigma Aldrich), as internal standards, it was subjected to acidic hydrolysis and processed for quantification. For acylcarnitines and fatty acid analysis API-4000 triple quadrupole mass spectrometer (AbSciex) coupled with HPLC system (Agilent) and CTC PAL HTS autosampler (PAL System) were used. Metabolites level was then normalized on protein content.

Statistical analyses

Statistical analyses were performed using the unpaired two- tailed Student's t-test, one way ANOVA or two way ANOVA, with Tukey's as post hoc test, with GraphPad PRISM (San Diego, CA, USA).

Results

Adipose tissue - specific *Hdac3* knock out promotes browning

Recently it has been reported that HDACs regulate metabolism and energy homeostasis in different tissues. We have previously demonstrated that inhibition of class I HDACs reduced body weight and ameliorated glucose tolerance in obese mice. Class I HDAC inhibitor, MS-275, induced browning of white adipose tissue. Moreover, silencing experiments suggested HDAC3 as a key player in mechanisms exerted by MS-275. For these reasons, we generated a murine model with *Hdac3* adipose ablation (H3atKO mice) by means of Cre-LoxP technology. We chose Adipoq-Cre mice to obtain adipose-specific knock out. H3atKO mice and Floxed littermates (controls) were fed low fat diet (LFD) for 24 weeks. Western blot analysis confirmed *Hdac3* knock out in adipose tissues (Figure 18).

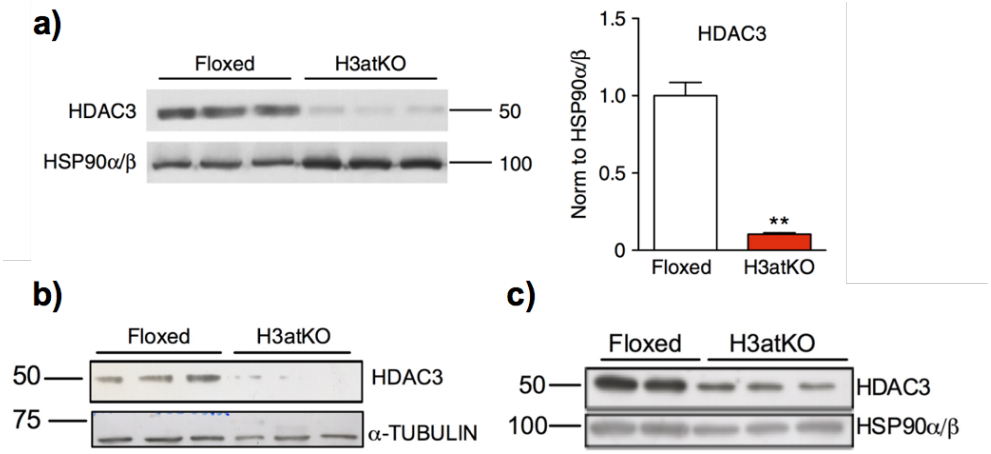

*Figure 18: western blotting of HDAC3, showing deletion of Hdac3 in IngWAT and related quantification (a), EpiWAT (b) and BAT (c) in H3atKO vs Floxed mice. Statistical analysis: Student's t test; **p<0.01 vs Floxed mice.*

H3atKO mice showed no differences in terms of body weight gain (Figure 19a). However, H3atKO mice displayed reduced visceral EpiWAT (Figure 19c) and a mild reduction of subcutaneous inguinal IngWAT (Figure 19b).

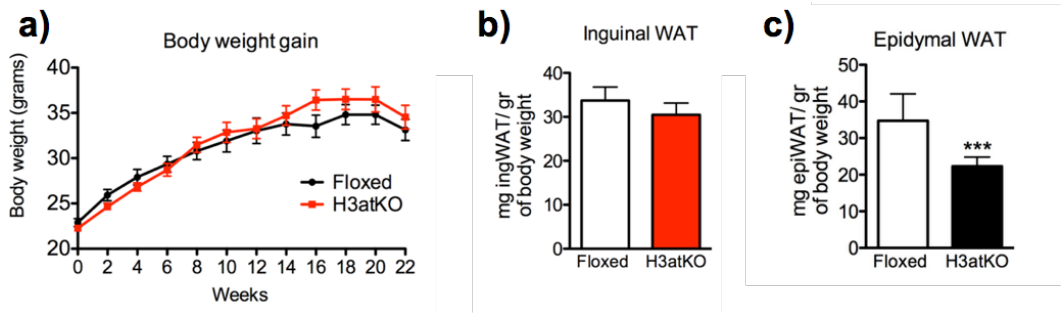

*Figure 19: a) Body weight gain of Floxed and H3atKO mice. b) Subcutaneous IngWAT weight of Floxed and H3atKO mice. c) Epididymal WAT weight of Floxed and H3atKO mice. Student's t test; ***p<0.001 vs Floxed mice.*

Most importantly, IngWAT of H3atKO mice appeared reddish, suggesting higher number of mitochondria (Figure 20a). H&E staining revealed increased number of multilocular adipocytes (Figure 20b-c), typical of brown adipose tissue, with no reduction of adipocyte size (Figure 20d). IHC analysis demonstrated increased UCP1 staining in IngWAT of H3atKO, which corresponds to increased UCP1 expression (Figure 20e), thus suggesting higher thermogenic capacity of H3atKO mice. This data was, in fact, paralleled by cold challenge test which showed increased capacity of H3atKO mice to maintain body temperature during 24 hours of exposure to 4°C (Figure 20f).

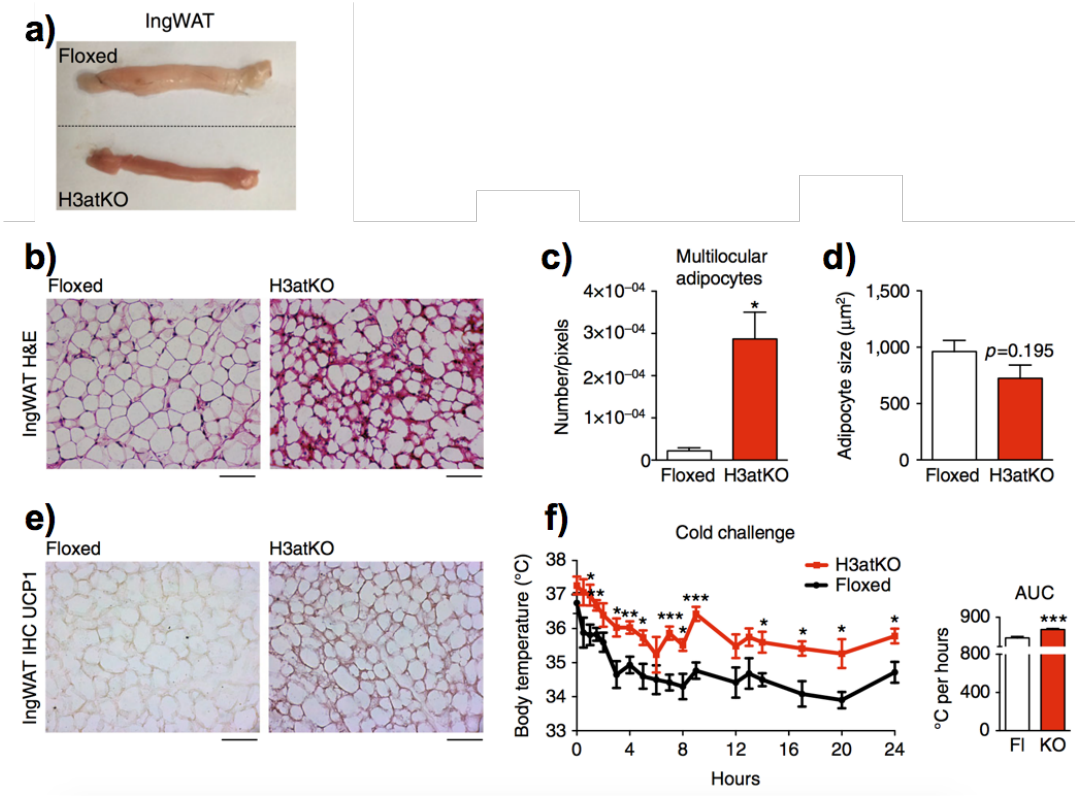

*Figure 20: a) IngWAT of Floxed and H3atKO mice. b) IngWAT H&E staining of Floxed vs H3atKO mice. Scale bar is 100 µm. c) Number of multilocular adipocytes in IngWAT of Floxed vs H3atKO mice. d) Adipocyte size quantification of Floxed vs H3atKO mice. e) IHC staining of UCP1 in IngWAT of Floxed vs H3atKO mice. Scale bar is 100 µm. f) Body temperature measurements of Floxed vs H3atKO mice exposed to 4°C for 24 h and related area under curve (AUC). Student's t test; *p<0.05; **p<0.01; ***p<0.001 vs Floxed mice.*

Regarding plasma lipids, we detected reduced levels of triglycerides (Figure 21a), non-esterified fatty acids (NEFA) (Figure 21b), with no difference in cholesterol (Figure 21c). Taken together, these data clearly showed induction of browning in IngWAT upon *Hdac3* ablation.

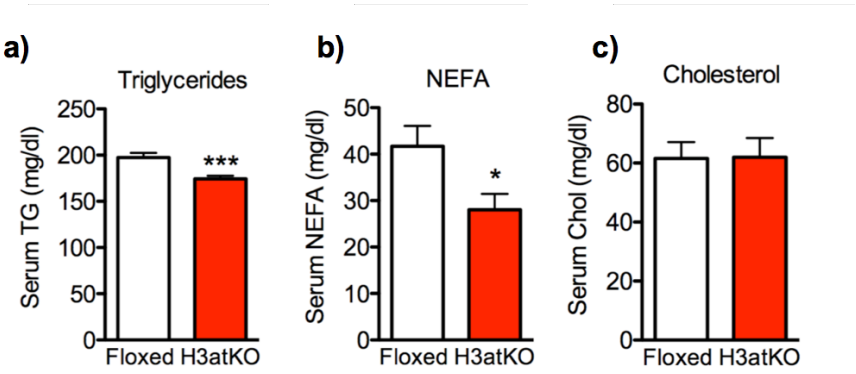

*Figure 21: levels of plasma lipids in Floxed vs H3atKO mice, in particular triglycerides (a), NEFA (b) and cholesterol (c). Student's t test; *p<0.05; ***p<0.001 vs Floxed mice.*

Hdac3 ablation reprograms gene expression in white adipose tissue

Considering that HDAC3 is an epigenomic regulator of gene expression, we decided to perform RNA-Sequencing analysis in IngWAT in collaboration with Dr. Béatrice Desvergne Laboratory, University of Lausanne. To this end, we analysized transcriptome in H3atKO and Floxed mice fed standard diet. We found 2246 downregulated and 1429 upregulated genes, indicating that *Hdac3* knock out did not increase globally gene expression (Figure 22a-b). Moreover, upregulated genes belonged to functional annotations related to mitochondria, fatty acid metabolism, respiratory chain and oxidoreductase activity, suggesting that *Hdac3* ablation induced lipid and oxidative gene program in IngWAT.

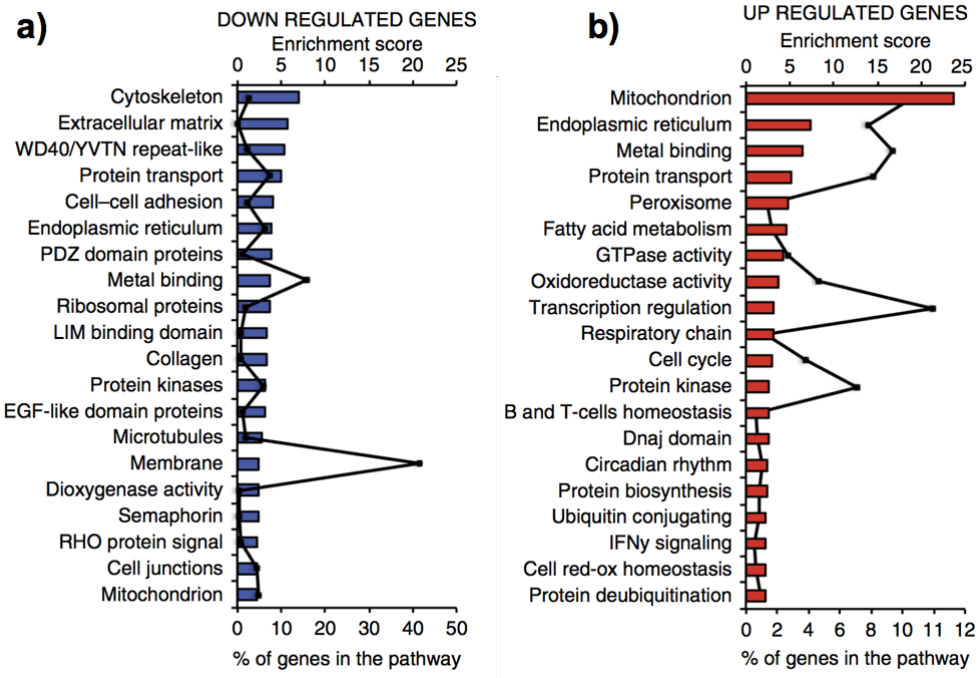

Figure 22: RNA-Seq analysis of Floxed and H3atKO IngWAT. a) Downregulated genes. b) Upregulated genes.

Therefore, to confirm these data we performed qPCR in H3atKO and Floxed mice fed LFD for 24 weeks IngWAT. We detected increased expression of genes important for adipocyte functionality (*Pparg, Fabp4, Adipoq, Glut4, Plin*) (Figure 23a) and TCA cycle and oxidative metabolism (*Idh3a, Bckdhb, Cox7a1, Ppargc1-a*) (Figure 23b). Furthermore, we found strongly increased expression of browning genes (*Ucp1, Dio2, Ppara, Prdm16, Adrb3, Vegfa*) (Figure 23c).

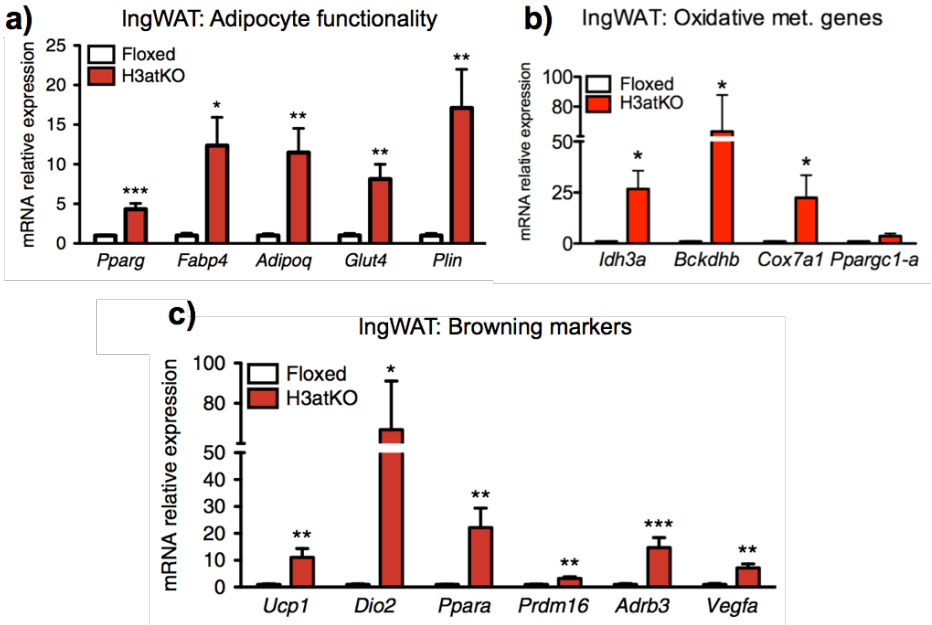

*Figure 23: gene expression analysis by qPCR in Floxed vs H3atKO IngWAT. a) Adipocyte functionality and differentiation genes. b) Genes related to oxidative metabolism. c) Browning markers. Student's t test; *p<0.05; **p<0.01; ***p<0.001 vs Floxed mice.*

These data suggested that *Hdac3* knock out reprogrammed gene expression toward lipid and oxidative metabolism. With respect to visceral EpiWAT, we found similar results upon *Hdac3* knock out, though in a smaller degree. In fact, there was no difference in terms of histology and number of multilocular adipocytes, but increased expression of adipocyte markers, browning and oxidative metabolism genes was observed also in EpiWAT.

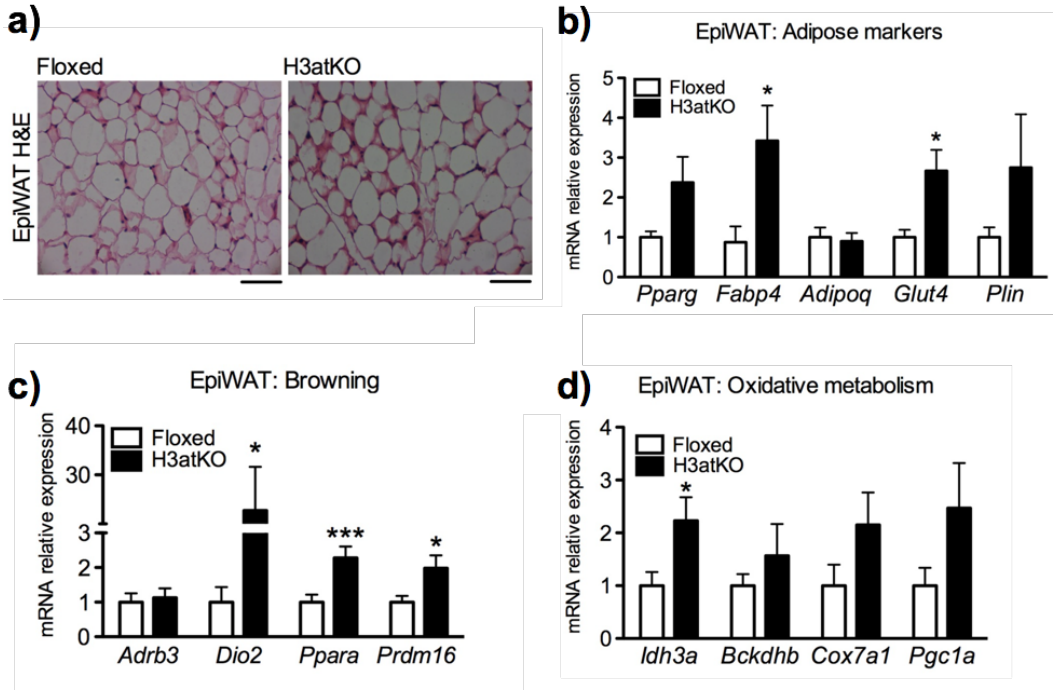

*Figure 24: a) EpiWAT H&E staining of Floxed and H3atKO mice. Scale bar is 100 µm. b, c, d) Gene expression of adipose markers (a), browning markers (b) and oxidative metabolism genes (d) in EpiWAT of Floxed and H3atKO mice. Student's t test; *p<0.05; ***p<0.001 vs Floxed mice.*

Hdac3 adipose knock out rewires metabolism

Transcriptome analysis revealed that *Hdac3* knock out induced gene program linked to lipid and oxidative metabolism. Therefore, we analysed metabolites level in IngWAT. As indicated by heatmap of metabolites (Figure 25), H3atKO mice displayed metabolic remodelling with metabolite levels globally reduced versus Floxed mice.

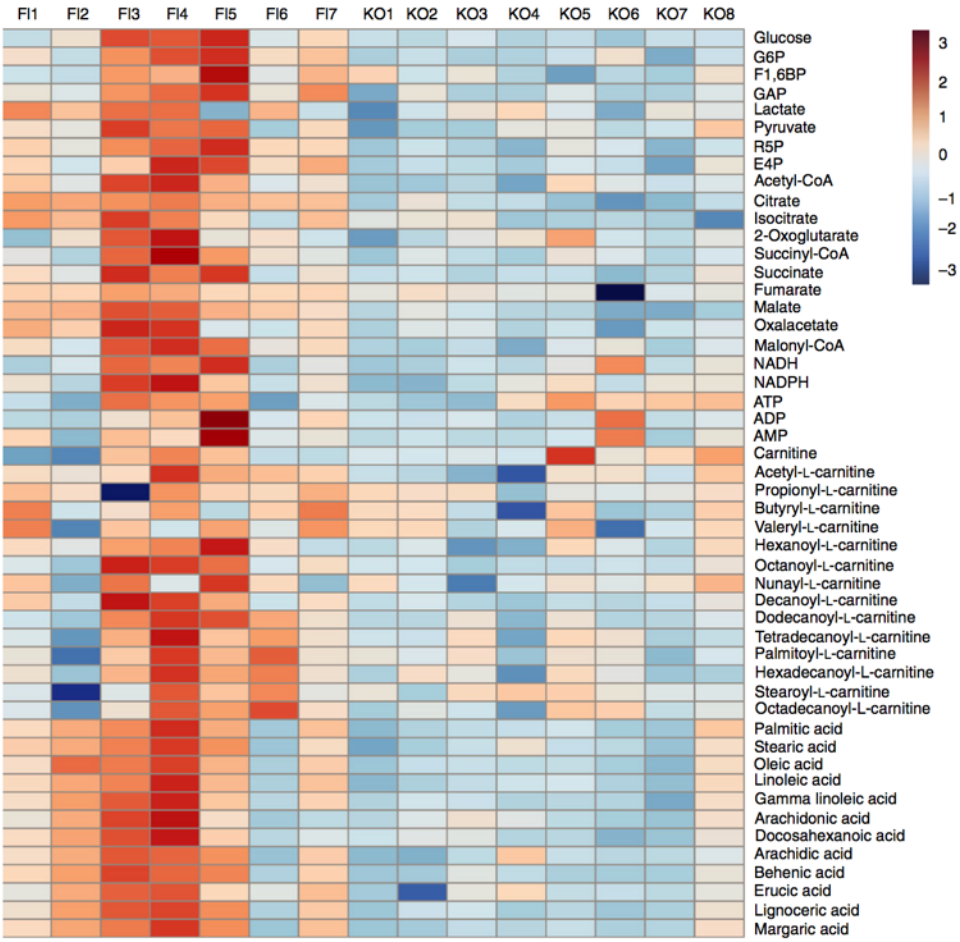

Figure 25: heatmap of metabolite levels in IngWAT of Floxed and H3atKO mice.

Volcano plot showed citrate as the most reduced metabolite upon *Hdac3* ablation (Figure 26a). In fact, we detected a strong reduction of citrate levels, along with that of acetyl-CoA (Figure 26b). The striking reduction of citrate prompted us to investigate more in depth citrate synthesis in H3atKO mice. As a matter of fact, we found increased expression of *Cs* (*citrate synthase*), suggesting higher citrate condensation, paralleled by increased expression of *Slc25a1*, which exports citrate out of mitochondrion, and *Acly*, which catalyzes the enzymatic conversion of citrate to citosolic oxaloacetate and acetyl-CoA (Figure 26c). These data suggested increased utilization of citrate in IngWAT of H3atKO mice.

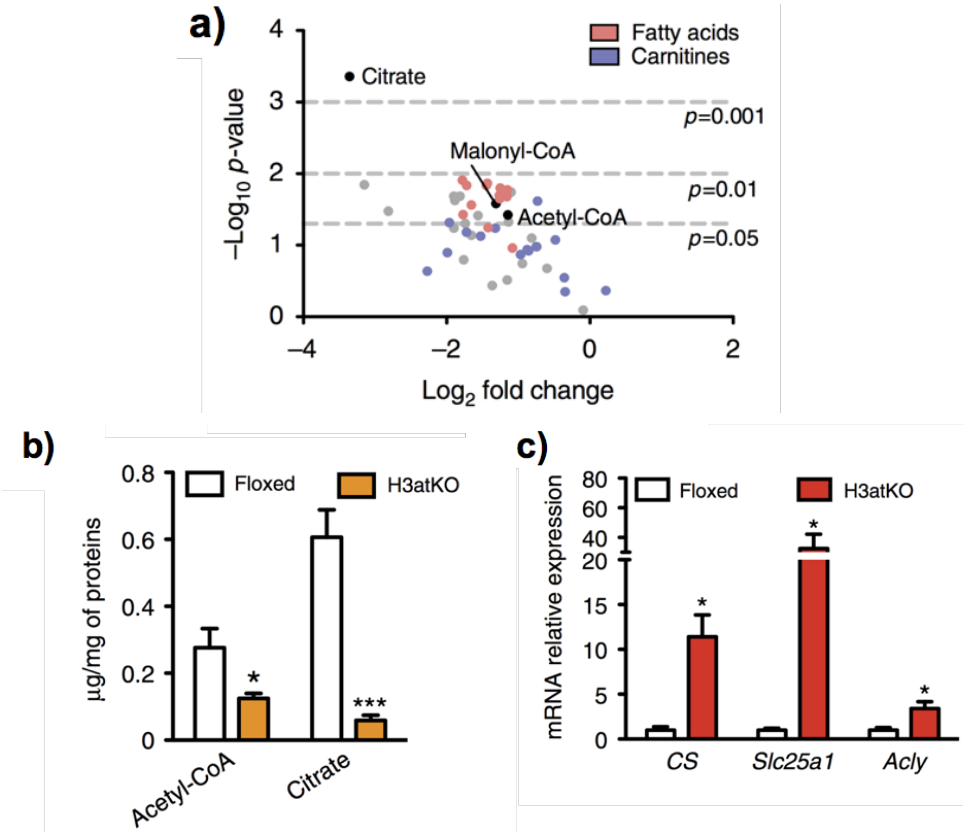

*Figure 26: a) Volcano plot of IngWAT metabolites. b) Acetyl-CoA and citrate levels in IngWAT of Floxed and H3atKO mice. c) Expression of genes related to citrate metabolism in IngWAT of Floxed and H3atKO mice. Student's t test; *p<0.05; ***p<0.001 vs Floxed mice.*

One of citrate possible sources is the mitochondrial conversion of glycolitic pyruvate to acetyl-CoA, catalyzed by pyruvate dehydrogenase complex (PDH), and the following condensation of acetyl-CoA and oxaloacetate. Therefore, we moved to investigate glicolysis and glucose metabolism. Glucose and glycolitic intermediates glucose 6-phosphate, fructose 1,6-bisphosphate and dihydroxyacetone phosphate/glyceraldehyde phosphate (DHAP/GAP) were reduced in H3atKO mice (Figure 27a), suggesting higher glycolitic flux and metabolite consumption. In parallel, we found increased expression of *pyruvate kinase* (*Pkm*) (Figure 27b), which generates pyruvate, but also increased expression of *pyruvate dehydrogenase kinase 4* (*Pdk4*), which blocks PDH by phosphorylation. In fact, we found increased phosphorylation of PDH at Ser293 and Ser300 in IngWAT of H3atKO mice (Figure 27c), suggesting that pyruvate conversion to acetyl-CoA is inhibited upon *Hdac3* ablation. Increased expression of *Mpc1*, *Pcx* and *Pck1* (Figure 27b) suggested that glycolitic pyruvate is preferentially converted

to anaplerotic oxaloacetate, which can be also used to feed glycolysis via conversion to phosphoenolpyruvate by PCK1.

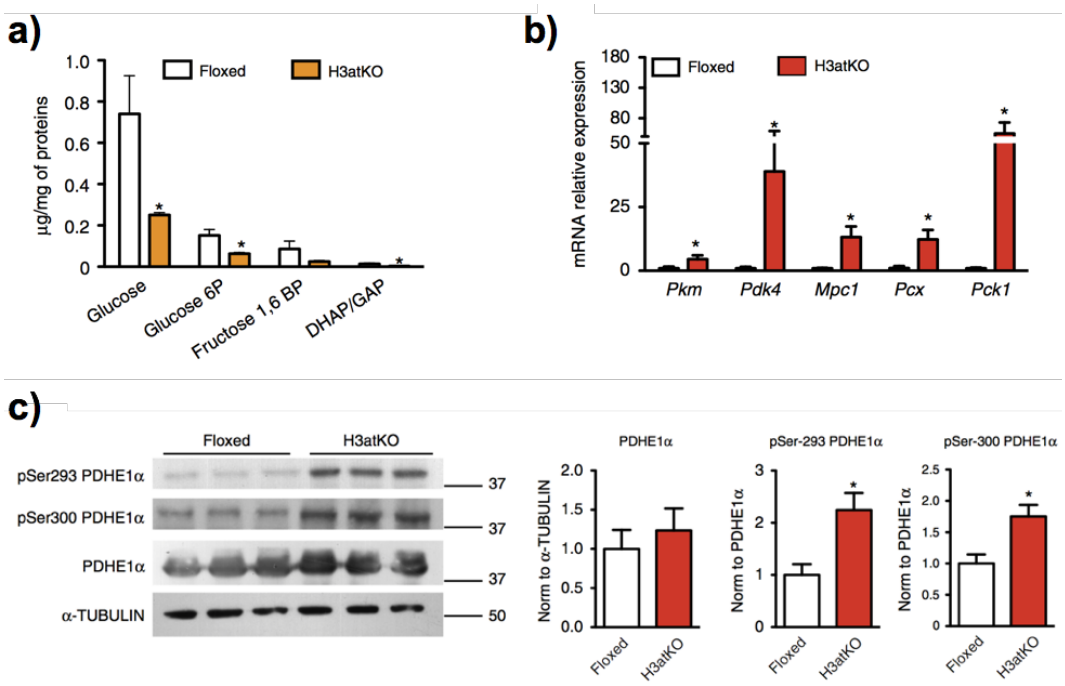

*Figure 27: a) Levels of glycolytic intermediates in IngWAT of Floxed and H3atKO mice. b) Expression of genes related to glucose metabolism in IngWAT of Floxed and H3atKO mice. c) Phosphorylation of Ser293 and Ser300 PDH analyzed by Western Blotting and related quantification in IngWAT of Floxed and H3atKO mice. Student's t test; *p<0.05 vs Floxed mice.*

Considering that glucose is not preferentially used to synthesize citrate in H3atKO mice, another possible source of mitochondrial acetyl-CoA is fatty acid β-oxidation. We, therefore, moved to analyze lipid metabolism. Mass spectrometry analysis revealed decreased levels of both saturated and unsatured fatty acids in IngWAT of H3atKO mice (Figure 28a). Importantly, we also found decreased levels of malonyl-CoA (Figure 28b), which in the mitochondria negatively modulates β-oxidation via CPT1 inhibition. Actually, in this case it is not possible to discriminate between mitochondrial or cytosolic malonyl-CoA. Even though, it is possible to speculate that β-oxidative flux was not reduced by malonyl-CoA mediated inhibition.

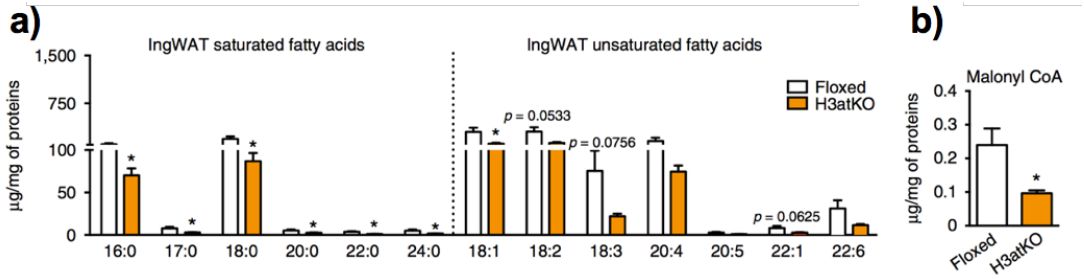

*Figure 28: a) Analysis of fatty acids levels in IngWAT of Floxed and H3atKO mice. b) Malonyl-CoA levels in IngWAT of Floxed and H3atKO mice. Student's t test; *p<0.05 vs Floxed mice.*

In parallel, we found increased expression of genes important for lipolysis (*Lipe*, *Atgl*) and β-oxidation (*Acsl1*, *Acox1*, *Cpt1b*, *Slc25a20*, *Acadl*, *Acadm*, *Hadh*) (Figure 29a). This was confirmed also at protein level for ATGL and ACADL (Figure 29b). These data suggested that β-oxidation was highly active upon *Hdac3* ablation and that this metabolic route was preferentially used as source for synthesizing citrate. However, we detected increased expression of genes important for *de novo* fatty acid synthesis, among which *ChREBPβ*, the master regulator of lipogenesis in the adipose tissue (Figure 29c).

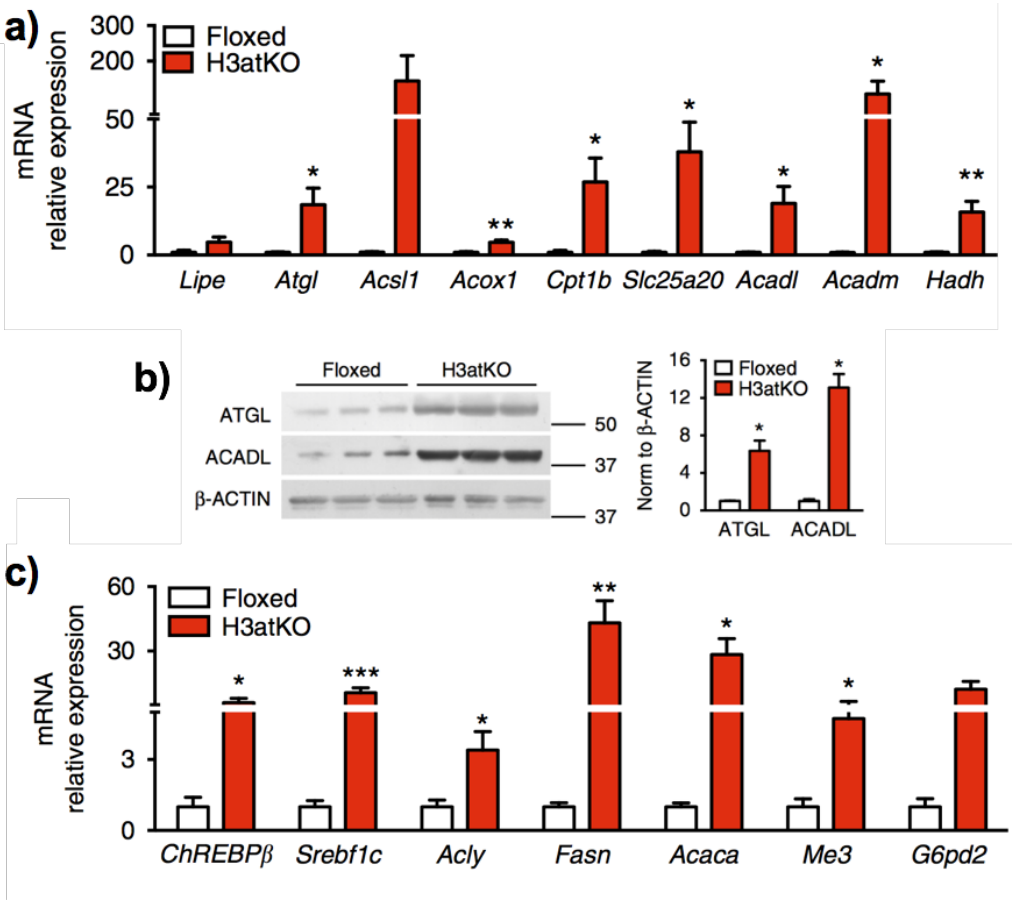

*Figure 29: a) Expression of genes related to lipolysis and fatty acid β-oxidation in IngWAT of Floxed and H3atKO mice. b) ATGL and ACADL Western Blotting and related quantification in IngWAT of Floxed and H3atKO mice. c) Expression of lipogenic genes in IngWAT of Floxed and H3atKO mice. Student's t test; *p<0.05; **p<0.01; ***p<0.001 vs Floxed mice.*

Consequently, we hypothesized that citrate is exported from mitochondria and converted by ACLY to cytoplasmic acetyl-CoA which, in turn, is precursor for fatty acid synthesis. This hypothesis could explain reduced levels of citrate in H3atKO mice IngWAT.

In vitro Hdac3 silencing recapitulates H3atKO phenotype

We have observed that *Hdac3* ablation *in vivo* caused a deep metabolic remodelling. Peculiar of H3atKO metabolic phenotype was the concomitant activation of lipolysis and fatty acid β-oxidation and lipogenesis, at least at gene expression and metabolite levels. To further confirm these data and deepen molecular mechanisms underlying H3atKO phenotype, we set up an *in vitro* model. We used C3H/10T1/2 mesenchimal stem cell line that can be differentiated to mature adipocytes. We silenced *Hdac3* at the beginning of differentiation protocol (day 0) with adenoviral vectors containing short hairpin sequences (ShHdac3). Empty adenoviral vectors were used as control (Scramble). After 9 days of differentiation, we confirmed by western blot effective *Hdac3* silencing (Figure 30).

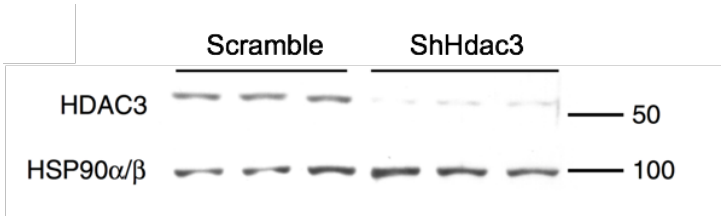

Figure 30: western blotting confirmed Hdac3 silencing in C3H/10T1/2 cell line.

ShHdac3 infected cells showed increased expression of adipocyte differentiation and functionality markers (*Pparg, Fabp4, Adipoq, Glut4, Plin, C/EBPα*) (Figure 31a). In fact, after *Hdac3* silencing we detected higher number of differentiated cells (Figure 31b) and more lipid accumulation as assessed by ORO staining (Figure 31c).

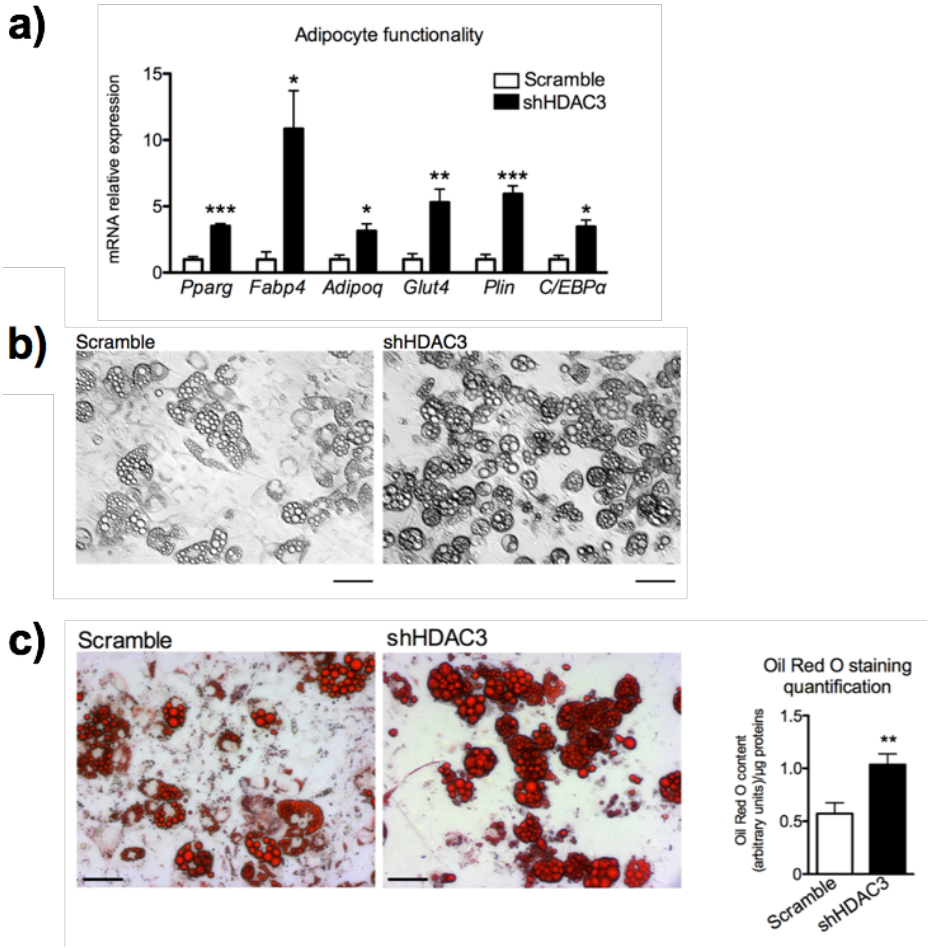

*Figure 31: a) Gene expression of adipocyte functionality markers in Scramble vs ShHdac3 treated C3H/10T1/2 cells. b) Morphology of Scramble vs ShHdac3 treated C3H/10T1/2 cells. Scale bar is 50 µm. c) Oil Red O staining in Scramble vs ShHdac3 treated C3H/10T1/2 cells and related quantification. Scale bar is 100 µm. Student's t test; *p<0.05; **p<0.01; ***p<0.001 vs Scramble.*

Moreover, ShHdac3 treated cells displayed increased expression of browning genes (*Ucp1, Adrb3, Ppara, Prdm16, Cidea*, *Elovl3*) (Figure 32).

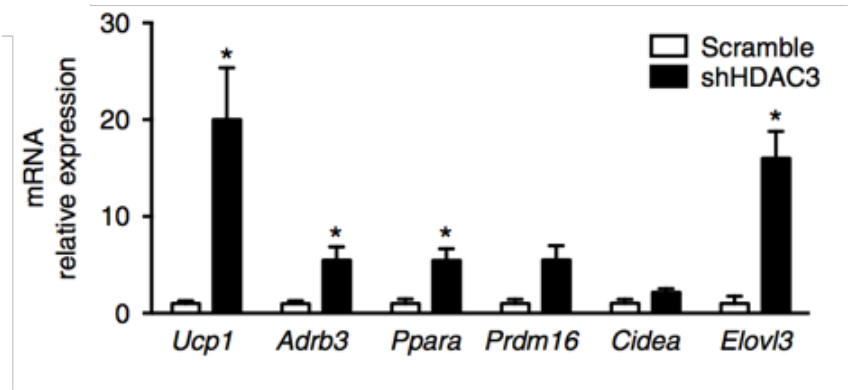

*Figure 32: gene expression of browning markers in Scramble vs ShHdac3 treated C3H/10T1/2 cells. Student's t test; *p<0.05 vs Scramble.*

Considering expression of metabolic genes, qPCR analysis showed increased expression of genes important for glucose and citrate metabolism (*Pkm2, Pdk4, Mpc1, Pcx, Cs, Acly, Slc25a1, Acss2*) (Figure 33a), lipolysis and fatty acid β-oxidation (*Cd36, Lpl, Lipe, Atgl, Acadl, Acadm, Hadh, Cpt1b*) and *de novo* lipogenesis (*ChREBPβ, Srebf1c, Acly, Fasn, Acaca, G6pd2*) (Figure 33b), similarly to what observed *in vivo*.

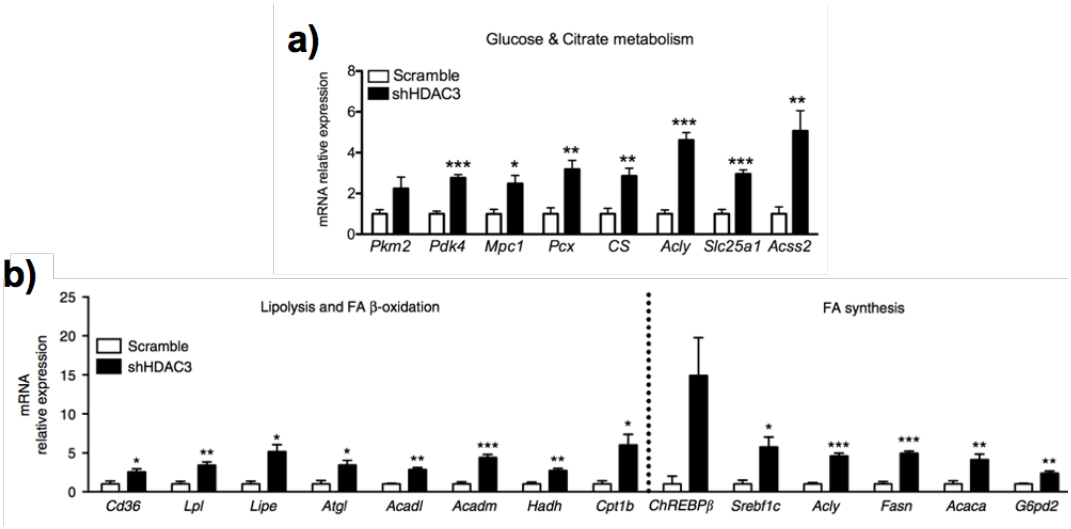

*Figure 33: a) Expression of glucose and citrate metabolism related genes in Scramble vs ShHdac3 treated C3H/10T1/2 cells. b) Expression of lipid futile cycle related genes in Scramble vs ShHdac3 treated C3H/10T1/2 cells. Student's t test; *p<0.05; **p<0.01; ***p<0.001 vs Scramble.*

Taken together, these results demonstrated that ShHdac3 cells presented similar phenotypical features observed in H3atKO mice and that this *in vitro* model can be used as a tool for examining molecular mechanisms underlying *Hdac3* inactivation in adipose tissue.

^{13}C labelling experiments confirms fatty acid futile cycle upon *Hdac3* silencing

Concurrent activation of fatty acid β-oxidation and lipogenesis was demonstrated to occur both *in vivo* in H3atKO mice and *in vitro* in ShHdac3 treated cells at level of gene expression and metabolites. Therefore, to further confirm these results, we treated ShHdac3 and Scramble cells with [U-^{13}C]palmitate at the end of differentiation. Firstly, we measured increased glycerol release in ShHdac3 treated cells, as result of increased triglycerides hydrolysis. (Figure 34).

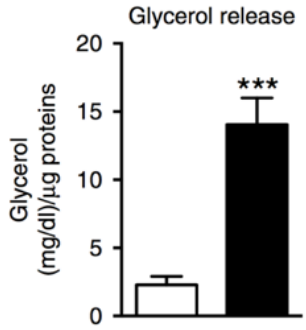

*Figure 34: measurement of glycerol release in Scramble (white bar) vs ShHdac3 treated C3H/10T1/2 cells (black bar). Student's t test; ***p<0.001 vs Scramble.*

After [U-^{13}C]palmitate treatment, we analysed by mass spectrometry metabolites isotopomers. With respect to citrate, we found decreased levels of citrate + 1 (Figure35).

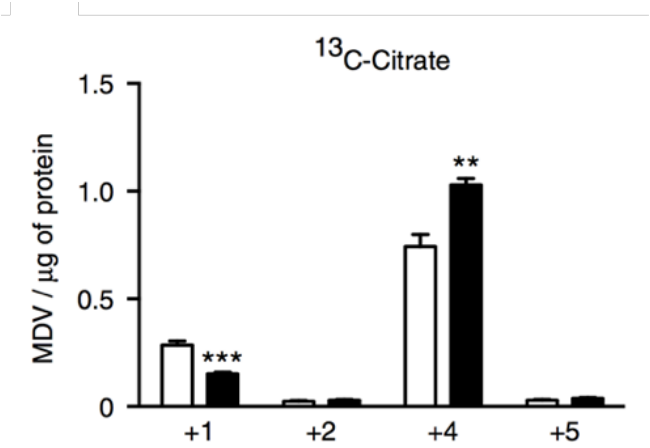

*Figure 35: levels of citrate +1, +2, +4, +5 isotopomers in Scramble (white bar) vs ShHdac3 treated C3H/10T1/2 cells (black bar). Student's t test; **p<0.01; ***p<0.001 vs Scramble.*

This isotopomer is formed after three rounds of TCA cycle: the first one incorporates 2 ^{13}C from labelled palmitate to citrate, forming citrate + 2, whose levels were not changed upon *Hdac3* silencing (Figure 35). In the second round of TCA cycle two C from not labelled (cold) palmitate are added to oxaloacetate + 2, forming citrate + 2; then 1 ^{13}C carbon exits TCA cycle as CO_2 (Figure 36).

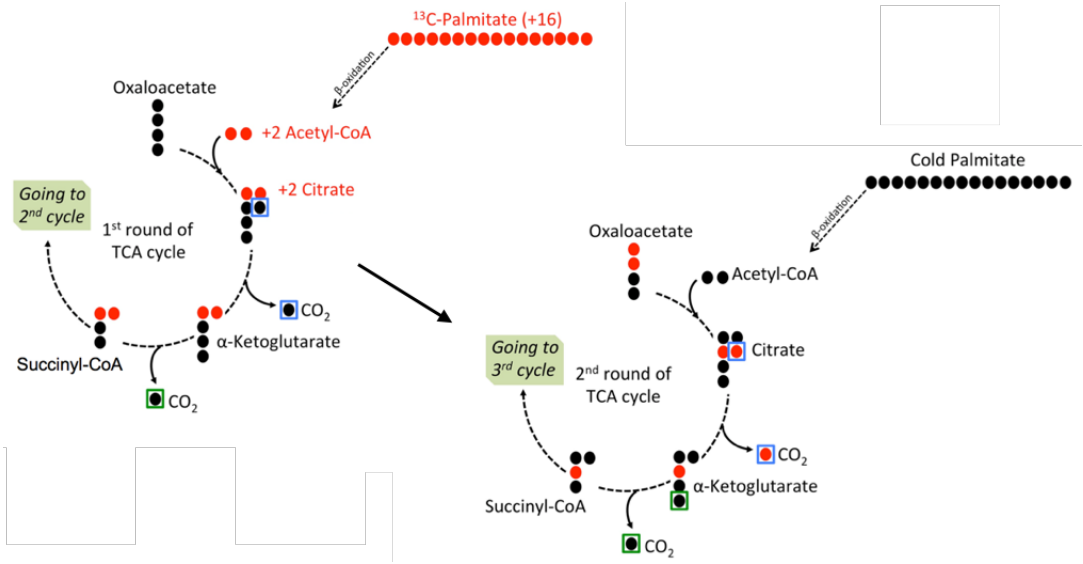

Figure 36: schematic representation of ^{13}C incorporation in metabolite isotopomers from labeled palmitate.

Finally, in the third round two C from unlabelled or cold palmitate are added to resulting oxaloacetate + 1, forming citrate + 1. This isotopomer then can exit TCA cycle and it can be used as substrate by ACLY to produce acetyl-CoA + 1 (Figure 37).

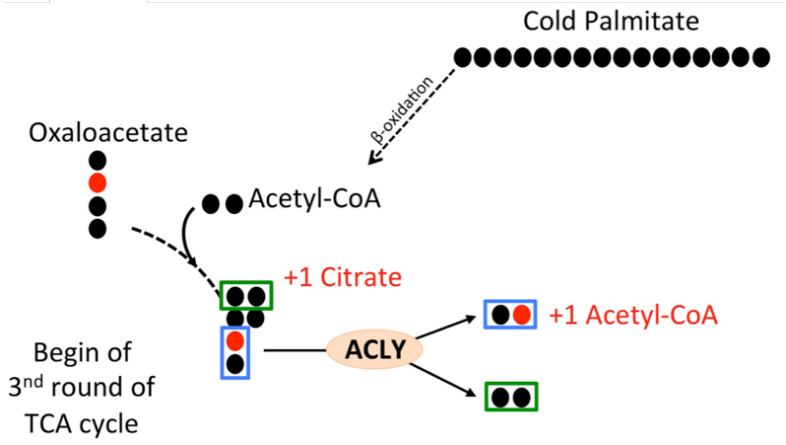

Figure 37: schematic representation of ^{13}C incorporation in metabolite isotopomers from labeled palmitate.

In fact, we found increased levels of acetyl-CoA + 1 isotopomer. The concurrent reduction of citrate + 1 and increase of acetyl-CoA + 1 indicated higher ACLY activity in ShHdac3 treated cells (Figure 38).

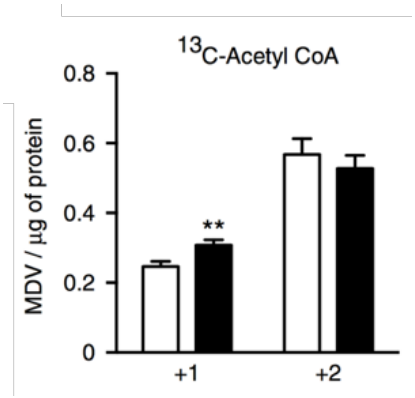

*Figure 38: levels of acetyl-CoA + 1 and acetyl-CoA + 2 isotopomers in Scramble (white bar) vs ShHdac3 treated C3H/10T1/2 cells (black bar). Student's t test; **p<0.01 vs Scramble.*

We also detected increased levels of citrate + 4 (Figure 35), which is formed after two rounds of TCA cycle with two following additions of 2 ^{13}C from labelled palmitate to oxaloacetate (Figure 39).

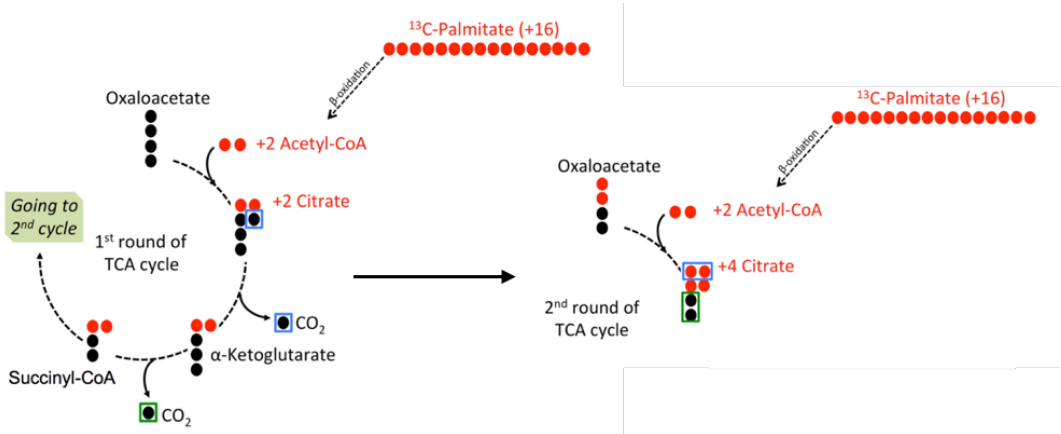

Figure 39: schematic representation of ^{13}C incorporation in metabolite isotopomers from labeled palmitate.

This data suggested increased flux of fatty acid β-oxidation and TCA cycle in Hdac3-silenced cells. Furthermore, levels of palmitate + 2 (Figure 40a-c) were increased in ShHdac3 treated cells paralleled by a mild increase, though not statistically significant, of malonyl-CoA + 2, + 3 isotopomers (Figure 40b).

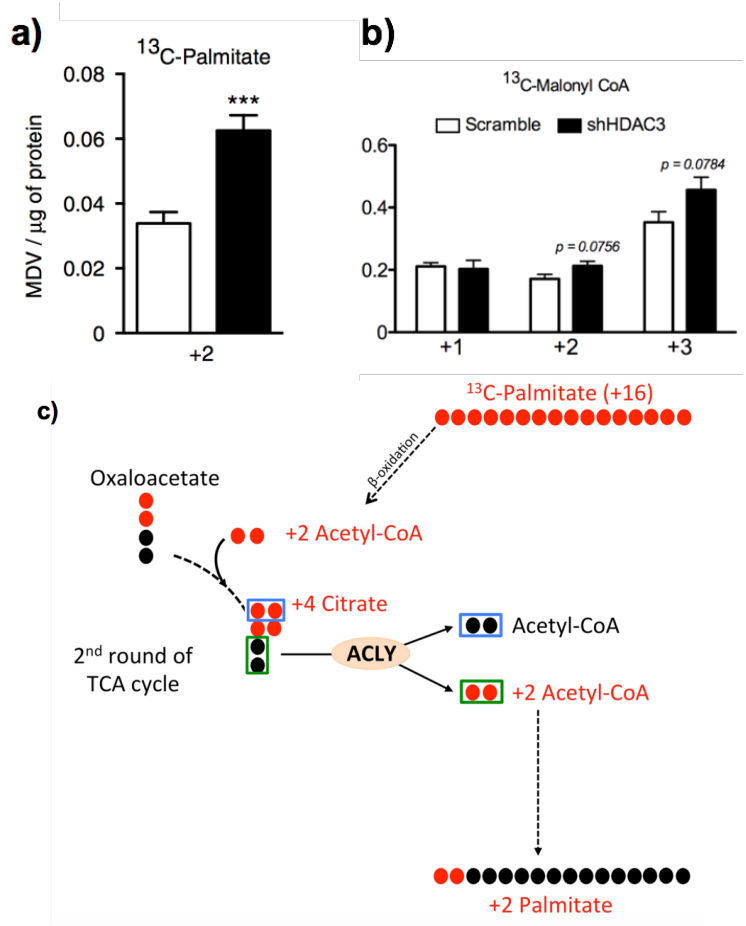

*Figure 40: levels of palmitate + 2 (a) and malonyl-CoA + 1, + 2, + 3 (b) isotopomers in Scramble (white bar) vs ShHdac3 treated C3H/10T1/2 cells (black bar). c) Schematic representation of ^{13}C incorporation in metabolite isotopomers from labeled palmitate. Student's t test; ***p<0.001 vs Scramble.*

These results suggested increased *de novo* lipogenesis with acetyl-CoA from palmitate used as precursor. Taken together, these data highlighted increased lipolysis, fatty acid β-oxidation and TCA cycle upon *Hdac3* silencing. Acetyl-CoA from β-oxidation is used as source for *de novo* fatty acid synthesis via increased ACLY activity. This highlighted the onset of futile cycle of fatty acid utilization and resynthesis in ShHdac3 treated cells.

Hdac3 ablation increases histone acetylation in specific chromatin regions

Hdac3 ablation in adipose tissue caused browning of WAT, accompanied by the onset of fatty acids futile cycle. Rewiring of lipid metabolism was paralleled by transcriptional reprogramming. These results prompted us to deepen molecular

mechanisms underlying these effects. HDAC3 belongs to a family of enzymes that regulate histone acetylation. It has been showed that *Hdac3* deletion caused hyperacetylation on specific chromatin regions with no increased global histone acetylation (Montgomery et al. 2008). Our data were in agreement with this previous finding (data not shown). Moreover, it has been reported the presence of a *Pparg* enhancer marked by acetylation on lysine 27 of histone H3 (H3K27ac) in white adipose tissue (Ramlee et al. 2014). Another study reported that in differentiated brown adipocytes two enhancers located at -13 and -5 kb upstream TSS of *Ucp1* are acetylated (Abe et al. 2015). Therefore, we decided to perform ChIP-qPCR on IngWAT of Floxed and H3atKO mice. We found increased acetylation at *Pparg* enhancer and at -5kb *Ucp1* enhancer of H3atKO mice (Figure 41a). This result was confirmed also *in vitro* where we detected increased acetylation at *Pparg* enhancer and at both -13 and -5kb *Ucp1* enhancers in ShHdac3 versus Scramble treated C3/H10T1/2 differentiated adipocytes (Figure 41b).

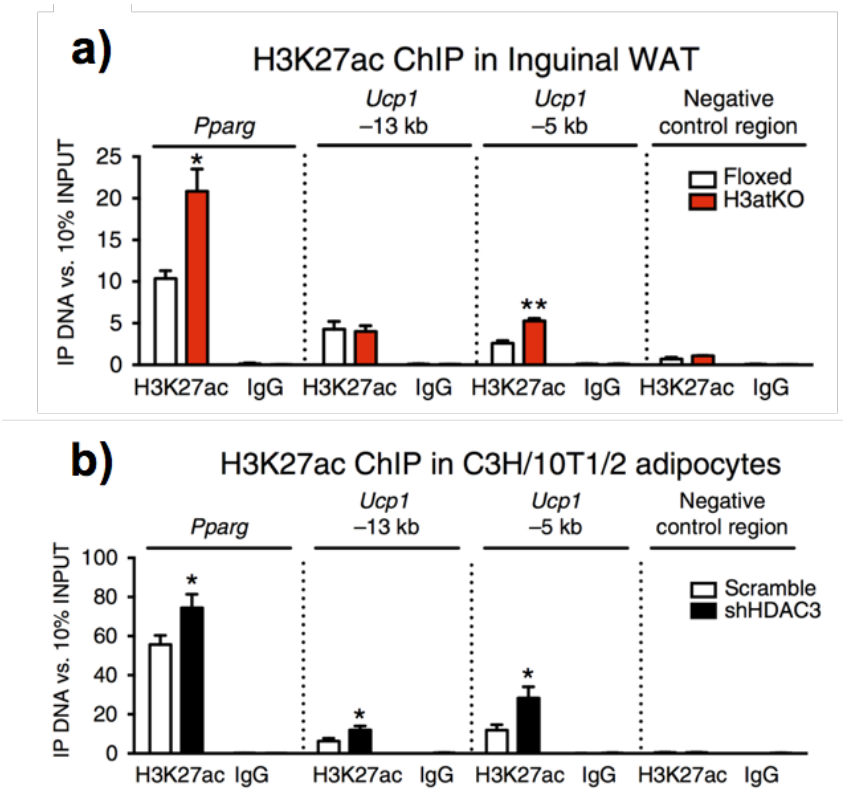

*Figure 41: a) ChIP-qPCR of H3K27ac at Pparg and Ucp1 enhancers in IngWAT of Floxed vs H3atKO mice. Student's t test; *p<0.05; **p<0.01 vs Floxed mice. b) ChIP-qPCR of H3K27ac at Pparg and Ucp1 enhancers in Scramble vs ShHdac3 treated C3H/10T1/2 cells. Student's t test; *p<0.05 vs Scramble.*

Furthermore, by analyzing already published ChIP-Seq experiments (GSE63964), we observed the presence of H3K27ac peaks at -15, -11, -3.5 and -1.6 kb upstream from *Ppara* coding region in BAT samples that were absent in WAT samples. Considering that H3K27ac generally marks active enhancers, we considered these regions as putative elements regulating *Ppara* transcription in BAT. We hypothesized that hyperacetylation at these regions could be present also in WAT during browning. Therefore, we investigated these chromatin regions in our model. As a matter of fact, we measured increased H3K27ac at -15, -11 and -1.6 kb regions in H3atKO IngWAT (Figure 42a). This result was again confirmed also *in vitro* where hyperacetylation was found at -15 and -11 kb putative regulatory regions in ShHdac3 treated cells (Figure 42a).

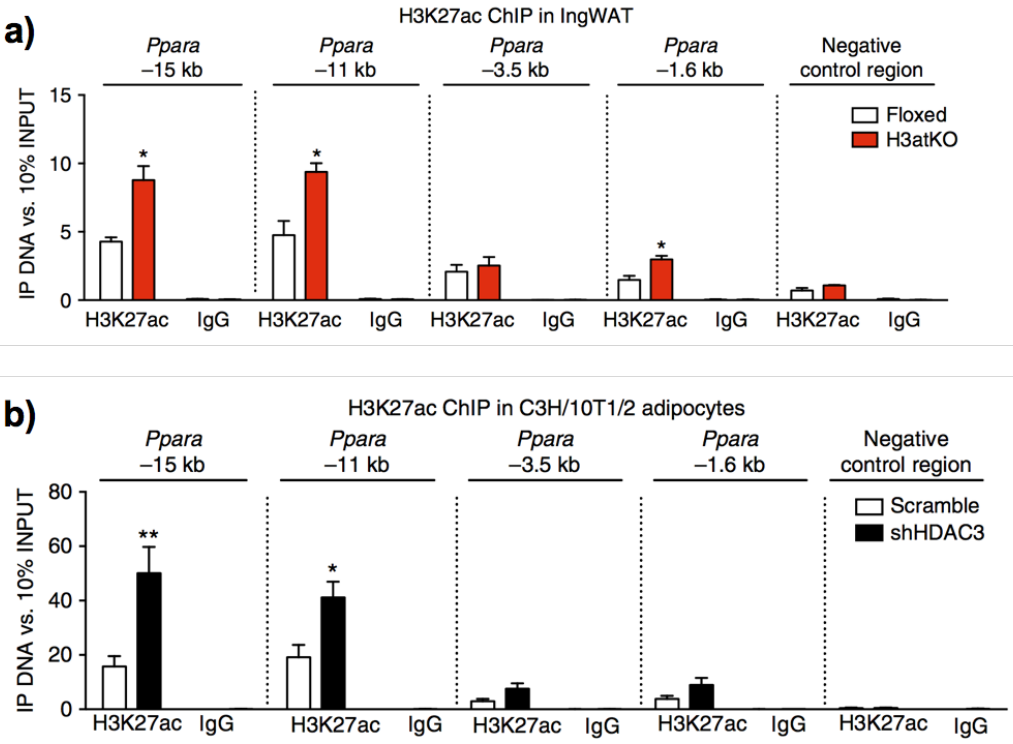

*Figure 42: a) ChIP-qPCR of H3K27ac at Ppara putative regulatory regions in IngWAT of Floxed vs H3atKO mice. Student's t test; *p<0.05 vs Floxed mice. b) ChIP-qPCR of H3K27ac at Ppara putative regulatory regions in Scramble vs ShHdac3 treated C3H/10T1/2 cells. Student's t test; *p<0.05; **p<0.01 vs Scramble.*

These data indicated that *Hdac3* ablation remodelled chromatin in specific regions. Hyperacetylation in these regions consequent to *Hdac3* ablation increased the expression of *Pparg, Ucp1* and *Ppara,* key genes in H3atKO phenotype.

ACLY is fundamental for H3atKO phenotype

Hdac3 ablation caused hyperacetylation of *Pparg*, *Ucp1* and *Ppara* regulatory regions. At this regard, it has been recently demonstrated that in the nucleus ATP-citrate lyase provides acetyl groups for histone acetylation. In our model we found increased *Acly* expression. However qPCR did not distinguish between cytosolic and nuclear ACLY. Therefore, we performed IF experiments in IngWAT from Floxed and H3atKO mice. We found increased nuclear ACLY localization in H3atKO mice (Figure 43).

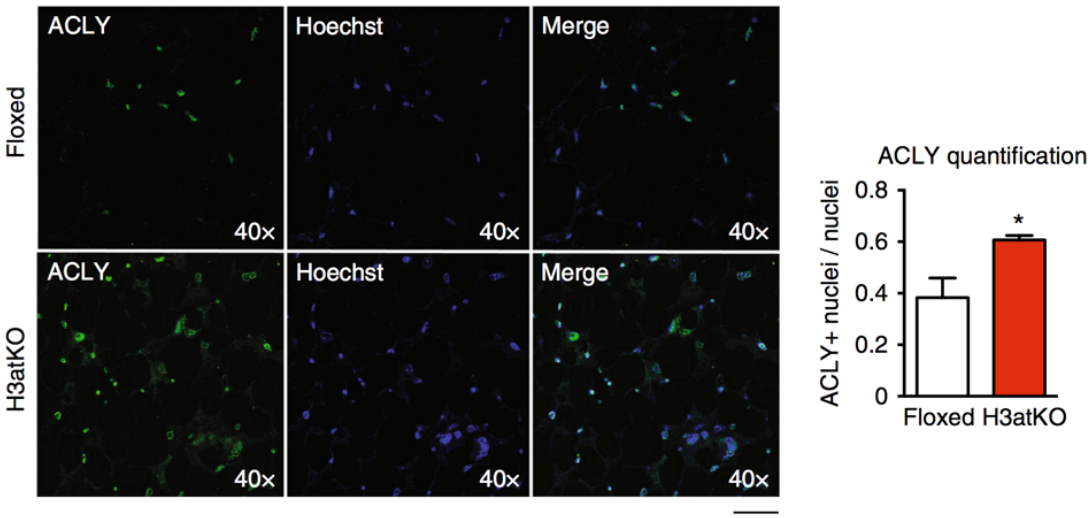

*Figure 43: ACLY immunofluorescence analysis in IngWAT of Floxed and H3atKO mice and related quantification of ACLY nuclear localization. Scale bar is 40 μm. Student's t test; *p<0.05 vs Floxed mice.*

This data suggested that ACLY had a dual role in H3atKO metabolism: it supplied cytosolic acetyl-CoA for fatty acid synthesis and, on the other hand, it sustained hyperacetylation of *Pparg*, *Ucp1* and *Ppara* regulatory regions, by providing nuclear acetyl-CoA. To deepen ACLY role in mechanisms exerted by adipose *Hdac3* ablation, we decided to co-silence *Hdac3* and *Acly* in C3H/10T1/2 cells at day 0 of differentation. Western blot analysis confirmed that ShAcly treatment abolished *Acly* expression (Figure 44).

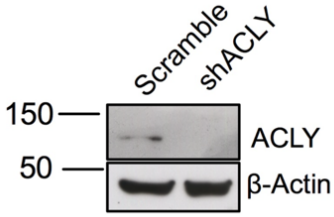

Figure 44: western blotting confirmed Acly silencing in C3H/10T1/2 cell line.

At the end of differentation, both ShAcly and ShHdac3 + ShAcly co-silenced cells appeared less differentiated compared to Scramble or ShHdac3 treated cells (Figure 45c). Importantly, co-silencing reduced H3K27 acetylation at *Pparg* enhancer (though not statistical significant), at -5 kb *Ucp1* enhancer and at -15, -11 kb *Ppara* putative regulatory regions compared to ShHdac3 treated cells (Figure 45b). In fact, upregulation of key genes *Ucp1, Ppara, Pparg, Glut4, Pdk4, Pcx, Atgl, Acadl, Fasn* in ShHdac3 treated cells was prevented by *Acly* silencing (Figure 45c).

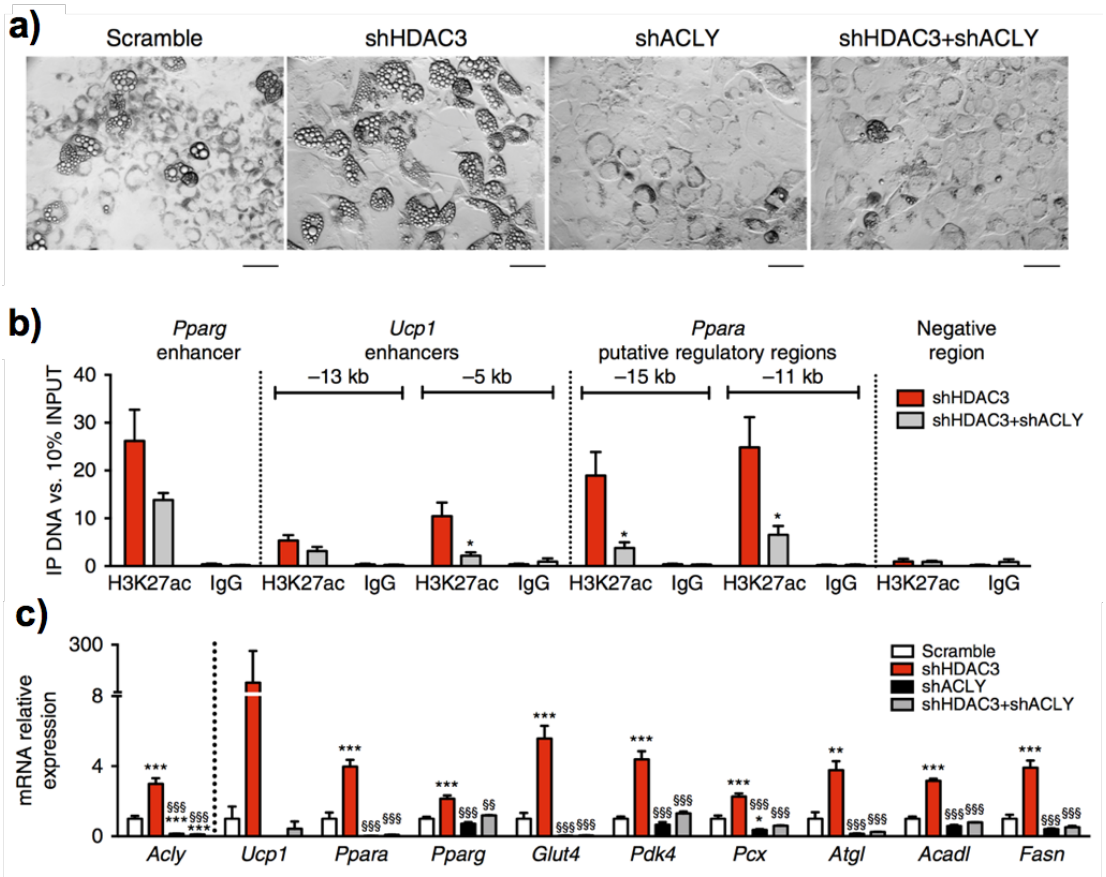

*Figure 45: a) Morphology of Scramble, ShHdac3, ShAcly and ShHdac3 + ShAcly treated C3/H10T1/2 cells. Scale bar is 50 µm. b) ChIP-qPCR of H3K27ac at Pparg and Ucp1 enhancers and Ppara putative regulatory regions in ShHdac3 and ShHdac3 + ShAcly treated C3/H10T1/2 cells. Student's t test; *p<0.05; **p<0.01; ***p<0.001 vs ShHdac3. c) Expression of genes important for metabolic rewiring upon Hdac3 ablation in Scramble, ShHdac3, ShAcly and ShHdac3 + ShAcly treated C3/H10T1/2 cells. One way ANOVA, Tukey as post hoc test; **p<0.01, ***p<0.001 vs. Scramble, §§p<0.01, §§§p<0.001 vs. shHdac3.*

However, cytosolic acetyl-CoA for *de novo* lipogenesis can be generated also from acetate via Acetyl-CoA Synthetase, ACSS2. For these reasons, we also performed *Acss2* and *Hdac3* co-silencing in C3H/10T1/2 cells at day 0 of differentation. Western blot analysis confirmed *Acss2* knock down upon ShAcss2 treatment (Figure 46).

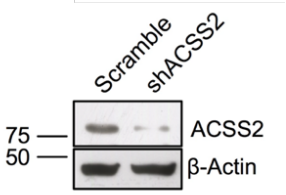

Figure 46: western blotting confirmed Acss2 silencing in C3H/10T1/2 cell line.

Contrary to what seen with *Acly* knock down, ShAcss2 co-silencing did not abrogate gene expression upregulation (Figure 47a). In fact, cell morphology of ShAcss2 treated cells appeared comparable to that of Scramble or ShHdac3 cells (Figure 47b).

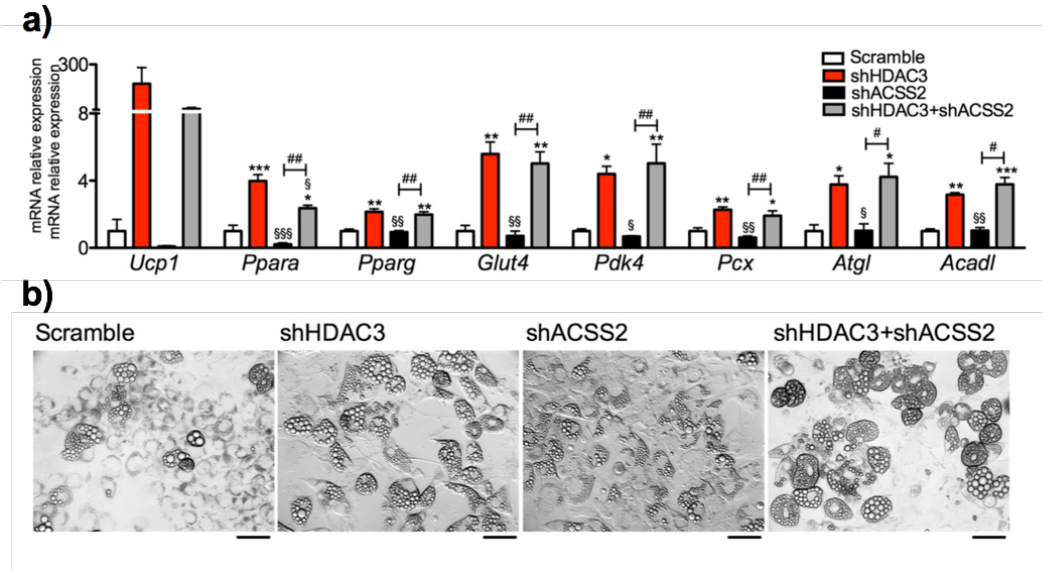

*Figure 47: a) Expression of genes important for metabolic rewiring upon Hdac3 ablation in Scramble, ShAcss2, ShAcss2 and ShHdac3 + ShAcss2 treated C3/H10T1/2 cells. One way ANOVA, Tukey as post hoc test; *p<0.05, **p<0.01, ***p<0.001 vs Scramble, §p<0.05, §§p<0.01, §§§p<0.001 vs shHdac3, #p<0.05, ##p<0.01, vs shAcss2. b) Morphology of Scramble, ShHdac3, ShAcss2 and ShHdac3 + ShAcss2 treated C3/H10T1/2 cells. Scale bar is 50 µm.*

These results ruled out the effects consequent to *Hdac3* ablation were dependent on ACSS2 activity. On the contrary, these data demonstrated that ACLY played

a relevant role in regulating both metabolism and epigenetic regulation of transcription in H3atKO mice.

High fat diet attenuates H3atKO phenotype

Hdac3 ablation induced browning of WAT, accompanied by peculiar metabolic rearrangement. In light of these promising results, we next asked whether *Hdac3* knock out was able to counteract obesity. To this end, we fed H3atKO and Floxed mice with high fat diet (HFD) for 24 weeks. Surprisingly, we observed no differences in body weight gain (Figure 48a), no amelioration of glucose clearance as measured by glucose tolerance test (GTT) (Figure 48b). Upon cold exposure, H3atKO mice were no longer able to maintain higher body temperature than Floxed mice (Figure 48c), as observed with LFD. In fact, we did not observe nor multilocular adipocytes in H&E histological pictures (Figure 48d) neither increased expression of browning markers (Figure 48e).

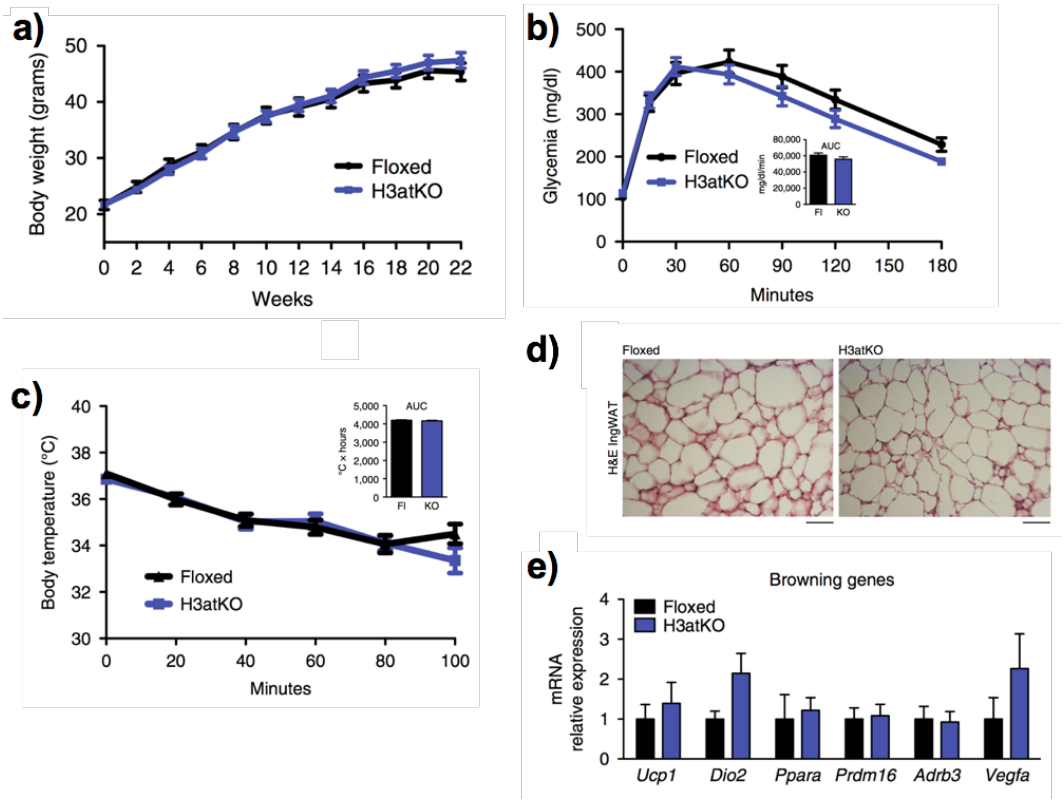

Figure 48 a) Body weight gain in HFD fed Floxed and H3atKO mice. b) Glycaemia levels during glucose tolerance test (GTT) and related area under the curve (AUC) in HFD fed Floxed and H3atKO mice. c) Body temperature measurements upon exposure to 4°C for 100 minutes and related area under the curve (AUC) of HFD fed Floxed and H3atKO mice. d) IngWAT H&E in HFD fed Floxed and H3atKO mice. Scale bar is

100 µm. e) Expression of genes related to browning in HFD fed Floxed and H3atKO mice. Student's t test.

Gene expression reprogramming was absent when H3atKO were fed HFD: in fact, we measured expression of several genes belonging to biological patterns relevant for H3atKO metabolic rewiring (adipocyte functionality, oxidative metabolism, fatty acid β-oxidation, lipolysis, lipogenesis and glucose and citrate metabolism) (Figure 49 a-d) but we did not detect any differences, except for *Fasn* expression.

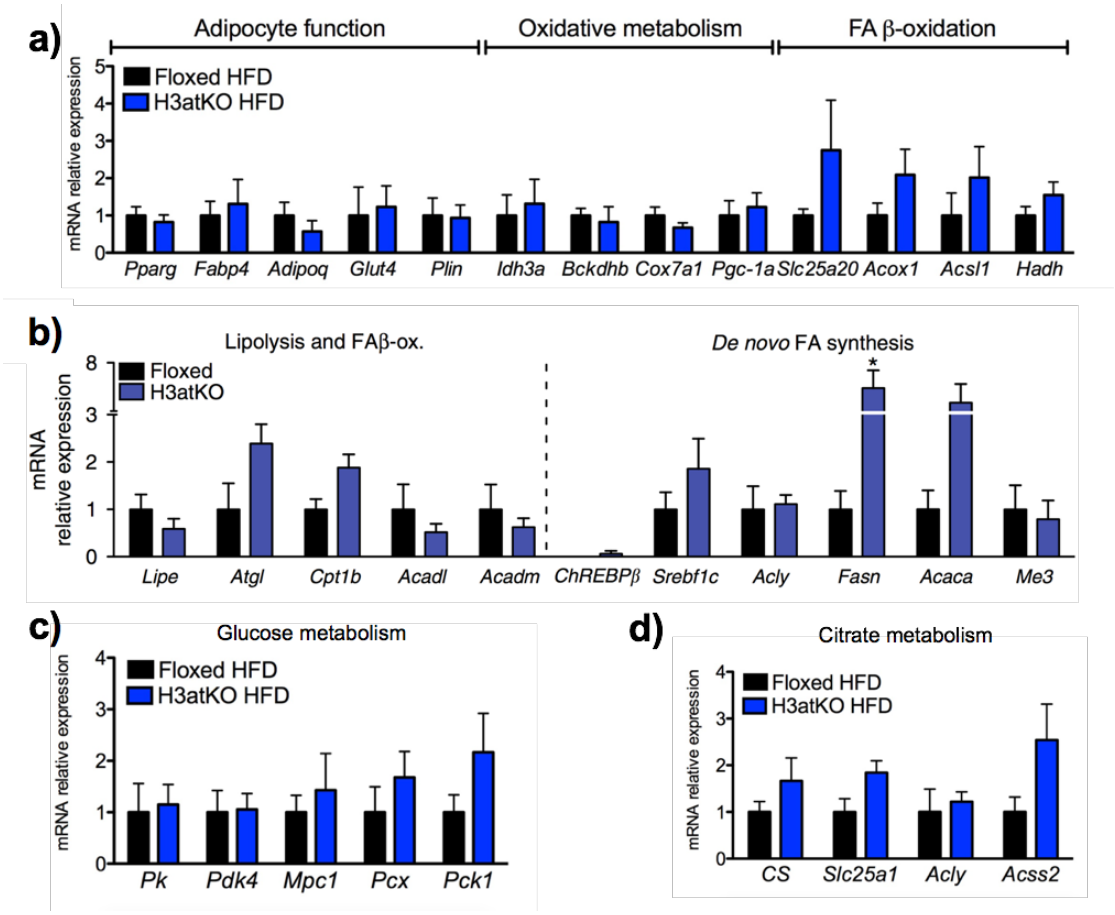

*Figure 49: analysis of expression of genes related to adipocyte functionality, oxidative metabolism and fatty acid β-oxidation (a), lipolysis and fatty acid β-oxidation and lipogenesis (b), glucose metabolism (c) and citrate metabolism (d) in HFD fed Floxed and H3atKO mice. Student's t test; *p<0.05 vs Floxed mice.*

Therefore, this suggests that futile cycle of fatty acid was not induced at least in terms of gene expression when H3atKO were fed HFD.

Metabolomic analysis (Figure 50a-b) did not highlight any specific metabolic pattern, thus suggesting that also at metabolite level *Hdac3* ablation did not exert any effect during exposure to high fat diet.

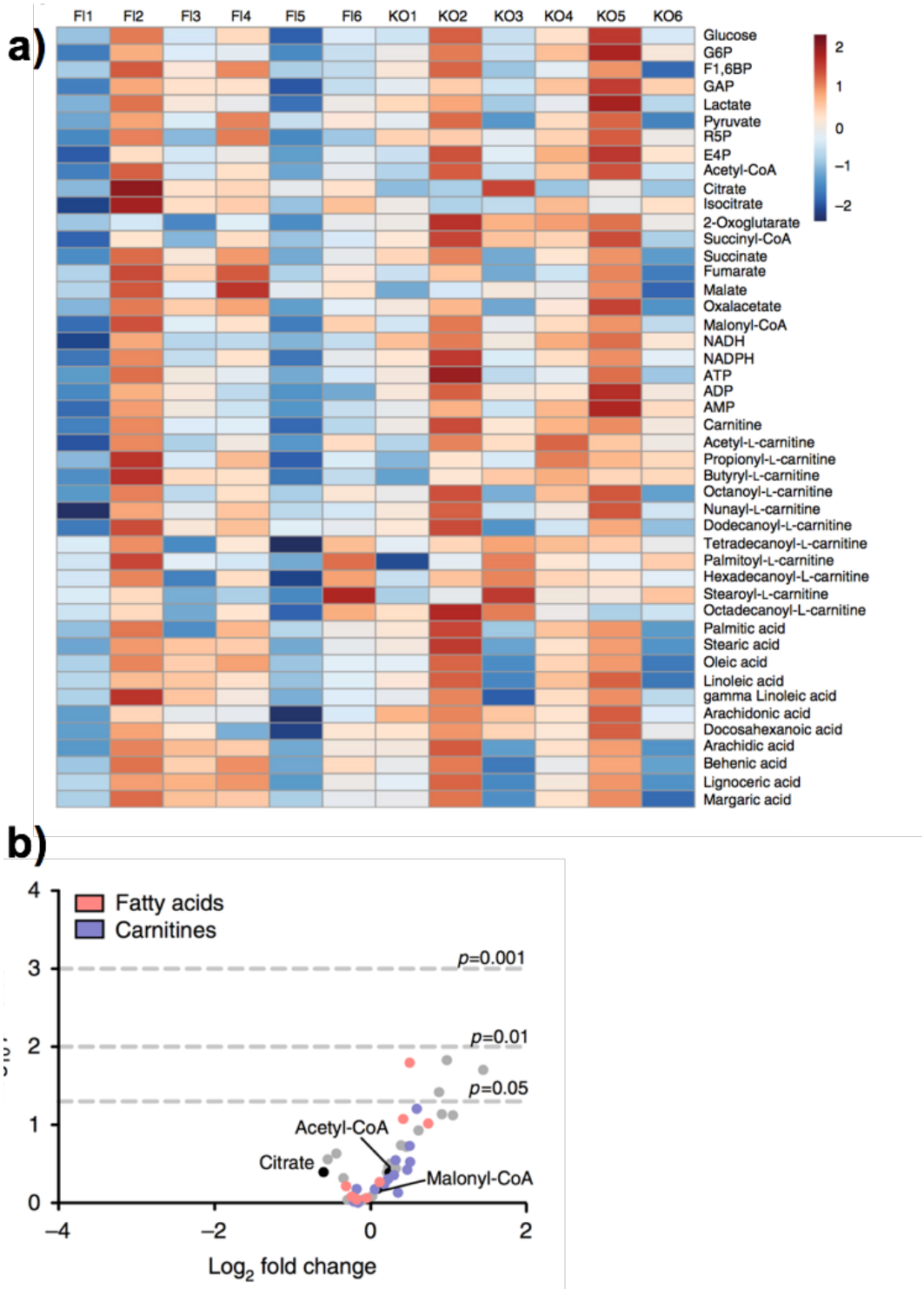

Figure 50: heatmap (a) and volcano plot (b) of metabolites in HFD fed Floxed and H3atKO IngWAT.

Moreover, chromatin hyperacetylation at *Pparg*, *Ucp1* enhancers (Figure 51a) and *Ppara* putative regulatory regions (Figure 51b) was absent in HFD fed H3atKO mice.

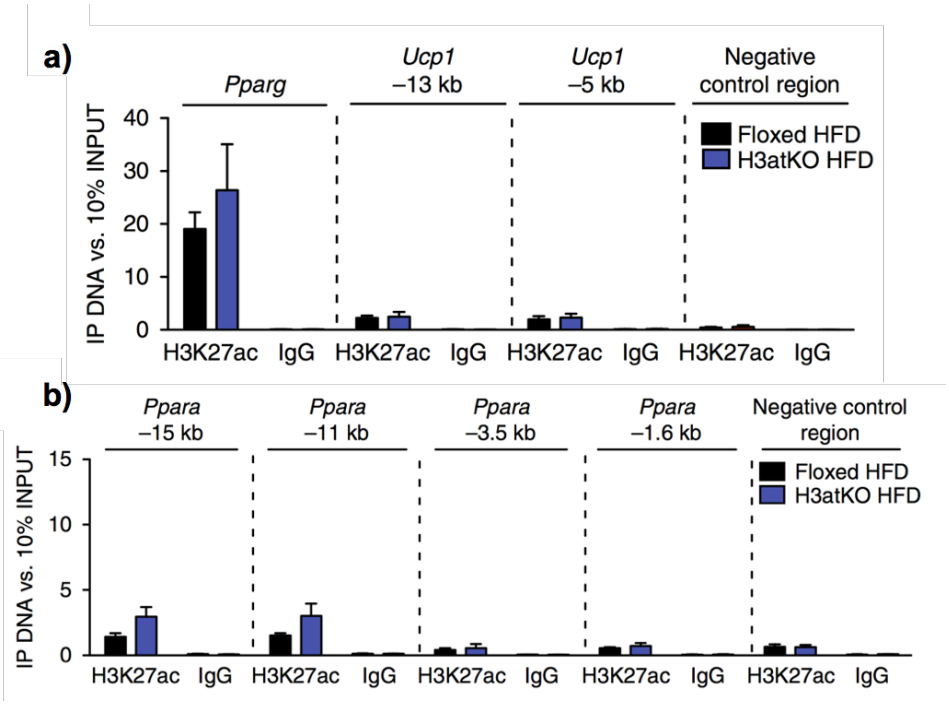

Figure 51: ChIP-qPCR of H3K27ac at Pparg and Ucp1 enhancers (a) and Ppara putative regulatory regions (b) in IngWAT of HFD fed Floxed and H3atKO mice. Student's t test.

Unlike expected, effects of adipose *Hdac3* ablation were blunted by high fat feeding and H3atKO displayed same obesity-like features of Floxed mice.

Metabolic dysregulation in high fat dietary regimen overcomes the effects of *Hdac3* knock out

To understand why during HF feeding H3atKO did not display any protective phenotype, we considered how high fat diet might deregulate lipid metabolism in WAT. At this regard, it has been previously showed that HFD could reduce levels of lipases in adipose tissue (Shen et al. 2007). In our model, ATGL expression was increased in H3atKO mice both in LFD and HFD (Figure 52). However, increased levels of ATGL protein in H3atKO LFD fed mice were significantly reduced during HF feeding.

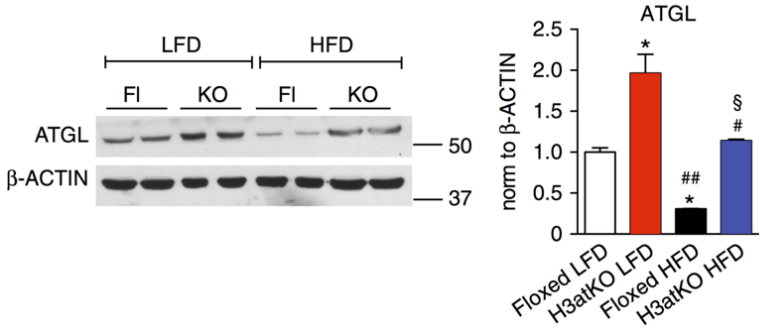

*Figure 52: western blotting of ATGL levels in LFD and HFD fed Floxed and H3atKO mice. Two way ANOVA, Tukey as post hoc test; *p 0.05 vs. Floxed LFD, #p<0.05, ##p<0.01 vs. H3atKO LFD, $p<0.05 vs. Floxed HFD.*

Of note, ATGL releases FFAs that are activators of PPARs. At this regard, another key feature of H3atKO metabolic remodelling was the activation of PPARs regulatory network via increased acetylation of regulatory regions increasing *Ppara* and *Pparg* expression. When H3atKO mice were fed HFD, both *Ppara* (Figure 53a) and *Pparg* (Figure 53b) expression was decreased compared to that of LFD fed H3atKO mice.

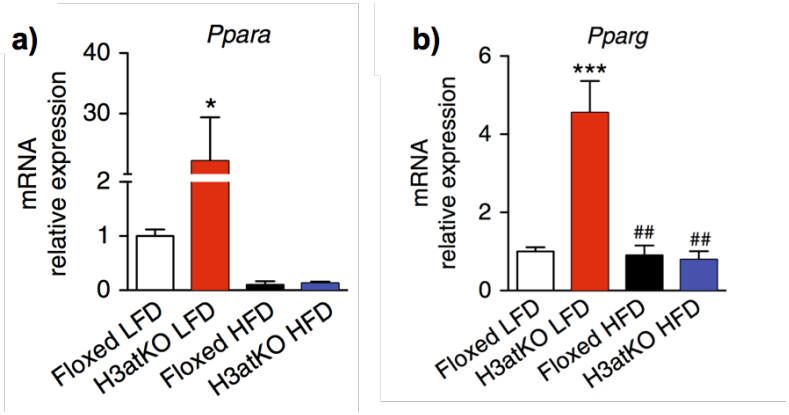

*Figure 53: IngWAT expression of Ppara (a) and Pparg (b) in LFD and HFD fed Floxed and H3atKO mice. Two way ANOVA, Tukey as post hoc test; *p 0.05, ***p<0.001 vs. Floxed LFD, ##p<0.01 vs. H3atKO LFD.*

These data suggested that PPARs regulatory network was no longer induced in HFD fed H3atKO because of lack of PPARs expression and activation. One of related consequences is that lypolitic program regulated by PPARα was not induced during HF feeding. Moreover, PPARα positively regulates expression of *Pdk4*, whose PDH inhibition is fundamental for H3atKO fatty acid futile cycle. As a matter of fact, *Pdk4* expression is not increased in HFD fed H3atKO mice as result of loss of PPARα activation (Figure 54a). This was paralleled by reduced phosphorylation of Ser293 and Ser300 PDH in HFD fed H3atKO mice compared to levels of LFD fed H3atKO mice (Figure 54b-c).

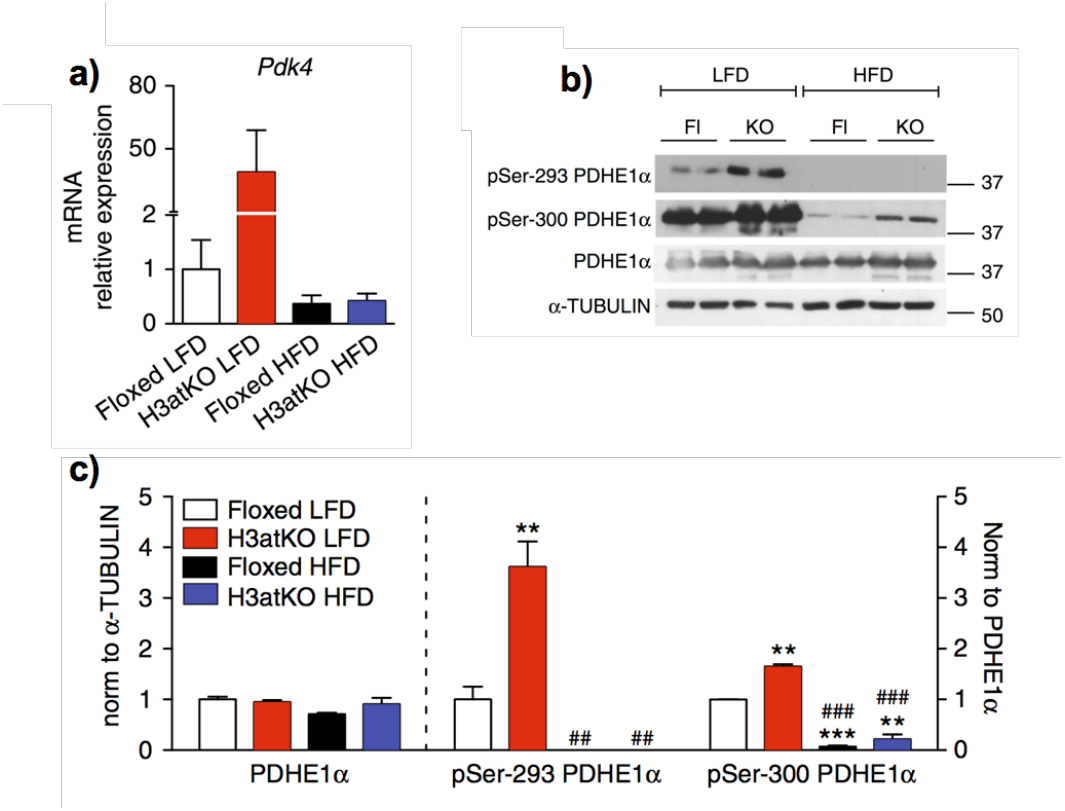

*Figure 54: a) Pdk4 expression in LFD and HFD fed Floxed and H3atKO mice. b-c) Western blotting analysis (b) of Ser293 and Ser300 PDH phosphorylation levels and related quantification (c) in IngWAT of LFD and HFD fed Floxed and H3atKO mice. Two way ANOVA, Tukey as post hoc test; **p<0.01, ***p<0.001 vs. Floxed LFD, ##p<0.01, ###p<0.001 vs. H3atKO LFD.*

Therefore, this suggested that conversion of glucose-derived pyruvate to acetyl-CoA was no longer blocked during HF feeding and that β-oxidation did not provide acetyl-CoA to feed TCA cycle and citrate synthesis. Moreover, these data suggested that PPARα played a relevant role in H3atKO phenotypical changes during LFD and that the block of its activation by HF feeding contributed to abrogate *Hdac3* ablation effects. To further confirm these results, we treated *Hdac3* silenced and Scramble C3/H/10T1/2 cells with PPARα inhibitor GW6471. As expected, GW6471 treatment attenuated *Hdac3* silencing effects on expression of key genes *Pparg*, *Glut4*, *Pdk4*, *Ucp1*, *Acadl*, *Acly*, *Fasn* (Figure 55a) and strongly reduced number of differentiated adipocytes (Figure 55b).

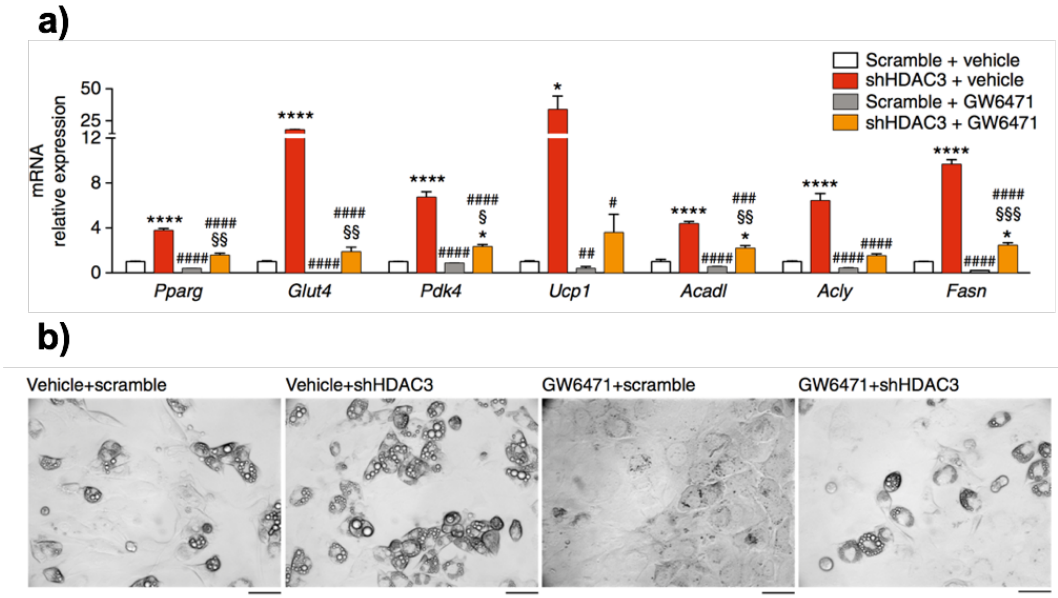

*Figure 55: a) Expression of key genes of H3atKO phenotype in Scramble or ShHdac3 C3/H10T1/2 cells treated with vehicle or GW6471. Two-way ANOVA, Tukey as post hoc test; *p<0.05, ****p<0.0001 vs. Scramble + Vehicle, ###p<0.001, ####p<0.0001 vs. ShHdac3 + Vehicle, §p<0.05, §§p<0.01, and §§§p<0.001 vs. Scramble + GW6471.*
b) Morphologic analysis of Scramble or ShHdac3 C3/H10T1/2 cells treated with vehicle or GW6471. Scale bar is 50 µm.

These *in vitro* results further confirmed that PPARα is a pivotal actor in mechanisms underlying H3atKO phenotype. Furthermore, another important metabolic route of H3atKO phenotype is lipogenesis, whose principal regulator in adipose tissue is ChREBPβ. In fact, *ChREBPβ* expression is increased in LFD fed H3atKO mice (Figure 56a). However, as already demonstrated in literature, its expression is reduced upon HF feeding in H3atKO mice. At this regard, *ChREBPβ* expression was shown to be regulated by glucose cellular level via ChREBPα (Herman et al. 2012). Intracellular glucose levels in adipose tissue are mainly regulated by GLUT4 transporter, which is PPARγ target gene. In fact, we found reduced levels of *Glut4* mRNA in HFD fed H3atKO mice compared to those of LFD fed H3atKO mice (Figure 56b), as result of reduced PPARγ activity.

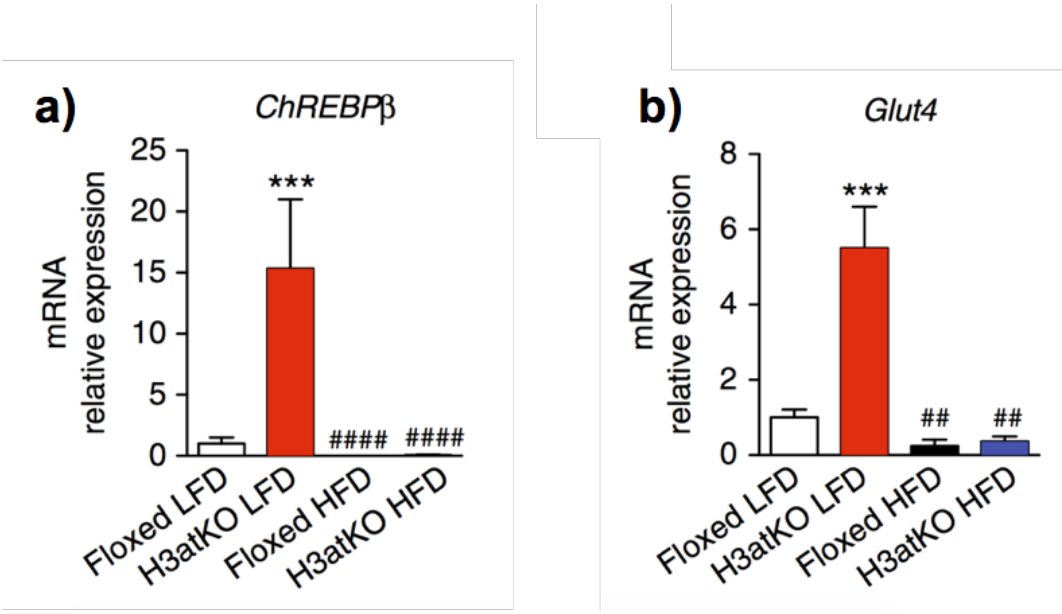

*Figure 56: expression of ChREBPβ (a) and Glut4 (b) in LFD and HFD fed Floxed and H3atKO mice. Two-way ANOVA, Tukey as post hoc test; ***p<0.001 vs. Floxed LFD, ##p<0.01, ####p<0.0001 vs. H3atKO LFD*

Therefore, these data suggested that HFD fed H3atKO displayed less adipose intracellular glucose levels leading to reduced *ChREBPβ* expression. Taken together, these results indicated that also lipogenic pathway was impaired when H3atKO mice were exposed to high fat feeding.

Immunophenotyping revealed immune remodelling of adipose tissue upon *Hdac3* knock out

It has been demonstrated that resident immune cells play relevant roles in the pathophysiology of adipose tissue. For these reasons, we investigated immunophenotype of adipose tissue in H3atKO mice. To this end, we fed Floxed and H3atKO mice with LFD for 4 weeks and we performed FACS analysis on visceral WAT (ViscWAT) in collaboration with Prof. Catapano and Prof. Norata Laboratory of Lipoproteins, Immunity and Atherosclerosis, Università degli Studi di Milano. We chose visceral WAT because the augmentation of this adipose compartment is classically involved in negative effects exerted by adipose resident immune cells on systemic metabolism during obesity. Firstly, ViscWAT of H3atKO mice weighed less than that of Floxed mice, confirming our previous results (Figure 57a). FACS analysis showed increased number of $CD45^+$ cells (Figure 57b), which represent leukocytes, in ViscWAT of H3atKO mice. Among leukocytes, number of dendritic cells ($Cd11c^+$ MHCII) (Figure 57c) was not

different between Floxed and H3atKO mice. Interestingly, we found increased number of neutrophils (Ly6G$^+$) (Figure 57d), monocytes (Ly6C$^+$) (Figure 57e) and macrophages (F4/80$^+$ MHCII) (Figure 57f).

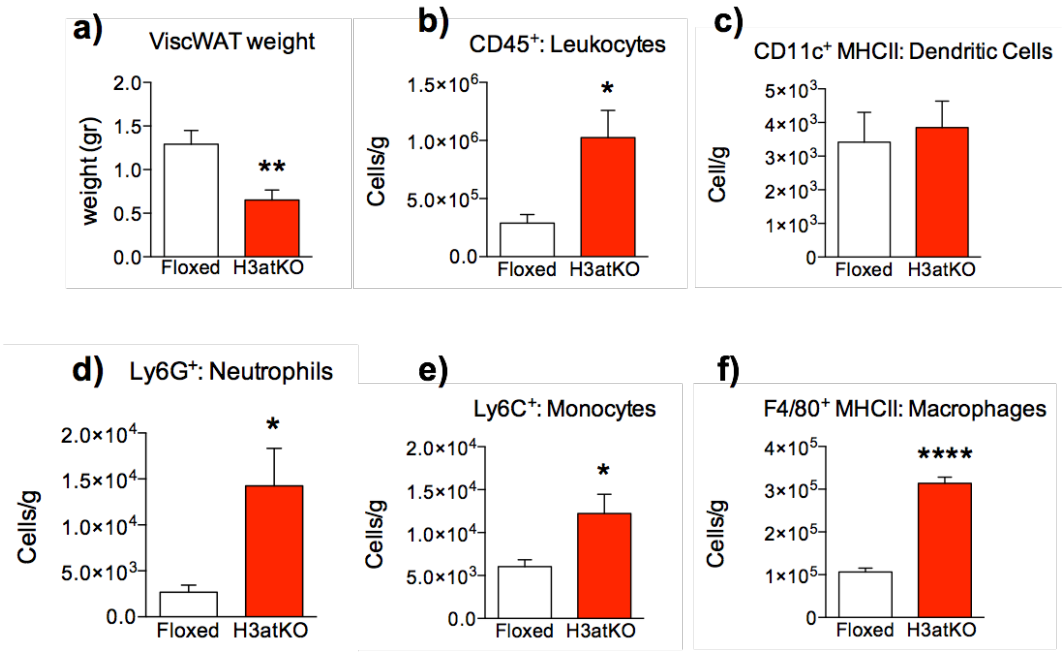

*Figure 57: a) ViscWAT weight of LFD fed Floxed and H3atKO mice. b-f) Analysis of immune cells number in ViscWAT of LFD fed Floxed and H3atKO mice, in particular leukocytes (b), dendritic cells (c), neutrophils (d), monocytes (e) and macrophages (f). Student's t test; *p<0.05; **p<0.01; ****p<0.0001 vs Floxed mice.*

We also analyzed macrophages subsets within ViscWAT and, surprisingly, we found 10% increase of M1 percentage (% Cd11c$^+$/F4/80$^+$MHCII) (Figure 58a) and reduction of M2 percentage (% Cd206$^+$/F4/80$^+$MHCII) (Figure 58b).

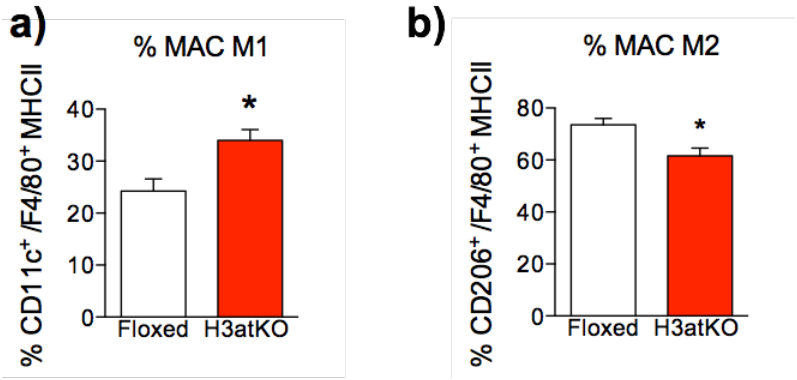

*Figure 58: percentage of M1 macrophages (a) and M2 macrophages (b) in ViscWAT of LFD fed Floxed and H3atKO mice. Student's t test; *p<0.05 vs Floxed mice.*

In parallel, we analyzed gene expression in epididymal visceral WAT. qPCR analysis showed increased expression of M1 markers *Il6* and *Nos2*, with no change in *Ccl2* expression (Figure 59a-c). However, also M2 marker *Ym1* expression was increased, accompanied by a trend of increase in *Arg1* and *Cx3cr1* expression, though not statistical significant (Figure 59d-f).

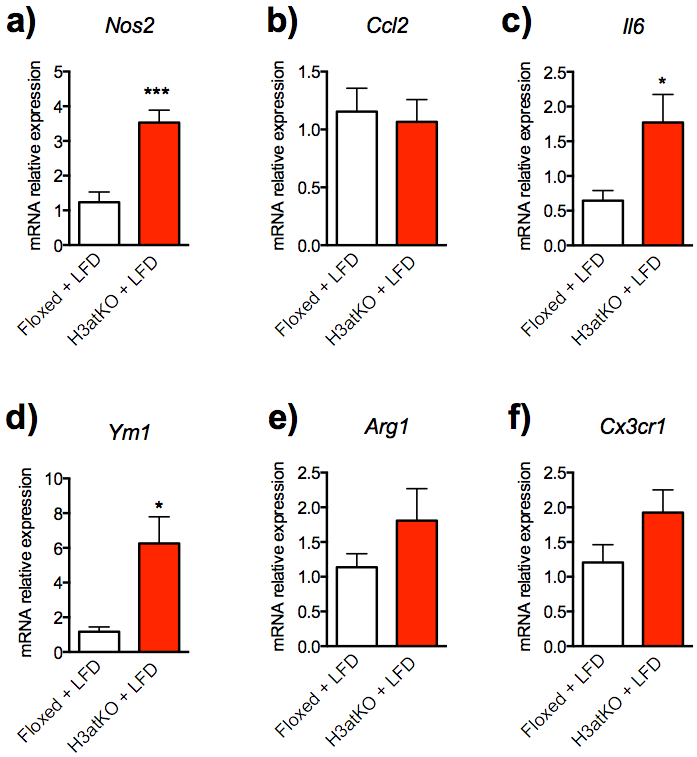

*Figure 59: expression of M1 macrophage (a, b, c) and M2 macrophage (d, e, f) markers in EpiWAT of LFD fed Floxed and H3atKO mice. Student's t test; *p<0.05; ***p<0.001 vs Floxed mice.*

With respect to adaptive immunity, H3atKO ViscWAT displayed increased number of both $CD4^+$ (Figure 60a) and $CD8^+$ T lymphocytes (Figure 60b). However, none of $CD4^+$ and $CD8^+$ subsets (Teffector memory TEM, Tcentral memory TCM, Teffector, Tnaïve) (Figure 60c-d) showed different percentage between Floxed and H3atKO mice. Of note, T regulatory cells (Treg, % $CD25^+$ $FoxP3^+/CD4^+$) were not different between two phenotypes (Figure 60e).

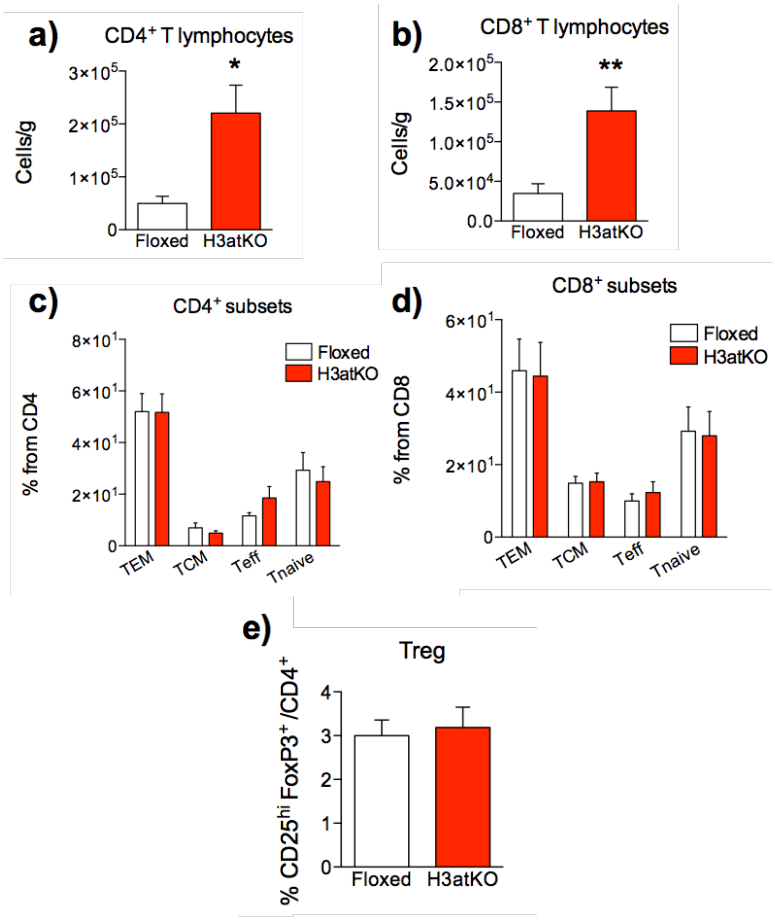

*Figure 60: analysis of adaptive immune cells number in ViscWAT of LFD fed Floxed and H3atKO mice, in particular CD4⁺ (a), CD8⁺ (b), CD4⁺ subsets (c), CD8⁺ subsets (d) and Treg (e). Student's t test; *p<0.05; **p<0.01 vs Floxed mice.*

To understand whether increased number of immune cells in H3atKO ViscWAT resulted from increased local proliferation or increased recruitment from systemic circulation, we analyzed levels of immune cells in bone marrow and blood of Floxed and H3atKO mice. We found no differences in CD45⁺ leukocytes in bone marrow (Figure 61a). Moreover, number of circulating neutrophils (Figure 61b), monocytes (Figure 61c) and monocitic subsets (Ly6C high, intermediate and low) (Figure 61d) was not different in blood.

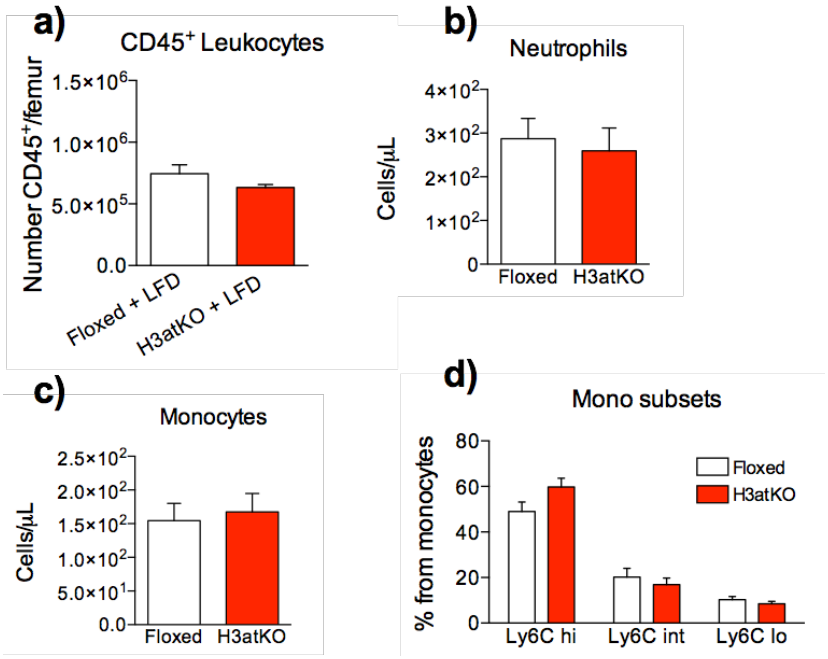

Figure 61: levels of leukocytes in bone marrow (a), neutrophils (b), monocytes (c), monocyte subsets (d) in blood of LFD fed Floxed and H3atKO mice. Student's t test.

Similarly, number of $CD4^+$ T cells (Figure 62a), $CD8^+$ T cells (Figure 62b), related subsets and basal Treg cells ($CD4^+ CD25^+$) showed no difference in blood (Figure 62c-d).

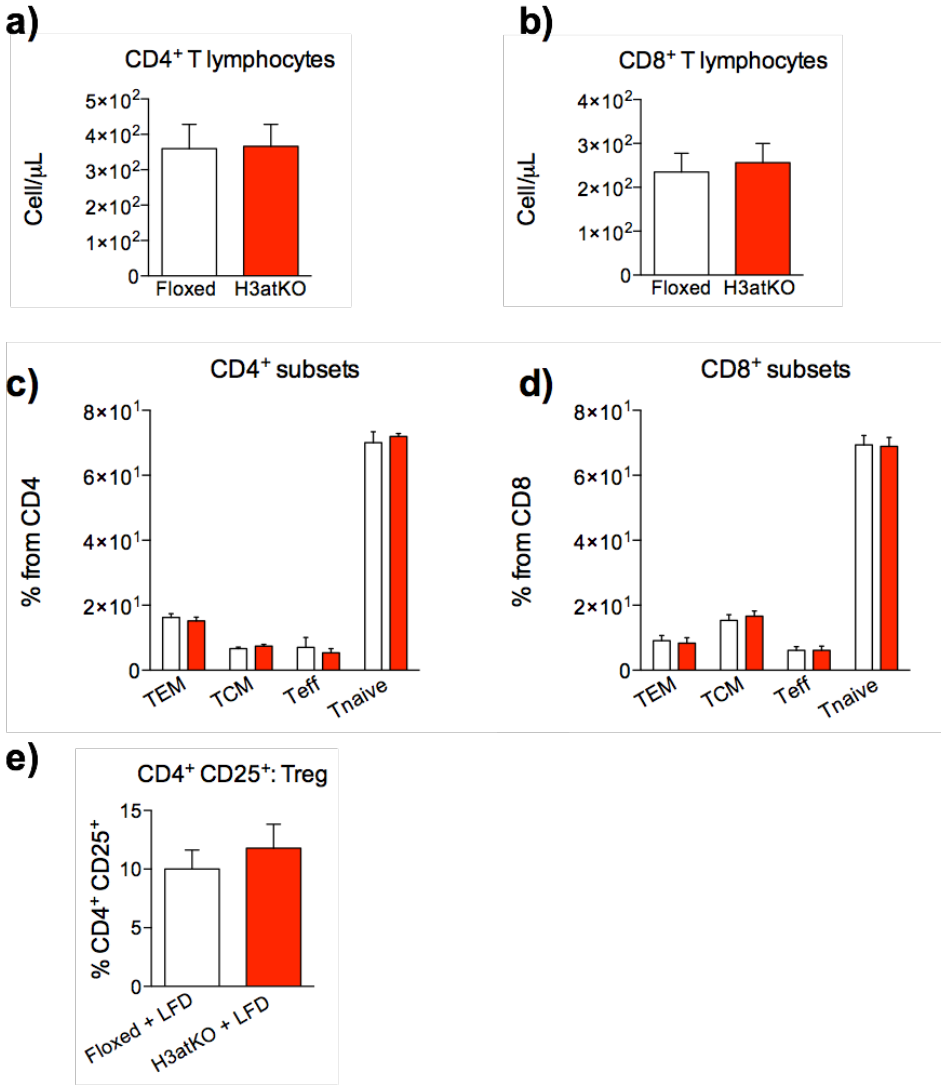

Figure 62: levels of CD4⁺ (a), CD8⁺ (b), CD4⁺ subsets (c), CD8⁺ subsets (d) and basal Treg cells in blood of LFD fed Floxed and H3atKO mice. Student's t test.

These data suggested that increased number of immune cells in adipose tissue was a result of increased local proliferation rather than increased recruitment. Taken together, these data indicated that adipocyte-specific *Hdac3* ablation redefined population of resident immune cells within visceral adipose tissue, increasing presence of both innate and adaptive immune cells. Interestingly, H3atKO mice displayed increased percentage of M1 macrophages.

Immunoremodeling of H3atKO ViscWAT is not altered by high fat diet

In obesity adipose tissue resident macrophages (ATMs) participate to worsen systemic metabolism leading to atherosclerosis and cardiovascular disease. In

particular M1 macrophages have a major role in these mechanisms. In H3atKO mice we found increased number of macrophages with increased percentage of M1 subset. These results prompted us to investigate whether these effects were maintained or even worsen during high fat diet consumption. To this end, we fed Floxed and H3atKO littermates HFD for 4 weeks to detect early effects of high fat diet consumption. After dietary exposure we analyzed ViscWAT immunophenotype by FACS. After 4 weeks of HFD consumption, ViscWAT weight was not statistically different between two phenotypes, even though a trend of reduction in H3atKO mice was still present (Figure 63a). FACS analysis showed a striking increase in the number of $CD45^+$ leukocytes in H3atKO ViscWAT, even though it was not statistical significant (p-value: 0,0579) (Figure 63b). As measured in LFD fed mice, number of neutrophils ($Ly6G^+$) (Figure 63c), monocytes ($Ly6C^+$) (Figure 63d) and macrophages ($F4/80^+$ MHCII) (Figure 63e) was increased in H3atKO mice, with a slight increase, not statistical significant, of dendritic cells ($Cd11c^+$ MHCII) (Figure 63f).

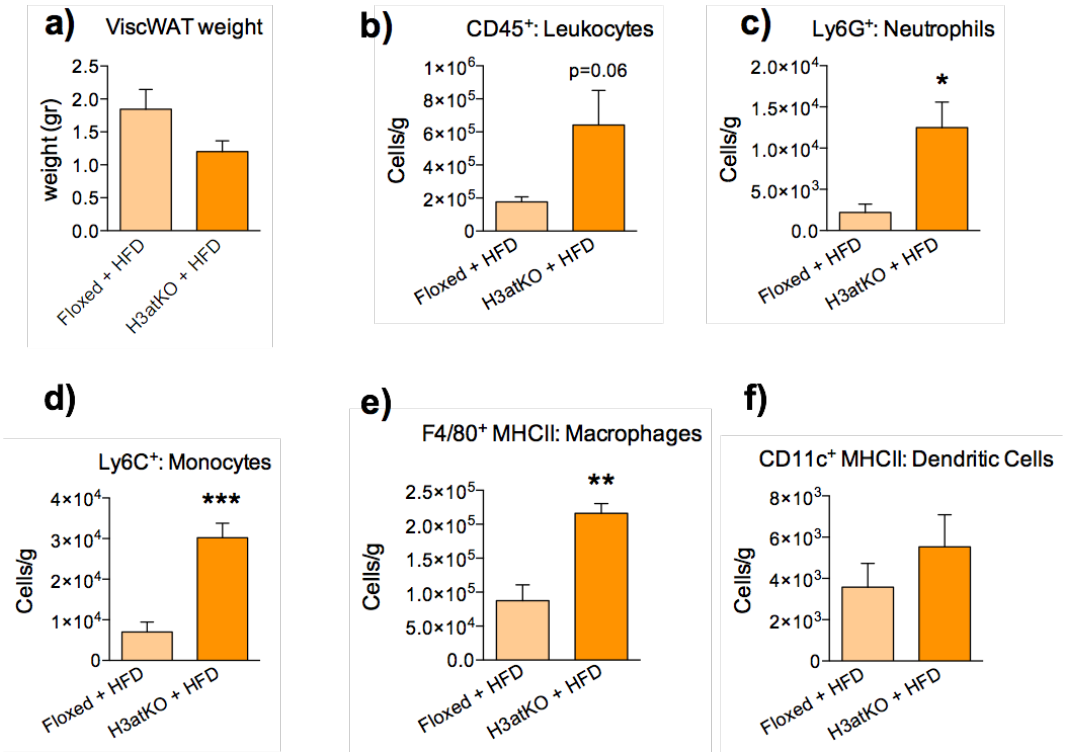

*Figure 57: a) ViscWAT weight of HFD fed Floxed and H3atKO mice. b-f) Analysis of immune cells number in ViscWAT of HFD fed Floxed and H3atKO mice, in particular leukocytes (b), neutrophils (c), monocytes (d), macrophages (e), and dendritic cells (f). Student's t test; *p<0.05; **p<0.01; ***p<0.001 vs Floxed mice.*

Among macrophages, we found no differences nor in percentage of M1 (% Cd11c^{+}/F4/80^{+}MHCII) (Figure 64a) neither M2 (% Cd206^{+}/F4/80^{+}MHCII) (Figure 64b) subsets.

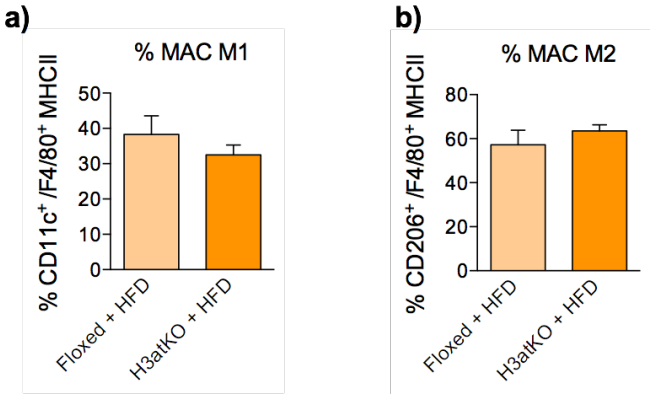

Figure 64: percentage of M1 macrophages (a) and M2 macrophages (b) in ViscWAT of HFD fed Floxed and H3atKO mice. Student's t test.

In particular, by comparing M1 percentage between two diets, we found that HFD consumption caused around 15% increase in % M1 subset in Floxed mice, whereas HFD did not change that of H3atKO mice (Figure 65). These data indicated that HFD consumption did not cause a further increase of M1 macrophages in ViscWAT upon *Hdac3* ablation, suggesting that *Hdac3* ablation might exert protective effect against HFD.

	FLOXED	H3atKO
LOW FAT DIET	24,24	34,01
HIGH FAT DIET	38,32	32,53

Figure 65: comparison of M1 macrophage percentage between LFD and HFD fed Floxed and H3atKO mice.

Furthermore, qPCR analysis showed a general increased expression of M1 (*Il6, Ccl2, Nos2*) (Figure 66a-c) and M2 markers (*Ym1, Arg1, Cx3cr1*) (Figure 66d-f), with only *Cx3cr1* expression reaching statistical meaning.

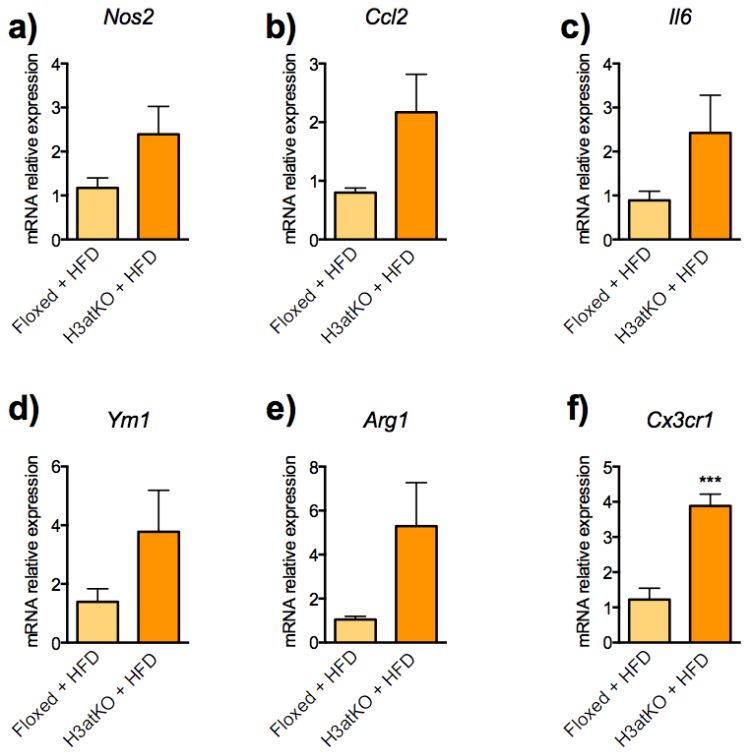

*Figure 66: expression of M1 macrophage (a, b, c) and M2 macrophage (d, e, f) markers in EpiWAT of HFD fed Floxed and H3atKO mice. Student's t test; ***p<0.001 vs Floxed mice.*

Similar to what found during LFD feeding, HFD fed H3atKO mice displayed increased levels of $CD4^+$ (Figure 67a) and $CD8^+$ T cells (though not statistical significant) (Figure 67b), with no prevalence of any T cell subset (Teffector memory TEM, Tcentral memory TCM, Teffector, Tnaïve) (Figure 67c-d), neither Treg cells (% $CD25^+$ $FoxP3^+/CD4^+$) (Figure 67e).

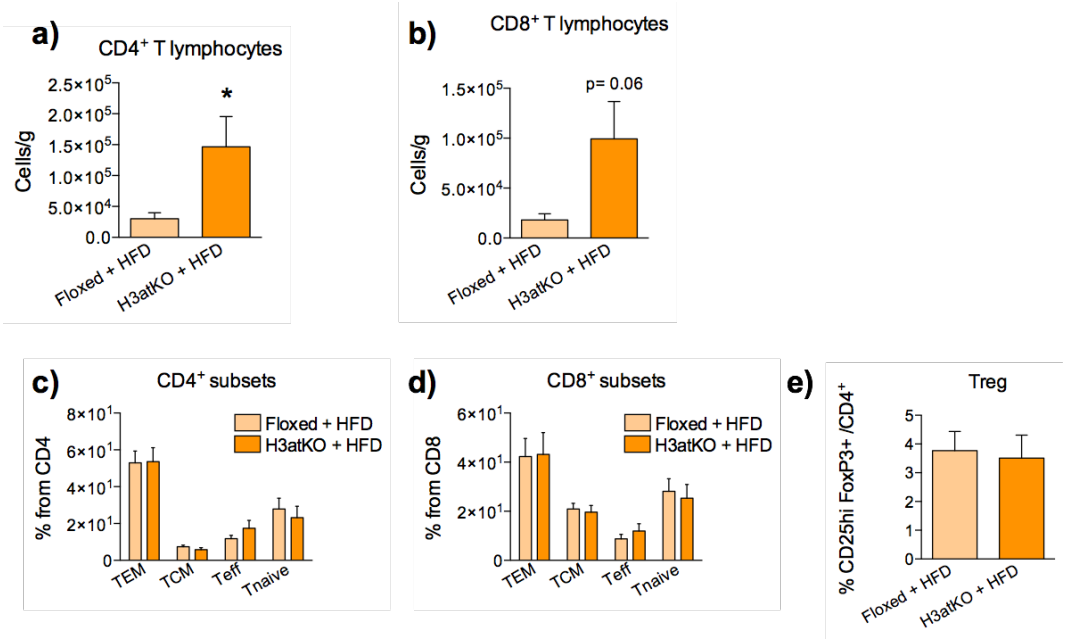

*Figure 67: analysis of adaptive immune cells number in ViscWAT of HFD fed Floxed and H3atKO mice, in particular CD4+ (a), CD8+ (b), CD4+ subsets (c), CD8+ subsets (d) and Treg (e). Student's t test; *p<0.05 vs Floxed mice.*

Bone marrow and blood analysis did not show any difference in leucocytes (Figure 68a), neutrophils (Figure 68b), monocytes (Figure 68c) and related subsets (Ly6C high, intermediate and low) (Figure 68d).

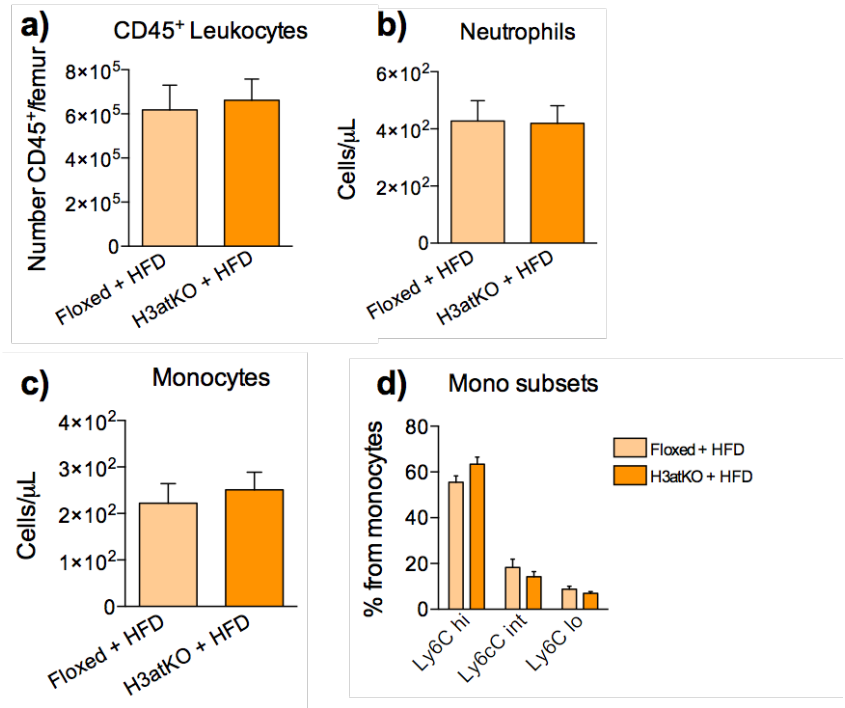

Figure 68: levels of leukocytes in bone marrow (a), neutrophils (b), monocytes (c), monocyte subsets (d) in blood of HFD fed Floxed and H3atKO mice. Student's t test.

Similarly, levels of $CD4^+$, $CD8^+$ T cells and related subsets were not changed upon HFD feeding (Figure 69a-d).

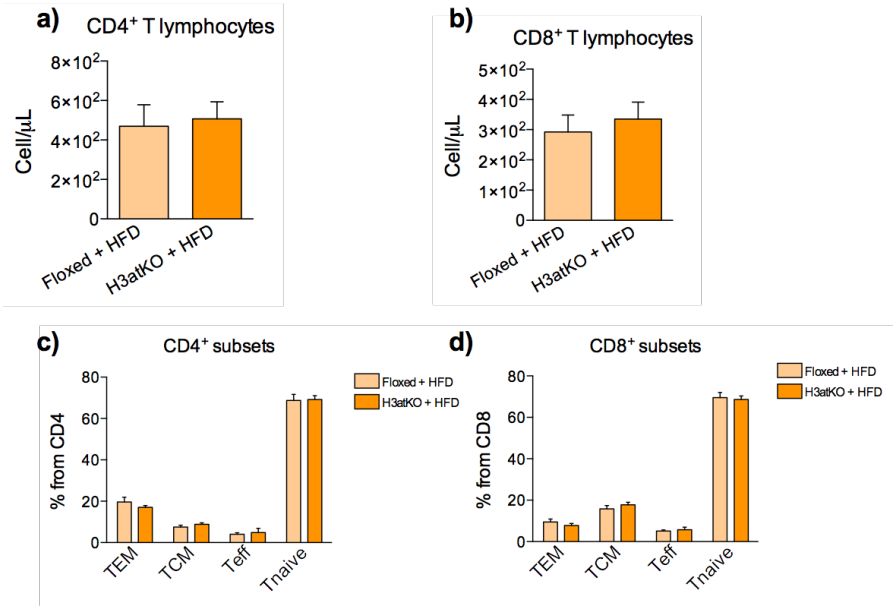

Figure 69: levels of $CD4^+$ (a), $CD8^+$ (b), $CD4^+$ subsets (c), $CD8^+$ subsets (d) in blood of HFD fed Floxed and H3atKO mice. Student's t test.

However basal not activated Treg cells ($CD4^+$ $CD25^+$) levels showed a slight increase in H3atKO mice fed HFD (Figure 70).

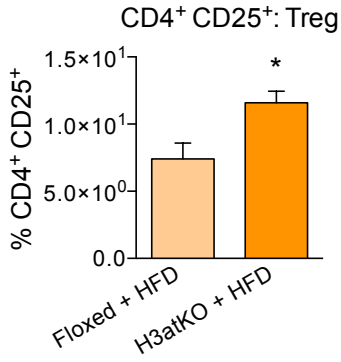

*Figure 70: levels of circulating basal Treg cells in HFD fed Floxed and H3atKO mice. Student's t test; *p<0,05 vs Floxed mice.*

Taken together, these data indicated that number of adipose immune cells in HFD fed H3atKO tended to increase similarly to what measured in LF feeding.

This suggested that ViscWAT immunoremodeling upon *Hdac3* ablation was maintained during early phase of high fat diet exposure.

Could HDAC3 be involved in thermogenic response to cold?

Hdac3 ablation in WAT reprogrammed gene expression leading to the onset of a futile cycle of fatty acid β-oxidation and *de novo* synthesis. It has been shown that this peculiar metabolism is actually typical of BAT (Mottillo et al. 2014; Yu et al. 2018). It helps, in fact, to sustain and provide energetic requirements of the thermogenic process. At this regard, we analysed expression of metabolic genes in BAT vs IngWAT of Floxed mice. BAT displayed higher expression of BAT markers, as expected (Figure 71). Interestingly, BAT showed strongly higher expression of genes belonging to glucose and citrate metabolism, like *Pdk4,* and fatty acid β-oxidation and synthesis (Figure 71), thus confirming that BAT gene program is characterized by higher expression of genes favouring fatty acid futile cycle.

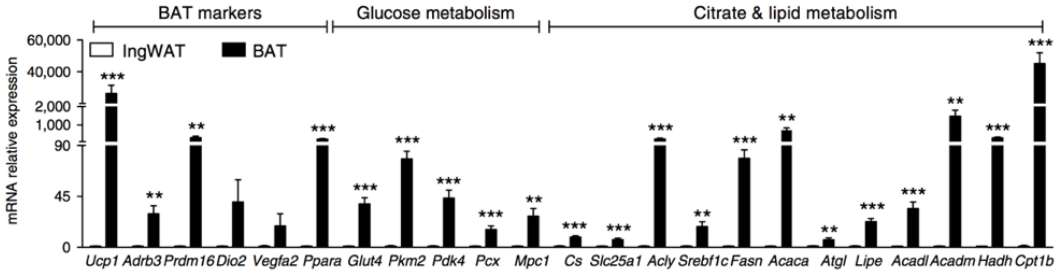

*Figure 71: expression of genes related to BAT activity, glucose, citrate and lipid metabolism in IngWAT vs BAT. Student's t test; **p<0.01; ***p<0.001 vs IngWAT.*

These data, together with already published evidences (Mottillo et al. 2014), led us to hypothesize that *Hdac3* ablation in WAT unlocked transcriptional program similar to BAT and to that evoked by cold exposure in WAT leading to browning. Therefore, we exposed Floxed and H3atKO mice to 4°C for 24 hours to induce WAT cold response and browning and we analysed gene expression in IngWAT. As expected, IngWAT showed strong increased expression of *Ucp1* and *Ppara* when Floxed mice were exposed to 4°C vs 22°C (Figure 72). Strikingly, cold exposure boosted expression of *Idh3a, Glut4, Pdk4, Cs, Atgl, Acadl, Acly, Fasn* in IngWAT of Floxed mice (Figure 72). The expression of same genes was augmented in H3atKO mice at 22°C. Of note, H3atKO mice exposed to 4°C expression pattern was in most cases similar to that of H3atKO mice at 22°C.

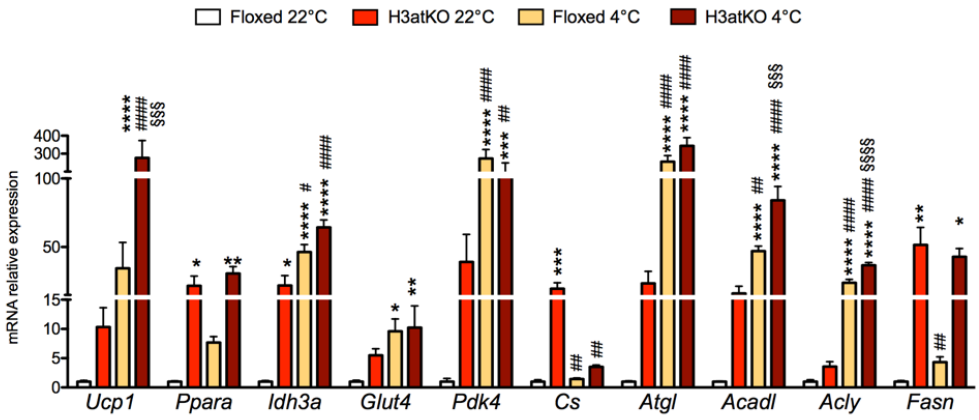

*Figure 72: expression of key genes for H3atKO phenotype in IngWAT of Floxed and H3atKO mice exposed to 4°C or at 22°C. Two way ANOVA, Tukey as post hoc test; *p<0.05, **p<0.01, ***p<0.001, ****p<0.0001 vs Floxed 22°C, #p<0.05, ##p<0.01, ###p<0.001, ####p<0.0001 vs H3atKO 22°C, §§§p<0.001, §§§§p<0.0001 vs Floxed 4°C.*

These data indicated that *Hdac3* ablation induced in IngWAT the expression of metabolic genes similarly to cold exposure, suggesting that HDAC3 may be involved in WAT thermogenic response upon cold exposure.

Discussion

Adipose *Hdac3* ablation induces browning of WAT, sustained by metabolic rewiring toward futile cycle of lipid oxidation and synthesis

Adipose tissue is not merely a site of energy storage but it also plays a central role in the regulation of systemic metabolism (Rosen & Spiegelman 2013). Recent discovery of beige adipocytes paved the way for novel therapeutical approaches for treatment of obesity and related disorders. Our previous results showed that inhibition of class I HDACs ameliorated metabolic phenotype of obese murine models, with a peculiar role played by HDAC3 (Galmozzi et al. 2013; A. Ferrari et al. 2017). Based on these preliminary data we generated a mouse model lacking HDAC3 only in adipose tissues, by breeding $Hdac3^{fl/fl}$ (Floxed) x Adipoq-Cre Tg mice in C57BL/6J background. We found that genetic inactivation of *Hdac3* in adipose tissues induced browning of IngWAT, paralleled by increased thermogenic capacity upon cold exposure. Of note, *Hdac3* ablation effects were also observed, though to a lesser extent, in visceral epididymal WAT (EpiWAT), probably due to the fact that ViscWAT is less prone to undergo browning (Kajimura et al. 2015). In fact, subcutaneous adipocytes feature peculiar cell-autonomous characteristics different from that of visceral depot (Rosen & Spiegelman 2013). Sequencing of whole transcriptome in IngWAT highlighted induction of gene pathways related to lipid oxidative metabolism. Of note, *Hdac3* ablation induced also gene repression, indicating that *Hdac3* knock out did not de-repress gene expression in uncontrolled fashion but rather HDAC3 governs specific gene pathways of metabolic regulation. This is in line with other findings showing that HDAC3 is not acting only as corepressor but also as coactivator of transcription (Emmett et al. 2017). Browning of H3atKO mice was sustained by the onset of peculiar metabolic phenotype. We found that glucose utilization is re-routed toward anaplerotic reactions feeding TCA cycle (e.g., conversion of pyruvate to oxaloacetate catalysed by pyruvate carboxylase). Conversely, FAs were preferentially oxidized to provide acetyl-CoA for citrate synthesis. FFAs are activators of UCP1-mediated uncoupling: on the one hand FAs directly activate UCP1 (Fedorenko et al. 2012), on the other hand β-oxidation produces higher amount of reducing equivalents (i.e., NADH and $FADH_2$), that, in turn, supply electron transport chain and uncoupling. However, we observed concomitant activation of *de novo* lipogenesis. As expected from previous findings (Herman et al. 2012), the increased expression of *ChREBPβ* isoform induced the lipogenic

gene pathway. Therefore, in this genetically modified mouse model, we observed an apparently paradoxical futile cycle of FAs metabolism, whereby FA β-oxidation and *de novo* FA biosynthesis pathways are active at the same time. The onset of lipid futile cycle is further strengthened by *in vitro* experiments with labelled palmitate, showing incorporation of labelled carbons to *de novo* synthesized palmitate. The concomitant activation of these opposite pathways appears to be typical of BAT metabolism upon cold or β_3-adrenergic stimuli, as demonstrated by previous findings (Mottillo et al. 2014; Yu et al. 2018). Moreover, BAT or activated beige adipocytes display UCP1-independent thermogenic mechanisms that rely upon futile cycles of creatine (Kazak et al. 2015) or Ca^{2+}/ATP hydrolysis (Ikeda et al. 2018). Based on these evidences, the occurrence of paradoxical metabolic pathways seems to be typical of BAT metabolism to sustain higher energy demand of the thermogenic process. Therefore, *Hdac3* ablation phenocopied, at least in part, BAT metabolism. These intriguing results prompted us to investigate molecular mechanisms underlying H3atKO phenotype. HDAC3 regulates transcription via epigenomic mechanisms. It is recruited to the genome, usually via formation of protein complex along with NCOR1 or NCOR2 (also known as SMRT), which are essential to mediate repression (Sun et al. 2013). Given that performing ChIP-qPCR experiments on coregulators of transcription in adipose tissue presents notable technical limitations, we decided to measure histone acetylation as a read-out of HDAC3 activity. Histone acetylation was not globally increased upon *Hdac3* ablation (data not shown), as previously reported by others (Montgomery et al. 2008). Therefore, we focused on specific chromatin regions with a potential role in determining effects consequent to *Hdac3* ablation. By exploiting literature (Ramlee et al. 2014; Abe et al. 2015) and published ChIP-Seq datasets, we found "hot regions" regulating *Pparg, Ucp1* and *Ppara* genes. When we interrogated chromatin, we found increased H3K27ac on these regions upon *Hdac3* ablation/silencing. PPARγ plays pivotal role in the regulation of adipogenesis and adipocyte function. In addition, ATGL and LPL are PPARγ target genes, therefore PPARγ activation might also be important to induce lipolysis and FA uptake upon *Hdac3* ablation. On the other hand, activation of PPARα gene network enhances FA β-oxidation. Moreover, PPARα positively regulates *Pdk4* expression, thus, in the context of H3atKO phenotype, PPARα activation also allowed to reroute glucose-derived pyruvate from production of acetyl-CoA to

anaplerotic synthesis of oxaloacetate. As a matter of fact, *in vitro* experiments with PPARα antagonist further demonstrated that this nuclear receptor contributed to establish metabolic rewiring upon *Hdac3* genetic inactivation. Thus, *Hdac3* ablation induced metabolic rewiring and browning by epigenetic regulation of key genes *Pparg*, *Ucp1* and *Ppara*. Histone acetylation in H3atKO mice was sustained by ACLY nuclear localization, as demonstrated by knockdown experiments showing that *Acly* silencing prevented hyperacetylation of chromatin regions. To summarize, *Hdac3* ablation-driven epigenetic changes in "hot chromatin regions" upregulated the expression of key genes *Pparg*, *Ucp1* and *Ppara*, thus inducing metabolic rewiring, which sustained browning of IngWAT.

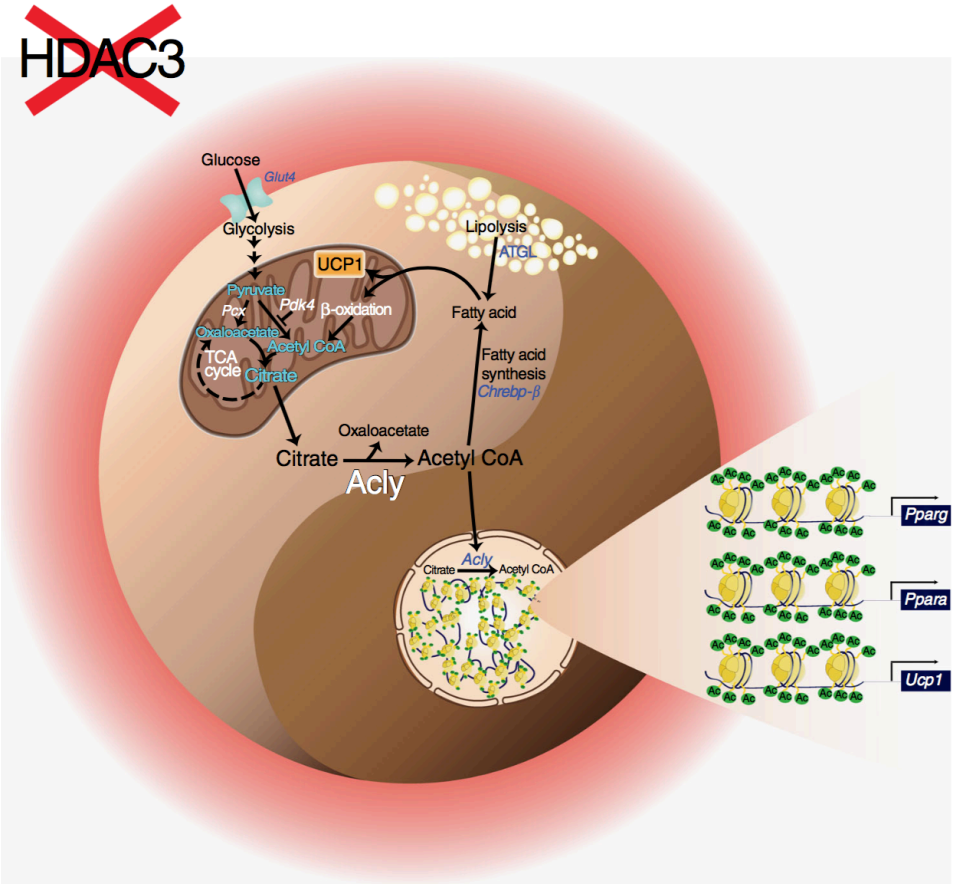

Figure 73: metabolic switch of H3atKO mice sustains thermogenesis (Alessandra Ferrari et al. 2017).

Transcription factors evoked by *Hdac3* ablation and activation of related regulatory networks is still a point that remains to be further investigated. While PPARγ and PPARα seem to emerge as pivotal actors in triggering molecular changes that determined metabolic rewiring and browning of IngWAT in H3atKO mice, the integration of different "omics" approaches would help to

further disentangle this issue. A possible approach would be to carry out ChIP-Seq experiments analysing H3K27ac and H3K4me3 enrichment peaks that would detect, respectively, enhancer and promoter regions involved in transcriptional reprogramming underlying effects consequent to *Hdac3* ablation. On the other hand, HDAC3 ChIP-Seq in IngWAT would identify genomic regions physiologically occupied by HDAC3. ATAC-Seq (Assay for Transposase-Accessible Chromatin followed by Sequencing) experiments in H3atKO IngWAT would highlight DNA fragments with greater chromatin openness which leads to binding of transcription factors and coregulators. Possibly, the use of bioinformatic tools, by integrating the results of these experiments, would help to identify the enrichment of specific transcription factors motifs upon *Hdac3* ablation and, consequently, infer candidate transcription factors involved in determining transcriptional and metabolic reprogramming upon *Hdac3* ablation. One example of these tools is HOMER (Hypergeometric Optimization of Motif EnRichment, available online at http://homer.ucsd.edu/homer/index.html), which contains several tools for *de novo* motif analysis in ChIP-Seq, ATAC-Seq and other "omics" experiments. The identification of these transcription factors may help to identify new possible targets that, once activated, trigger mechanisms, e.g. browning, that counteract obesity.

It is important to mention that our findings do not overlap the results reported by Emmett et al. (Emmett et al. 2017), which showed that pan-adipose and BAT-specific *Hdac3* knock out mice were not able to cope cold exposure. These discrepancies could be related to different Hdac3$^{fl/fl}$ strains used; however, the authors focused their attention on BAT-specific *Hdac3* knock out, showing that HDAC3 primed brown adipocytes to immediate thermogenic response, by allowing a basal tone of thermogenic gene expression. Their conclusion is not completely in contrast with our results, considering that in our model we did not detect any significant effect of *Hdac3* ablation in BAT (data not shown). However, recent findings support our conclusion on HDAC3 role in WAT (Liao et al. 2018). These authors found that pharmacologic HDAC3 inhibition increased expression of thermogenic genes both in BAT and inguinal SubWAT primary cells, regardless of mouse strain, and immortalized cell lines. Importantly, these authors reported the same observation also in human derived adipocytes. Moreover, PRDM16, a critical factor for BAT and beige development, was involved in mediating the effects of HDAC3 inhibition. These data support our

hypothesis of HDAC3 as a brake of metabolic program driving thermogenesis in IngWAT.

High fat diet blunts the effects of *Hdac3* ablation

The induction of browning and/or BAT activation confers protection against obesity and related disorders. The exciting phenotype observed in H3atKO mice prompted us to investigate whether *Hdac3* ablation exerted protective properties against obesity and related systemic metabolic dysfunction. However, when we exposed H3atKO mice to HFD for 24 weeks, we detected no difference in H3atKO mice compared to Floxed mice. To explain why HFD offset H3atKO phenotype, we focused on lipid metabolism regulation by HFD itself. Notably, it has been shown that HFD reduces levels of ATGL in adipose tissue (Shen et al. 2007). Therefore, the tissue is releasing less FFAs, which are known activators of PPARs. The expression of PPARs was not augmented in H3atKO mice fed HFD, which correlated with lack of increased acetylation of histone at chromatin regions regulating *Ppara* and *Pparg* genes. It is conceivable that PPARs were also less active, due to less availability of FFAs as ligands of these two nuclear receptors. Consequently, activation of PPARα- and PPARγ-regulated gene networks were blunted upon HFD feeding. As such, PDK4-mediated shift of glucose metabolism is overridden by HFD, because *Pdk4* is a known target gene of PPARα. Moreover, UCP1 was less active as well, due to the lack of FFAs. Therefore, HFD impaired UCP1 activation and PPARα-mediated regulation of lipolysis and fatty acid β-oxidation. In addition, *ChREBPβ* expression was also reduced in mice on HFD and, as a consequence, its target lipogenic genes. Therefore, in accordance with previous findings (Herman et al. 2012), *de novo* lipogenesis was diminished upon HF feeding. Overall, these evidences imply that HFD modulated by itself lipid metabolism, thus, by interfering with epigenomic regulation mediated by *Hdac3* ablation, HFD overcame H3atKO metabolic phenotype.

Immunophenotype of H3atKO ViscWAT reveals HDAC3 as a new possible regulator of immune function of adipose tissue

Innate and adaptive immune cells resident in adipose tissue play important role in the regulation of adipocytes function and systemic metabolism (Mathis 2013). Immune cells are not only involved in aetiology of obesity-related metabolic

disturbances but they also modulate physiological functions such as thermogenesis, adipose tissue angiogenesis and remodelling (Choe et al. 2016). The recent attention on immune partners in the pathophysiology of adipose tissue prompted us to analyse immunophenotype of H3atKO ViscWAT. Unexpectedly, we observed that *Hdac3* ablation in adipocytes also influenced the presence of immune cells in adipose tissue, with respect to both the innate and adaptive components of the immune system. In fact, we detected increased number of monocytes, neutrophils and macrophages and $CD4^+$ and $CD8^+$ T lymphocytes, with no increased prevalence of any T cell subsets. When considering macrophages, we noticed increased percentage of M1 over M2 macrophages, but gene expression of macrophage markers showed increase in both M1 and M2 markers upon *Hdac3* ablation. Of note, analysis of blood and bone marrow suggested that higher number of immune cells in H3atKO ViscWAT was caused by increased local proliferation rather than recruitment from systemic circulation. Adipocytes death induces recruitment of macrophages, in particular apoptotic-like cell death appeared to induce M2 macrophages recruitment (Fischer-posovszky et al. 2018). However, the recent study of Hill et al. (Hill et al. 2018) has revolutionized the classical M1/M2 paradigm, by the identification of different classes of macrophages ($CD9^+$ and $Ly6C^+$) that do not display predominant characteristics of M1 or M2 activation, as assessed by transcriptome analysis. At this regard, it has been recently demonstrated that M1 and M2 are both involved in tissue repairing processes after adipocyte death (Choe et al. 2016). In particular, Kato et al. (Kato et al. 2014) observed the presence of both M1 and M2 macrophages after fat grafting. The authors proposed the hypothesis whereby M1 macrophages are involved in phagocytosis of dead adipocytes, particularly in the regenerating zone, where adipogenesis supplies the tissue with newly differentiated adipocytes without fibrotic area. At the same time both M1 and M2 macrophages are involved in hypoxic and necrotic area where M1 absorption of extra lipids from necrotic cells is subsequently followed by M2-induced fibrogenesis. This study suggested possible unrecognized roles of M1 macrophages that are not necessarily detrimental for metabolic function. To explain the upsurge of macrophages in our H3atKO mouse, particularly M1, we are tempted to speculate that mechanisms of cell death and adipogenesis-driven cell renewal are activated upon *Hdac3* ablation. Possibly, increased metabolic rate induces cell death and macrophages are involved in removal of dead cells. However, the possible occurrence of these mechanisms remains to be further

investigated to test this hypothesis. Moreover, analysis of immunophenotype revealed that early HFD exposure did not substantially change the tendency of H3atKO ViscWAT to be enriched of immune cells. This indicates that *Hdac3* adipose-specific knock out caused rewiring of ViscWAT immunophenotype, which is maintained in the early phases of HFD exposure. Interestingly, HFD feeding did not increase the number of M1 macrophages in H3atKO mice, as opposed to Floxed control mice and in agreement with published literature. It would be of great interest to investigate whether genetic inactivation or pharmacological inhibition of HDAC3 in adipose tissue would confer protection against inflammation-related impairments in systemic metabolism and insulin sensitivity.

HDAC3 is emerging as a new possible regulator of thermogenic response to cold

Hdac3 ablation in adipose tissue rewired metabolism toward a futile cycle of fatty acid oxidation and synthesis that sustained thermogenesis and browning. Therefore, we propose HDAC3 as molecular brake of thermogenesis-supporting metabolism in WAT. By comparing gene expression in IngWAT between Floxed mice exposed at 4°C and H3atKO at room temperature, we noticed that *Hdac3* ablation induced similar gene expression pattern to that induced by cold in Floxed mice. These data were confirmed also in *in vitro* experiments showing that *Hdac3* silencing, phenocopied, at least in part, the effects consequent to β-adrenergic stimulation with isoproterenol in terms of gene expression and isotope labelled metabolites (data not shown). Interestingly, Liao et al. (Liao et al. 2018) recently showed that HDAC3 protein levels were markedly reduced upon chronic cold exposure both in BAT and inguinal SubWAT. Of note, *Hdac3* mRNA did not parallel the same pattern: in fact BAT *Hdac3* mRNA were slightly higher in BAT versus SubWAT at room temperature, as also observed by us (data not shown). However, BAT showed less amount of HDAC3 protein than SubWAT in mice kept at room temperature. In parallel, *Hdac3* mRNA showed mild increase only in SubWAT upon cold. Notably, another recent paper further strengthens the hypothesis that HDAC3 is involved in cold response. Yuliana et al. (Yuliana et al. 2018) reported that β-adrenergic stimulation by isoproterenol treatment increased H3K27ac at *Ucp1* enhancer and proximal regions in primary inguinal subcutaneous adipocytes. The authors also found that HDAC activity was

reduced upon isoproterenol treatment and that *Hdac3* and *Hdac8* expression inversely correlated with *Ucp1* expression. In addition, the authors found reduced HDAC3 recruitment at *Ucp1* enhancer and proximal regions after isoproterenol treatment. Finally, silencing *in vitro* experiments suggested that HDAC3 regulation of *Ucp1* expression relied on β-adrenergic stimulation, even though this result was not totally confirmed by pharmacological inhibition experiments.

Thus, our results, together with findings of other laboratories, strongly suggest HDAC3 as one of the actors involved in the regulation of thermogenic response to cold in WAT.

Conclusions

The evidences reported in this thesis demonstrated that HDAC3 is a molecular brake of metabolic program that supports thermogenesis and browning of white adipose tissue (WAT). By exploiting a mouse model with adipose-specific ablation of *Hdac3*, we discovered that *Hdac3* inactivation induced rearrangements of specific chromatin regions regulating the key genes *Pparg, Ppara* and *Ucp1*. In turn, this drove gene reprogramming that sustained a metabolic shift towards a futile cycle of fatty acid β-oxidation and *de novo* lipogenesis. According to this model, the futile cycle of fatty acid metabolism supports browning of WAT and increases the thermogenic capacity of WAT. However, *Hdac3* ablation was not able to prevent the metabolic impairments consequent to high fat diet exposure. This was due to impaired regulation of lipid metabolism by high fat diet exposure, which offset the phenotype induced by genetic inactivation of *Hdac3*. Adipose-specific *Hdac3* ablation also remodelled immunophenotype of visceral WAT, which was characterized by higher number of innate and adaptive immune cells both in low fat and in high fat diet. The role of immunoremodeling of ViscWAT on systemic metabolism and insulin sensitivity in H3atKO mice will be further elucidated in future experiments. Based on our results and on published literature by other investigators, we propose HDAC3 as a crucial regulator of adipose tissue metabolism and phenotype.

Bibliography

Abe, Y. et al., 2015. JMJD1A is a signal-sensing scaffold that regulates acute chromatin dynamics via SWI/SNF association for thermogenesis. *Nature communications*, 6(May), p.7052. Available at: http://www.pubmedcentral.nih.gov/articlerender.fcgi?artid=4432656&tool=pmcentrez&rendertype=abstract.

Benayoun, B.A., Pollina, E.A. & Brunet, A., 2015. Epigenetic regulation of ageing: Linking environmental inputs to genomic stability. *Nature Reviews Molecular Cell Biology*, 16(10), pp.593–610. Available at: http://dx.doi.org/10.1038/nrm4048.

Brown, C.C. et al., 2018. Minireview Toward an Understanding of How Immune Minireview.

Calderon-Dominguez, M. et al., 2015. Fatty acid metabolism and the basis of brown adipose tissue function. *Adipocyte*, 5(2), pp.98–118. Available at: http://www.tandfonline.com/doi/full/10.1080/21623945.2015.1122857\nhttp://www.ncbi.nlm.nih.gov/pubmed/27386151\nhttp://www.pubmedcentral.nih.gov/articlerender.fcgi?artid=PMC4916887.

Choe, S.S. et al., 2016. Adipose Tissue Remodeling : its Role in energy Metabolism and Metabolic Disorders. , 7(April), pp.1–16.

Cinti, S. et al., 2005. Adipocyte death defines macrophage localization and function in adipose tissue of obese mice and humans. , 46, pp.2347–2355.

Clearance, A.M. et al., 2016. Beige Adipocyte Maintenance Is Regulated by Article Beige Adipocyte Maintenance Is Regulated by Autophagy-Induced Mitochondrial Clearance. , pp.402–419.

Cummins, T.D. et al., 2014. Metabolic remodeling of white adipose tissue in obesity. *American journal of physiology. Endocrinology and metabolism*, 307(3), pp.E262–77. Available at: http://www.ncbi.nlm.nih.gov/pubmed/24918202.

Cypess, A.M. et al., 2009. Identification and Importance of Brown Adipose Tissue in Adult Humans. , pp.1509–1517.

Davina, W. et al., 2011. Eosinophils Sustain Adipose Alternatively Activated Macrophages Associated with Glucose Homeostasis. *Science*, (APRIL), pp.243–247.

Demerath, E.W. et al., 2015. Epigenome-wide association study (EWAS) of BMI, BMI change and waist circumference in African American adults identifies multiple replicated loci. *Human molecular genetics*, 24(15), pp.4464–4479.

Dick, K.J. et al., 2014. DNA methylation and body-mass index: A genome-wide analysis. *The Lancet*, 383(9933), pp.1990–1998.

Emmett, M.J. et al., 2017. Histone deacetylase 3 prepares brown adipose tissue for acute thermogenic challenge. *Nature*, 546(7659), pp.544–548. Available at: http://dx.doi.org/10.1038/nature22819.

Fedorenko, A., Lishko, P. V & Kirichok, Y., 2012. Mechanism of Fatty-Acid-Dependent UCP1 Uncoupling in Brown Fat Mitochondria. *CELL*, 151(2), pp.400–413. Available at: http://dx.doi.org/10.1016/j.cell.2012.09.010.

Feng, D. et al., 2012. A Circadian Rhythm Orchestrated By Histone Deacetylase 3 Controls Hepatic Lipid Metabolism. , 331(6022), pp.1315–1319.

Ferrari, A. et al., 2017. Attenuation of diet-induced obesity and induction of

white fat browning with a chemical inhibitor of histone deacetylases. *International Journal of Obesity*, 41(2), pp.289–298. Available at: http://dx.doi.org/10.1038/ijo.2016.191.

Ferrari, A. et al., 2018. Epigenome modifiers and metabolic rewiring: new frontiers in therapeutics. *Pharmacology & Therapeutics*, (xxxx). Available at: https://linkinghub.elsevier.com/retrieve/pii/S0163725818301463.

Ferrari, A. et al., 2017. HDAC3 is a molecular brake of the metabolic switch supporting white adipose tissue browning. *Nature Communications*, 8(1). Available at: http://dx.doi.org/10.1038/s41467-017-00182-7.

Ferrari, A. et al., 2012. Linking epigenetics to lipid metabolism: focus on histone deacetylases. *Molecular membrane biology*, 29(7), pp.257–66. Available at: http://www.ncbi.nlm.nih.gov/pubmed/23095054.

Feuerer, M. et al., 2009. Fat Treg cells: a liaison between the immune and metabolic systems. , 15(8), pp.930–939.

Fischer-posovszky, P. et al., 2018. Targeted Deletion of Adipocytes by Apoptosis Leads. , 152(April), pp.3074–3081.

Galmozzi, A. et al., 2013. Inhibition of class i histone deacetylases unveils a mitochondrial signature and enhances oxidative metabolism in skeletal muscle and adipose tissue. *Diabetes*, 62(3), pp.732–742.

Gao, X. et al., 2016. Acetate functions as an epigenetic metabolite to promote lipid synthesis under hypoxia. *Nature Communications*, 7(May), pp.1–14. Available at: http://dx.doi.org/10.1038/ncomms11960.

Haberland, M., Montgomery, R.L. & Olson, E.N., 2009. The many roles of histone deacetylases in development and physiology: Implications for disease and therapy. *Nature Reviews Genetics*, 10(1), pp.32–42.

Hankir, M.K., Klingenspor, M. & Pet, F., 2018. Brown adipocyte glucose metabolism : a heated subject. , pp.1–13.

Haslam, D. & James, W.P., 2005. Seminar - Obesity. *Lancet*, 366, pp.1197–209. Available at: http://www.ncbi.nlm.nih.gov/pubmed/16198769.

Herman, M.A. et al., 2012. A novel ChREBP isoform in adipose tissue regulates systemic glucose metabolism. *Nature*, 484(7394), pp.333–338.

Hill, D.A. et al., 2018. Distinct macrophage populations direct inflammatory versus physiological changes in adipose tissue. , pp.1–10.

Hong, S. et al., 2016. Dissociation of muscle insulin sensitivity from exercise endurance in mice by HDAC3 depletion. *Nature Publishing Group*, (December). Available at: http://dx.doi.org/10.1038/nm.4245.

Huh, J.Y. et al., 2014. Crosstalk between Adipocytes and Immune Cells in Adipose Tissue Inflammation and Metabolic Dysregulation in Obesity. , 37(5), pp.365–371.

Ikeda, K. et al., 2018. UCP1-independent signaling involving SERCA2b-mediated calcium cycling regulates beige fat thermogenesis and systemic glucose homeostasis. , 23(12), pp.1454–1465.

Jespersen, N.Z. et al., 2013. Short Article A Classical Brown Adipose Tissue mRNA Signature Partly Overlaps with Brite in the Supraclavicular Region of Adult Humans. *Cell Metabolism*, 17(5), pp.798–805. Available at: http://dx.doi.org/10.1016/j.cmet.2013.04.011.

Kajimura, S., Francisco, S. & Francisco, S., 2017. HHS Public Access. , 13(2), pp.69–70.
Kajimura, S., Spiegelman, B.M. & Seale, P., 2015. Brown and beige fat: Physiological roles beyond heat generation. *Cell Metabolism*, 22(4), pp.546–559. Available at: http://dx.doi.org/10.1016/j.cmet.2015.09.007.
Kato, H. et al., 2014. Degeneration, regeneration, and cicatrization after fat grafting: Dynamic total tissue remodeling during the first 3 months. *Plastic and Reconstructive Surgery*, 133(3), pp.303–313.
Kazak, L. et al., 2015. A Creatine-Driven Substrate Cycle Enhances Energy Expenditure and Thermogenesis in Beige Fat. *Cell*, 163(3), pp.643–655. Available at: http://www.sciencedirect.com/science/article/pii/S0092867415011976.
Knutson, S.K. et al., 2008. Liver-specific deletion of histone deacetylase 3 disrupts metabolic transcriptional networks. , 27(7), pp.1017–1028.
Kopelman, P.G., 2000. Obesity as a medical problem. , 404(April), pp.635–643.
Liao, J. et al., 2018. HDAC3-selective inhibition activates brown and beige fat through PRDM16. *Endocrinology*, 159(7), pp.2520–2527.
Longo, R. et al., 2017. Of mice and humans through the looking glass: 'reflections' on epigenetics of lipid metabolism. *Molecular Aspects of Medicine*, 54, pp.16–27. Available at: http://dx.doi.org/10.1016/j.mam.2017.01.005.
Lu, C. & Thompson, C.B., 2012. Metabolic regulation of epigenetics. *Cell Metabolism*, 16(1), pp.9–17. Available at: http://dx.doi.org/10.1016/j.cmet.2012.06.001.
Lumey, L.H. et al., 2007. Cohort profile: The Dutch Hunger Winter families study. *International Journal of Epidemiology*, 36(6), pp.1196–1204.
Mathis, D., 2013. Immunological goings-on in visceral adipose tissue. *Cell Metabolism*, 17(6), pp.851–859. Available at: http://dx.doi.org/10.1016/j.cmet.2013.05.008.
McDonnell, E. et al., 2016. Lipids Reprogram Metabolism to Become a Major Carbon Source for Histone Acetylation. *Cell Reports*, 17(6), pp.1463–1472.
Mihaylova, M.M. et al., 2011. Class IIa histone deacetylases are hormone-activated regulators of FOXO and mammalian glucose homeostasis. *Cell*, 145(4), pp.607–621. Available at: http://dx.doi.org/10.1016/j.cell.2011.03.043.
Min, S.Y. et al., 2016. HHS Public Access. , 22(3), pp.312–318.
Mitro, N. et al., 2007. Insights in the regulation of cholesterol 7α-hydroxylase gene reveal a target for modulating bile acid synthesis. *Hepatology*, 46(3), pp.885–897.
Montgomery, R.L. et al., 2008. Maintenance of cardiac energy metabolism by histone deacetylase 3 in mice. *Journal of Clinical Investigation*, 118(11), pp.3588–3597.
Mottillo, E.P. et al., 2014. Coupling of lipolysis and de novo lipogenesis in brown , beige , and white adipose tissues during chronic NL 3-adrenergic receptor activation. , 55.
Murano, I. et al., 2008. Dead adipocytes , detected as crown-like structures , are prevalent in visceral fat depots of genetically obese mice. , 49.

Nishimura, S. et al., 2009. CD8+ effector T cells contribute to macrophage recruitment and adipose tissue inflammation in obesity. *Nature Medicine*, 15(8), pp.914–920. Available at: http://www.nature.com/doifinder/10.1038/nm.1964.

Ramlee, M.K. et al., 2014. Histone H3 K27 acetylation marks a potent enhancer element on the adipogenic master regulator gene Pparg2. *Cell Cycle*, 13(21), pp.3414–3422.

Rosen, E.D. & Spiegelman, B.M., 2013. Review What We Talk About When We Talk About Fat.

Shabalina, I.G. et al., 2013. Report UCP1 in Brite / Beige Adipose Tissue Mitochondria Is Functionally Thermogenic. *CellReports*, 5(5), pp.1196–1203. Available at: http://dx.doi.org/10.1016/j.celrep.2013.10.044.

Shen, W.-J. et al., 2007. Effects of rosiglitazone and high fat diet on lipase/esterase expression in adipose tissue. *Biochimica et biophysica acta*, 1771(2), pp.177–84. Available at: http://www.ncbi.nlm.nih.gov/pubmed/17215164.

Shimazu, T. et al., 2012. Suppression of Oxidative Stress by B-Hydroxybutyrate, an Endogenous Histone Deacetylase Inhibitor. *Sciencexpress*, DOI: 10.11, pp.1–5.

Shinoda, K. et al., 2015. HHS Public Access. , 21(4), pp.389–394.

Sparks, L.M. et al., 2012. Beige Adipocytes Are a Distinct Type of Thermogenic Fat Cell in Mouse and Human.

Stein, A.D. et al., 2007. Anthropometric measures in middle age after exposure to famine during gestation: Evidence from the Dutch famine. *American Journal of Clinical Nutrition*, 85(3), pp.869–876.

Strahl, B.D. & Allis, C.D., 2000. The language of covalent histone modifications. *Nature*, 403(6765), pp.41–45.

Sun, Z. et al., 2013. Deacetylase-Independent function of HDAC3 in transcription and metabolism requires nuclear receptor corepressor. *Molecular Cell*, 52(6), pp.769–782.

Sun, Z. et al., 2011. Diet-induced lethality due to deletion of the Hdac3 gene in heart and skeletal muscle. *Journal of Biological Chemistry*, 286(38), pp.33301–33309.

Sun, Z. et al., 2012. Hepatic Hdac3 promotes gluconeogenesis by repressing lipid synthesis and sequestration. *Nature Medicine*, 18(6), pp.934–942. Available at: http://dx.doi.org/10.1038/nm.2744.

Talukdar, S. et al., 2013. HHS Public Access. , 18(9), pp.1407–1412.

Watson, P.J. et al., 2012. Structure of HDAC3 bound to co-repressor and inositol tetraphosphate. *Nature*, 481(7381), pp.335–340. Available at: http://dx.doi.org/10.1038/nature10728.

Weir, G. et al., 2018. Short Article Substantial Metabolic Activity of Human Brown Adipose Tissue during Warm Conditions and Cold- Induced Lipolysis of Local Triglycerides Short Article Substantial Metabolic Activity of Human Brown Adipose Tissue during Warm Conditions and Cold. *Cell Metabolism*, 27(6), pp.1348–1355.e4. Available at: https://doi.org/10.1016/j.cmet.2018.04.020.

Wellen, K.E. et al., 2009. ATP-citrate lyase links cellular metabolism to histone acetylation. *Science (New York, NY)*, 324(5930), pp.1076–1080. Available at: http://eutils.ncbi.nlm.nih.gov/entrez/eutils/elink.fcgi?dbfrom=pubmed&id=19461003&retmode=ref&cmd=prlinks.

Williams, E.P. et al., 2015. Overweight and Obesity : Prevalence , Consequences , and Causes of a Growing Public Health Problem. , pp.363–370.

Winer, D.A. et al., 2011. B Lymphocytes Promote Insulin Resistance through Modulation of T Lymphocytes and Production of Pathogenic IgG Antibody. *Nat Med*, 17(5), pp.610–617.

Winer, S. et al., 2009. Normalization of Obesity-Associated Insulin Resistance through Immunotherapy: CD4+ T Cells Control Glucose Homeostasis. *Nature medicine*, 15(8), pp.921–929.

Xu, H. et al., 2003. Chronic inflammation in fat plays a crucial role in the development of obesity-related insulin resistance Find the latest version : a crucial role in the development. , 112(12), pp.1821–1830.

Yu, X.X. et al., 2018. Cold elicits the simultaneous induction of fatty acid synthesis and NL -oxidation in murine brown adipose tissue : prediction from differential gene expression and confirmation in vivo. , pp.155–168.

Yuliana, A. et al., 2018. β-adrenergic Receptor Stimulation Revealed a Novel Regulatory Pathway via Suppressing Histone Deacetylase 3 to Induce Uncoupling Protein 1 Expression in Mice Beige Adipocyte. *International Journal of Molecular Sciences*, 19(8), p.2436. Available at: http://www.mdpi.com/1422-0067/19/8/2436.